Mutations in *BRCA1* and *BRCA2* Generate Distinct Ovarian Tumour Microenvironments and Differential Responses to Therapy

By Salar Farokhi Boroujeni

This thesis is submitted in partial fulfillment of the M.Sc. degree in Cellular and Molecular Medicine

Department of Cellular and Molecular Medicine, Faculty of Medicine,
University of Ottawa

Table of Contents

Abstract

Clinical trials are currently exploring the combinations of PARP inhibitors and immunotherapies in the treatment of ovarian cancer, but their effects on the ovarian tumour microenvironment (TME) remain unclear. Here, we investigate how olaparib, PD-L1 monoclonal antibodies and their combination can influence TME composition and survival of tumour-bearing mice. We further explored how *BRCA* mutations can influence the response to therapy. Olaparib and combination therapies similarly improved the median survival of *Brca1*- and *Brca2*-deficient tumour-bearing mice. Anti-PD-L1 monotherapy improved the survival of mice with *Brca1*-null tumours, but not *Brca2*-null tumours. A detailed analysis of the TME revealed that the olaparib monotherapy resulted in a large number of immunosuppressive and immunomodulatory effects in the more inflamed *Brca1*-deficient TME but not *Brca2*-deficient tumours. Anti-PD-L1 treatment was mostly immunosuppressive, resulting in a systemic reduction of cytokines and a compensatory increase of PD-L1. The results of the combination therapy generally resembled the effects of one or both of the monotherapies, along with unique changes observed in certain immune populations. *In-silico* analysis of RNA-seq also revealed numerous differences between *Brca*-mutated tumour models. In summary, these findings shed light on the influence of novel therapeutics and *BRCA* mutations on the ovarian TME.

Acknowledgements

First, I would like to express my deep appreciation and gratitude to my thesis supervisor, Dr. Barbara Vanderhyden, for her continuous support and guidance throughout my graduate studies. Her passion for science, along with her commitment to mentoring her students have been truly inspiring. She has always made herself available for my many questions and has been a beacon of hope both inside and outside the lab. From the moment I joined her lab in 2021, she has provided me with the academic freedom to explore my ideas and expand my intellectual curiosity by testing out new hypotheses and experiments. Her mentorship has encouraged me to work harder, solve difficult problems and expand my critical thinking, and I believe that the lessons that I have learned from her will be invaluable in my progress as a young scientist. I am honoured and privileged to have had such an outstanding mentor, and I cannot thank her enough for her contributions to my research journey and personal growth. I would also like to acknowledge my colleagues in the Vanderhyden lab for their invaluable support. Specifically, I would like to thank Dr. Galaxia Rodriguez and Dr. Kristianne Galpin, whose expertise in immunology were indispensable in ensuring the success of this project. I would also like to thank Elizabeth Macdonald who taught me how to work with mice, a skill that was crucial in the completion of the multiple animal studies of this project. I would also like to give credit to Edward Yakubovich, whose immense knowledge of computational biology equipped me with valuable tools to analyze and understand complex data sets and study the field of medicine in new ways. Last but certainly not least, I am eternally indebted to my parents for their never-ending support. They sacrificed all that they had to provide my siblings and I with the opportunity to move to a country where we could finally have the freedom to pursue our passion. I owe my success to their unending support and could not have done this without them.

List of Tables

List of Figures

List of Abbreviations

ACK	Aluminum chloride potassium
ACVS	Animal Care and Veterinary Services
Akt	Protein kinase B
APCs	Antigen presenting cells
ART	ADP-ribosyltransferase
BRCA	Breast cancer-associated gene/protein
BRCT	BRCA c-terminus domain
cGAS-STING	Cyclic GMP-AMP synthase-stimulator of interferon genes
CCL4	Chemokine CC motif ligand 4
CO_2	Carbon dioxide
CtIP	BRCA1-c-terminal-binding protein-interacting protein
CTL	Cytotoxic T lymphocyte
CTLA4	T-lymphocyte-associated protein 4
CXCL10	Chemokine (C-X-C motif) ligand 10
DCs	Dendritic cell
DMEM	Dulbecco's Modified Eagle's Medium
DMSO	Dimethyl sulfoxide
DSB	Double-stranded break
EDTA	Ethylenediaminetetraacetic acid
EOC	Epithelial ovarian cancer
FBS	Fetal bovine serum
FC	Fragment crystallizable
GM-CSF	Granulocyte-macrophage colony-stimulating factor
gMFI	Geometric mean fluorescence intensity
GSK3β	Glycogen synthase kinase-3 beta
HD	Helical domain
HGSOC	High grade serous ovarian carcinoma
HIF1A	Hypoxia induced factor 1 alpha
HR	Homologous recombination
HRD	Homologous recombination deficient
ICI	Immune checkpoint inhibitor
IFN-*a*	Interferon alpha
IFN-γ	Interferon gamma
IL-2	Interleukin 2
IL-6	Interleukin 6
IL-10	Interleukin 10
IL-11	Interleukin 11
IP	Intraperitoneal

LAG3	Lymphocyte activating 3
MDC1	Damage checkpoint protein 1
MDSC	Myeloid-derived suppressive cells
MHCII	Major histocompatibility complex 2
MNM	Nicotinamide mononucleotide
MRE11	Meiotic recombinase 11
MTT	3-(4,5-dimethylthiazol-2-yl)-2,5-diphenyl-2H-tetrazolium bromide
NAD	β-nicotinamide adenine dinucleotide
NAM	Nicotinamide
NAMPT	Nicotinamide phosphoribosyltransferase
NBS1	Nijmegen breakage syndrome protein 1
NF-*k*B	Nuclear factor kappa-light-chain-enhancer of activated B cells
NHEJ	Non-homologous end joining
NK	Natural killer
NMNAT	Nicotinamide mononucleotide adenylyl transferase
OCT	Optimal cutting temperature compound
OLA	Olaparib
PALB2	BRCA1-partner and localizer of BRCA2
PAR	Poly-ADP-ribose
PARP	Poly (ADP-ribose) polymerase
PARPi	Poly (ADP-ribose) polymerase inhibitor
PBS	Phosphate-buffered saline
PD-1	Programmed cell death protein 1
PD-L1	Programmed cell death ligand 1
PDX	Patient derived xenograft
PFA	Paraformaldehyde
PI3K	Phosphoinositide 3-kinase
PW	Peritoneal wash
RAP80	Ubiquitin-interacting motifs of receptor-associated protein 80
RNF8	RING finger protein 8
RPA	Replication proteins A
RPM	Revolutions per minute
RT-qPCR	Reverse transcription quantitative polymerase chain reaction
SD	Standard deviation
SH2	Src homology 2
SHP3	Src homology 2 domain-containing tyrosine phosphatase-2
SSB	Single-stranded break
TCR	T cell receptor
TGFβ	Transforming growth factor beta
TILs	Tumour infiltrating lymphocytes

TME	Tumour microenvironment
TNF*a*	Tumour necrosis factor alpha
Tregs	Regulatory T cells
VEGF	Vascular endothelial growth factor
VEGFR	Vascular endothelial growth factor receptor
WGR	Tryptophan-glycine-arginine rich domain
XRCC1	X-ray repair cross complementing 1

Introduction

1.1 Ovarian Cancer

Ovarian cancer refers to a group of malignancies which form primary tumours in the ovarian tissue[1]. This disease is the leading cause of death among gynecological malignancies, and it is the fifth leading cause of cancer-related death in women[2]. In Canada, there are about 3000 new cases of ovarian cancer diagnosed each year and in 2022, there were approximately 1950 deaths associated with this disease[3]. Although the survival rates of many solid cancers have improved over the past few decades, the improvements in the survival rates of ovarian cancer patients have been minimal since the 1990s[4]. Thus, in Canada the 5-year survival rate of this disease is less than 45% due to reasons such as the absence of early-stage disease-specific symptoms and lack of efficient screening tools[4,5]. Moreover, the high rates of relapse following initial treatment further reduce the survival rate of patients as recurrent cancers are less responsive to therapy[6].

Although the name of the disease may suggest that it is a single entity, ovarian cancer is in fact a group of distinct malignancies that share a common anatomical site of presentation[7,8]. Over 90% of ovarian tumours are thought to have an epithelial origin and are referred to as epithelial ovarian cancers (EOC)[7,8]. The five most common types of EOC which are distinguished based on their microscopic morphology include low- and high-grade serous, endometrioid, clear cell, and mucinous tumours[9]. EOCs are further categorized into two subtypes which are referred to as Type I and Type II[9,10]. Type I malignancies include low-grade serous and endometrioid cancers, which often develop in a stepwise manner similar to many other epithelial malignancies[9,10]. Type II cancers, however, are often more aggressive and common and account for 80% of ovarian cancer

associated fatalities.[8–10] They develop rapidly, include high-grade serous ovarian carcinomas (HGSOC), and are frequently diagnosed at an advanced stage[10].

Treatment of ovarian cancer is generally dependent on the pathological stage of the tumour and involves cytoreductive surgery and chemotherapy[11,12]. Women with early-stage EOCs often undergo unilateral salpingo-oophorectomy without the removal of the contralateral ovary or the uterus[13]. Depending on the presented features, the women may also receive adjuvant platinum chemotherapy[6]. For advanced stage EOCs, women typically undergo debulking surgery, which involves a combination of bilateral salpingo-oophorectomy as well as hysterectomy[13,14]. The standard chemotherapy regimen for advanced stage tumours involves a combination of platinum and taxane-based chemotherapy[6,15]. Following the initial surgery and chemotherapy, patients may also receive a maintenance therapy to eliminate residual cancer cells that could result in recurring tumours. These maintenance therapies include a variety of anti-angiogenic inhibitors[16], platinum-based agents[17,18], and immunotherapies[19]. Depending on the cancer genotype and presence of mutations in DNA repair pathways, however, patients can receive poly (ADP)-ribose polymerase inhibitors (PARPi) as maintenance therapy[20,21].

1.2 DNA Repair Mechanisms

1.2.1 The Role of BRCA in DNA Repair

The BReast Cancer-Associated genes (*BRCA*) 1 and 2 were first identified in 1990, and mutations in these genes were linked with the development of breast cancer[22]. BRCA1 and BRCA2 are central constituents of homologous recombination (HR), a mechanism through which cells repair double-stranded DNA breaks (DSBs) (**Figure 1**)[25–28]. BRCA1 is an 1,863 amino acids protein that is composed of 24 exons and is involved in early stages of HR, and initiates the steps

required for DNA resection[26]. BRCA2 is a large 3418 amino acids protein that is composed of 27 exons and is involved in the downstream steps of HR and aids the recombination of DNA[25] (**Figure 1**).

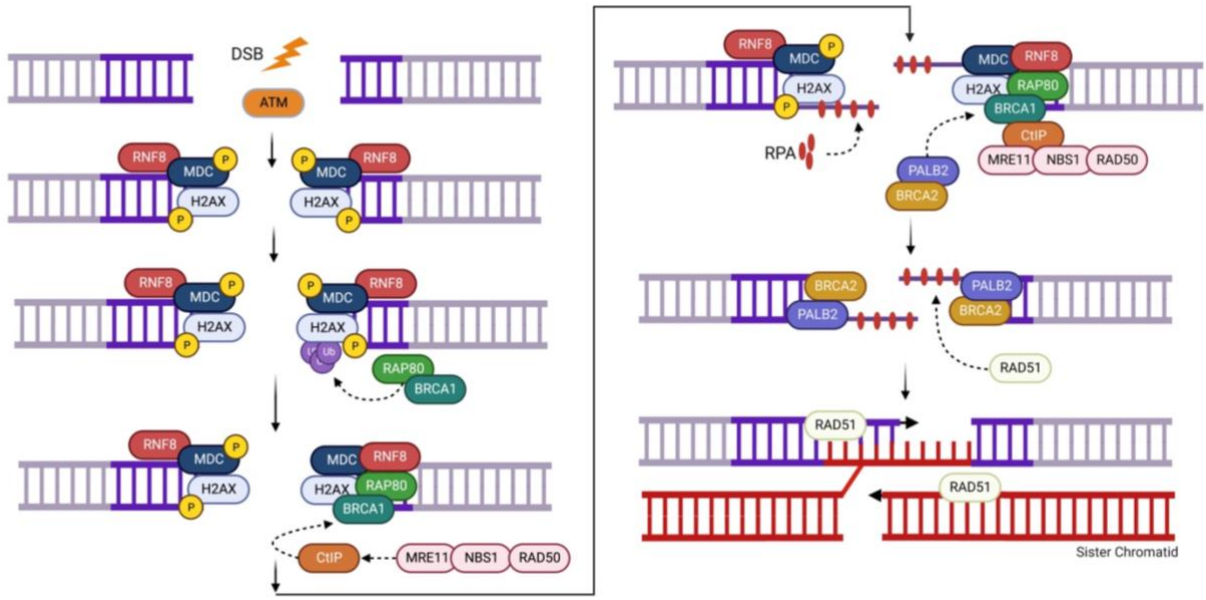

Figure 1. Molecular pathway for DNA repair through homologous recombination. Following the double-stranded DNA break, ataxia-telangiectasia mutated (ATM), a phosphoinositide 3-kinase, recognizes the DNA damage and phosphorylates the histone H2AXs. This results in the recruitment of damage checkpoint protein 1 (MDC1), a protein which is also phosphorylated by ATM and recruits RING finger protein 8 (RNF8), a ubiquitin ligase. RNF8 subsequently catalyzes the polyubiquitination of γH2AX, which attracts the ubiquitin-interacting motifs of receptor-associated protein 80 (RAP80). As RAP80 is in a complex with BRCA1, this protein is recruited to the site of damage. The BRCA1-c-terminal-binding protein-interacting protein (CtIP) then associates with the MRN complex which is composed of meiotic recombinase 11 (MRE11), RAD50 and Nijmegen breakage syndrome protein 1 (NBS1). This complex senses the double-stranded break and is responsible for the DNA resection which turns the double-stranded blunt ends into single-stranded overhangs. Replication proteins A (RPA) can then detect and bind to the overhangs, which prevents DNA folding and coordinates the assembly of repair proteins. Meanwhile, the BRCA1 partner and localizer of BRCA2 (PALB2) which is in a complex with BRCA2, interacts with BRCA1. This communication facilitates the replacement of RPAs with RAD51, a recombinase protein. RAD51 facilitates strand invasion of the sister chromatid which is used as a template to repair the DSB. Created using *BioRender*.

Since the 1990s, germline mutations in the *BRCA* genes have been also identified as primary risk factors of ovarian cancer as they are present in approximately 10-15% of patients[23,24]. Over 1600 mutations have been identified in *BRCA1* and they are in forms of nonsense and missense mutations as well as DNA deletions and insertions[29]. As this protein is composed of several domains which serve various functions, mutations in these domains can differentially influence the functions of this protein. For instance, mutations in the ovarian cancer cluster region (OCCR) which is between codons 1380 and 4062 of exon 11 of *BRCA1,* have been associated with increased risk of ovarian cancer due to impaired really interesting gene (RING) domain activity[30]. This compromised RING domain activity can prevent BRCA1 from interacting with other proteins such as ubiquitin-interacting motifs of receptor-associated protein 80 (RAP80), BRCA1-c-terminal-binding protein-interacting protein (CtIP) and inhibits the appropriate localization of this protein[31]. In contrast, over 1800 mutations have been detected in *BRCA2*[29]. In this larger protein, 3 unique OCCRs have been identified between codons 3249 and 7471 which are part of exon 11 of this gene[30]. Mutations in exon 11 of *BRCA2* have been associated with impaired binding to RAD51c, which is the recombinase protein that allows for strand invasion in DSB repair[32]. Therefore, the great variety in both the location and type of mutations in these genes can result in an abundance of biological consequences some of which, can completely impair the function of these proteins.

As a result of nonsense mutations in *BRCA1* and *BRCA2*, DSB repair cannot take place, and this results in continuous genome instability, high mutational load, chromosomal rearrangements, and overall defective genome maintenance[33]. Together, these phenotypes are referred to as BRCAness[34,35]. The importance of BRCA activity on cell survival becomes apparent in models of embryonic development[36,37]. Genome instability and DNA damage brought forth

through the absence of BRCA activity results in embryonic lethality and cell death in mouse models[37]. At a superficial level, these findings contradict the discovery that BRCA mutations result in tumorigenicity and uncontrolled cell survival. This paradox can be explained, at least in part, by the fact that most *BRCA*-mutated tumours also carry mutations in *TP53*, a tumour suppressor gene that induces cell cycle arrest and subsequent apoptosis upon detection of DNA damage[28]. *BRCA*-mutated cells harbouring *TP53* mutations can overcome cell cycle arrest and divide uncontrollably, initiating tumour onset.

1.2.2 The PARP Pathway

Although initially useful in allowing a cancer cell to survive, continuous accumulation of mutations can result in cell death, even in cancer cells. As such, *BRCA*-mutant cells have to rely on alternative single- or double-stranded DNA break repair mechanisms. For instance, nonhomologous end joining (NHEJ) is a DSB repair pathway that is alternative to HR, which simply involves the ligation of blunt DNA ends[38]. However, this method is highly error prone as direct ligation can require the deletion of DNA overhangs[38]. These deletions can later result in DNA indels and non-reversable chromosomal re-arrangements that can be detrimental to cell survival. As such, HR deficient (HRD) cells become heavily dependent on single-stranded break (SSB) repair mechanisms[39]. A prime example of SSB repair is the PARP repair pathway and the high reliance on this pathway is what allows for the survival of HRD ovarian cancer cells[39]. Enzymes in the PARP family of enzymes share the ability to catalyze the addition of poly-ADP-ribose (PAR) chains to target a protein by using β-nicotinamide adenine dinucleotide (NAD+) as the substrate[40]. This post-translational modification process is commonly referred to as PARylation[41].

The PARP1 enzyme is the most bioavailable PARP, and it consists of six main domains: three zinc finger domains (DNA binding), one BRCA c-terminus domain (BRCT), one tryptophan-glycine-arginine rich domain (WGR) and one catalytic domain which consists of a helical domain (HD) and an ADP-ribosyltransferase (ART) domain[42]. The PARP enzyme initially uses the zinc-fingers to detect SSB. Consequently, the catalytic ART domain uses the co-factor NAD+ to produce PAR chains[40,42]. The biosynthesis of NAD+ is vital for PARP activity and it is achieved through a variety of pathways. For example, NAD+ can be produced from the amino acid tryptophan which is absorbed from diet[43]. However, the major NAD biosynthesis mechanism is the salvage pathway where nicotinamide (NAM) is converted to nicotinamide mononucleotide (MNM) using the nicotinamide phosphoribosyltransferase (NAMPT)[44]. The NMN is then converted to NAD+ using the nicotinamide mononucleotide adenylyl transferase (NMNAT) family of enzymes[44].

Following the process of PARylaiton, the PAR chains attached to histones at the site of DNA damage attract DNA repair enzymes such as X-ray repair cross complementing-1 (XRCC1), which has a PAR-binding motif in its central catalytic domain[45,46]. XRCC1 then facilitates base excision repair by associating with other DNA repair enzymes such as DNA polymerase β and DNA ligase 3[45]. As the PARP pathway is reliable and less erroneous than NEHJ, HRD cells become heavily reliant on PARP activity. The over-reliance on this singular repair pathway makes *BRCA*-mutated ovarian cancer cells susceptible to PARPi, which are now commonly employed as maintenance therapy[20,21].

1.2.3 PARP Inhibitors

PARPi are a class of drug which competitively inhibit the binding of NAD+ to PARP's catalytic ART domain[47] (**Figure 2**). Alternatively, PARPi can induce the trapping of PARP onto

the DNA[48]. This trapping inhibits PARP from repairing the DNA, and also induces replication fork collapse and DSBs which eventually leads to apoptosis (**Figure 2**). In women with *BRCA*-mutated tumours, PARPi are commonly used as maintenance therapy following initial surgery and chemotherapy[20,21]. However, there is evidence to suggest that mutations in *BRCA* are not the only phenomenon that sensitizes cancer cells to PARPi toxicity as some *BRCA*-proficient tumours have also been noted to respond to PARPi therapy[49]. This may be due to the fact that there are several other genes involved in HR and mutations in any number of them (i.e., RAD51) can result in HRD. Furthermore, hypermethylation of HR genes may also result in the magnification of a HRD phenotype, thus making *BRCA*-proficient cells heavily reliant on PARP[50].

In HRD cells, PARPi take advantage of a phenomenon known as synthetic lethality where the occurrence of a single independent event is tolerable for cell survival, but their co-occurrence can be fatal[51]. Cells which are either BRCA or PARP deficient may still manage to repair their DNA and survive. However, inhibition of both pathways, whether through mutations or therapeutics, will be detrimental to cancer cell survival[51].

Olaparib, commonly known as Lynparza, was the first PARPi to be approved by the US Food and Drug Administration as a monotherapy in the treatment of advanced, *BRCA*-mutated ovarian cancers in 2014[52,53]. Three years later, the drug was approved for use to treat various forms of recurring ovarian cancer, irrespective of the patient's *BRCA* status. Since then, several other PARPi have been tested in clinical trials and currently, olaparib and niraparib are the only PARPi approved for use in Canada[54]. Although sold under several names, the pharmacokinetics of the various PARPi are similar. However, the efficiency of these drugs to inhibit PARP activity can vary. For instance, Talazoparib which is the latest PARPi approved for clinical study, has the greatest PARP1 trapping potential[55].

Although effective as a monotherapy, PARPi can also be administered as a co-therapy with other compounds[56,57]. For example, PARPi work exceptionally well in combination with genotoxic chemotherapies in platinum-sensitive cases of ovarian cancer[57,58]. Platinum-based chemotherapies often generate DNA adducts that result in cross-link formations and thus impaired DNA replication and transcription, and eventually induce apoptosis. Platinum resistance, however, is often closely linked with PARP hyperactivity in HRD patients[59]. The elevated expression of PARP can allow the cancer cells to rapidly repair the DNA damage induced by the adduct. As such, PARPi administration in combination with platinum-based therapies can help sensitize cancer cells to genotoxic compounds by preventing their ability to repair the damage[59]. In fact, in preclinical models olaparib administration has been shown to improve cisplatin-based cytotoxicity[60].

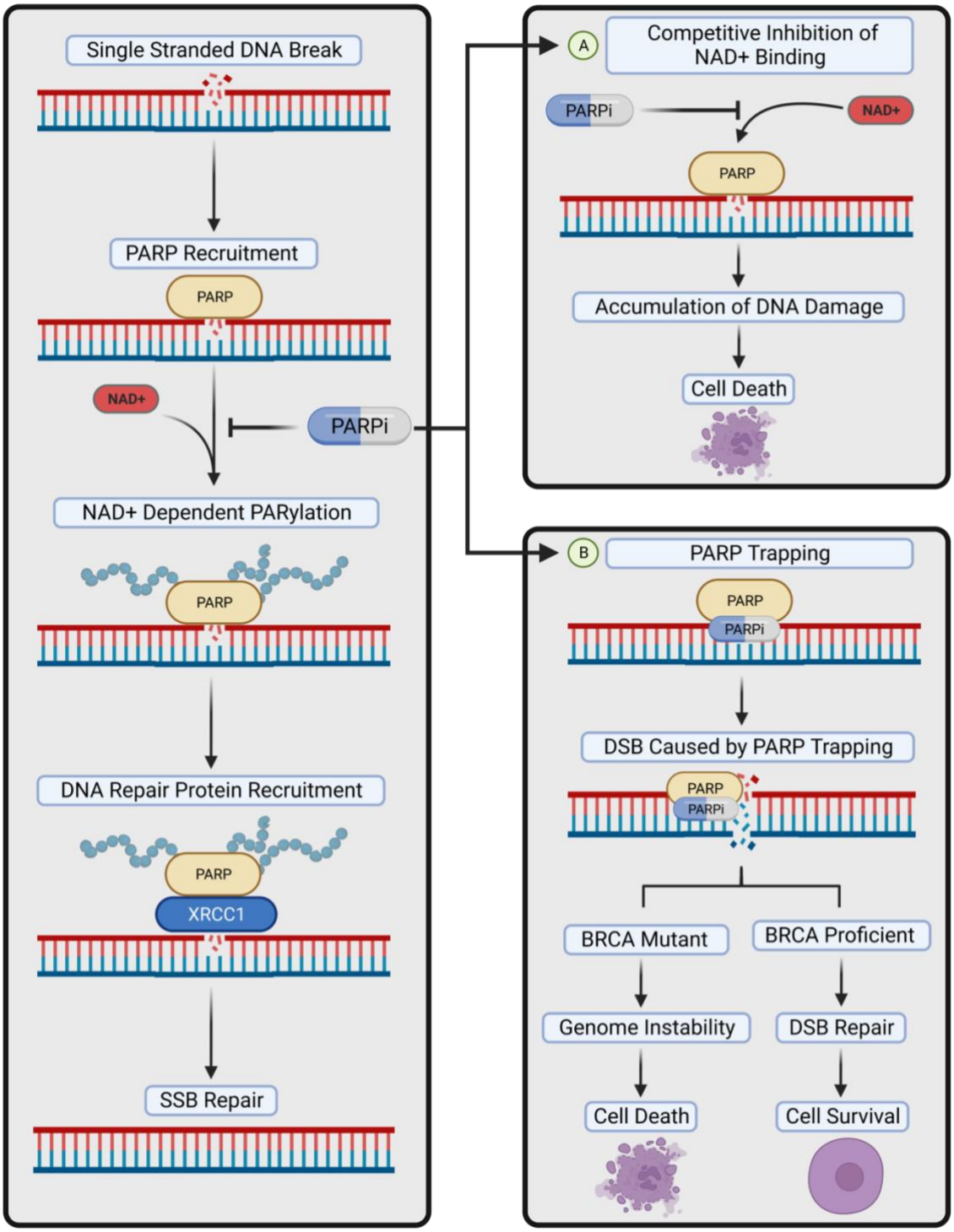

Figure 2. Schematic representation of PARP inhibitor's mechanisms of action. Under homeostatic conditions, PARP enzymes can repair DNA through base excision repair. However, PARP inhibitors can prevent PARP activity through both (A) competitive inhibition and (B) PARP trapping and result in apoptosis of *BRCA*-mutated cells. Created using *BioRender.* Inspired by Rose *et al*[61].

1.3 The Tumour Microenvironment

1.3.1 Overview of the Ovarian Tumour Microenvironment

Over the past decade, the tumour microenvironment (TME) has become a topic of interest to explore how the host's immune system can be modulated to destroy cancer cells[62]. Generally, the TME is composed of tumour cells, fibroblasts, epithelial cells, extracellular matrix, as well as cells from both the adaptive and innate arms of the immune system[62]. The dynamic interaction between these various factors can influence tumour progression and the antitumour response to therapy, and the immune surveillance that serves as a tool to target and kill cancer cells[63]. In the case of ovarian cancer, the TME is generally characterized as immunosuppressive or "cold"; a characteristic that is based on the unique immune composition of this TME[63,64].

A cold TME is often characterized by low rates of immune cell infiltration, impaired antigen presentation, or the presence of immunosuppressive immune cells such as myeloid-derived suppressive cells (MDSCs)[65], regulatory T cells (Tregs)[66] and M2 macrophages[67]. Not only do these cells impair the ability of the immune system to destroy tumour cells, but they also secrete factors that promote tumour growth. Abundant presentation of immune checkpoint molecules and exhaustion markers such as programmed cell death protein-1 (PD-1), programmed cell death ligand-1 (PD-L1), cytotoxic T-lymphocyte-associated protein-4 (CTLA4) or lymphocyte activating-3 (LAG3) all contribute to this cold phenotype as well[68]. Together, the combination of these immunosuppressive characteristics makes the TME immunologically destitute, thus rendering the immune system unable to slow down tumour progression.

In contrast, a "hot" TME is characterized by high rates of proinflammatory immune cell infiltration and is often associated with superior cancer prognosis. The elevated presence of tumour infiltrating lymphocytes (TILs) such as CD8+ and CD4+ T cells[69], natural killer (NK) cells[70], M1

macrophages[71], and antigen presenting cells (APCs) can aid in the generation of a strong anti-tumour immune response in hot TMEs. The TILs can also produce proinflammatory cytokines and chemokines which enhance the anti-tumoral response and attract more TILs from the circulation[69–71]. Furthermore, hot tumours are characterized by the presence of neoantigens on the surface of tumour cells, which make it easier for TILs to identify and attack the cancer cells[72]. The enhanced efficiency of the immune system to implement an anti-tumour response result in reduced tumour progression and improved patient survival. Recently, immunotherapies have been developed with the aim to transform the cold ovarian TME hot and ameliorate patient outcomes[19,64,73].

1.3.2 Immunotherapy

Immunotherapies are an emerging type of cancer treatment that boosts the patient's immune system to target and kill cells[64]. These immunomodulatory treatments can enhance the ability of TILs to activate and kill cancer cells. One example of such immunotherapies are the immune checkpoint inhibitors (ICIs), that bind to immune checkpoint molecules and inhibit their immunosuppressive function[74,75]. Effector T cells use the T-cell receptor (TCR) to recognize cells in their vicinity[76]. Upon recognition of a cell ligand, immune checkpoint molecules which are co-signaling pathways that modify TCR responses, can act in a negative feedback loop and prevent the effector T cells from mounting a response against that cell[76]. Although this is useful in preventing autoimmunity, it can also become an issue with regards to cancer cell detection. By expression of checkpoint molecules, tumour cells are able to dampen immune responses and thus escape immune surveillance[77]. For example, PD-L1 molecules on the surface of a tumour cell can interact with PD-1 on the surface of T cells and attenuate their anti-tumour action[75]. Consequently, monoclonal antibodies that target PD-1/PD-L1 interactions have been developed as

immunotherapies. Results of various clinical studies show an average overall response rate of 9 to 36% to anti-PD-1/PD-L1 monoclonal antibodies in ovarian cancer patients[78]. This limited efficacy may be improved through combination therapies such as anti-PD-L1 plus olaparib and the clinical trials testing such combinations are currently ongoing (NCT02953457).

1.3.3 Influence of *BRCA* Mutations on Ovarian TME Composition

Clinically, *BRCA* mutations have been simply regarded as HR defects, and *BRCA1*- and *BRCA2*-mutated tumours have been treated as the same disease. However, recent data have shown that patients with *BRCA1* mutations tend to have a higher risk of developing ovarian cancer by the age of 80; 44% (95% C.I, 36%-53%) for *BRCA1* and 17% (95% C.I, 11%-25%) for *BRCA2*[79]. Similarly, the 5-year survival rate is shorter for patients with *BRCA1*-mutated tumours[80]. Such differences point to the possibility that these proteins are involved in pathways other than genome maintenance, and therefore can potentially influence TME composition.

For instance, the high tumour mutational burden (TMB) that results from HRD can result in the presentation of neoantigens on tumour cells[81,82]. This neoantigen load may allow for improved detection of these cells through immune surveillance[81]. In preclinical models of breast cancer, mutations in *Brca1* and *Brca2* have been shown to influence response to immune checkpoint blockade. Interestingly, this effect was different in the two models, with anti-PD-l blockade only resulting in improved survival of mice harbouring *Brca1*-mutated tumours[81].

Neoantigen presentation as a result of *Brca*-mediated differences in mutational landscapes can also influence the infiltration of TILs in the TME. For instance, *Brca*-mutated ovarian TMEs have a higher abundance of CD3+ and CD4+ T cells, as well as enhanced expression of immune checkpoint molecules[83]. Furthermore, mutations in *BRCA* are associated with higher secretion of

various proinflammatory cytokines such as tumour necrosis factor alpha (TNF-*a*) in the TMEs[84]. In summary, the TME is a dynamic entity which can be influenced by both treatment and mutations in DNA repair genes. However, the changes resulting in the ovarian TME as a consequence of both specific HR mutations and exposure to therapeutics such as PARPi remain largely unknown.

1.3.4 Syngeneic Models of Cancer

For many years, patient-derived xenograft (PDX) models which are developed by the transplant of human cancer cells into immunodeficient mice were the gold standard in the study of cancer treatments in preclinical stages[85]. However, the lack of immune activity in these animals limits their use for the study of the influences of the immune system on the TME during response to treatment. Consequently, the lack of robust immunity prevents the development of reliable immunomodulatory therapies. The increased use of syngeneic models in recent years has allowed researchers to address this issue by using cancer cells that were derived from the host's species[86,87]. Injecting cancer cells which were developed in a relatively homogeneous model such as C57BL/6 mice back into those animals reduces the risk of tissue rejection that is seen in immunocompetent mice as the cells express similar surface antigens. For instance, the ID8 cell line developed by Roby *et al.* in 2000 was created by repeated passaging of ovarian surface epithelial cells isolated from C57BL/6 mice[86]. Since then, the model has been genetically modified to replicate various genetic abnormalities found in the human disease (e.g., mutations in *Trp53*, *Brca1* and *Brca2*), to enable further study of the influence of these mutations on tumour development[88,89]. The various ID8 cell lines are now frequently used as syngeneic models of ovarian cancer, and our lab has been using this model to study the influence of various treatments such as oncolytic viruses on the TME composition.

1.4 Rationale and Hypothesis

Although PARPi and immunotherapies are commonly tested in the treatment of ovarian cancer, the effects of these therapies on the composition of the ovarian TME remains unknown. As such, we hypothesize that following the administration of these treatments, the characteristics of the ovarian TME can be defined and manipulated to boost the immune response, ultimately to design more effective combination therapies. In light of recent evidence that indicates the potential differences in *BRCA1* vs. *BRCA2*-mutated cancers, we further hypothesized that tumours with different *Brca* mutations will be respond differently to treatment and therefore we analyzed how the *Brca* status of ovarian tumours influenced the TME composition and response to therapy.

Objectives:

Aim 1: To assess the response of *Brca*-mutated ovarian cancer cells to PARPi treatment *in vitro.*

Aim 2: To assess the response of syngeneic *Brca*-mutated ovarian tumours and their TME to PARPi, anti-PD-L1 antibody and their combination *in vivo.*

Aim 3: To use *in-silico* analysis of RNA sequencing data to compare the TME of *Brca*-mutated models of ovarian cancer.

Methods

2.1 Mouse Ovarian Cancer Cell Lines

For both the *in vivo* and *in vitro* sections of this project the ID8 cell lines were used. The cell lines included the ID8 *Trp53*$^{-/-}$, ID8 *Trp53*$^{-/-}$ *Brca1*$^{-/-}$, and ID8 *Trp53*$^{-/-}$ *Brca2*$^{-/-}$ cells which were created using CRISPR-Cas9-mediated knockouts and were provided by Dr. Iain McNeish[88,89]. All three cell lines were cultured using Dulbecco's Modified Eagle's Medium (DMEM) (Corning, #10-013-CV) supplemented with 4% Fetal Bovine Serum (FBS) (ThermoFisher, #12483-020) and 1x Insulin-Transferrin-Sodium-Selenium (Sigma-Aldrich Roche, #11074547001). The cells were incubated at 37^{o}C and 5% carbon dioxide (CO_2).

2.2 *In Vitro* Analyses

2.2.1 AlamarBlue Assays

In order to assess cancer cell viability in response to PARPi treatment, ID8 cells were treated with olaparib, and viability was assessed using AlamarBlue assays. ID8 cells were seeded in a 96-well plate at a density of 1.0 x 10^3 cells/well 24 hours prior to the start of treatment. A stock of olaparib (MedChemExpress; HY-10162) was prepared by dissolving the drug in dimethyl sulfoxide (DMSO) at a concentration 25.57 mM. Media with various concentrations of olaparib (0, 1, 5 and 10 μM) were prepared by dissolving the DMSO/olaparib stock mixture in DMEM media. The original culture media were then aspirated from the wells and replaced with media containing various concentrations of olaparib.

After the 24-hour treatment period, the media were aspirated from each well and replaced with DMEM media containing 10% AlamarBlue cell viability reagent (ThermoFisher; #DAL1100). The plate was incubated in the dark for 3 hours. Following the incubation, the plate

read was performed using a Bio-Tek Microplate Reader for which the absorbance and emission wavelengths were set at 530 and 590 nanometers, respectively. The data collected from the treated cells were normalized to the untreated samples, for which the cells were hypothetically 100% viable. The average results of three experiments each containing three technical replicates were pooled for statistical analyses.

2.2.2 Flow Cytometry of *In Vitro* Treated Samples

Flow cytometry was used to assess the effects of olaparib treatment on ID8 cells. The cells were seeded in a 6-well plate at a density of 6.0 x 10^4 cells/ well and treated with 10 μM olaparib for 24 hours. The negative control group received DMSO, and the positive control group was treated with recombinant 0.2 ng/ml mouse interferon gamma (IFN-γ; Fisher Scientific, 315-05). Following the treatment, the cells were collected in 1.5 mL Eppendorf tubes and washed using phosphate-buffered saline (PBS) (ThermoFisher; #14190-144). The cells were then incubated in the Fixable Viability Stain (BD BioSciences; #564406) in a 1:1000 dilution for 15 minutes. The cells were washed with PBS supplemented with 2% FBS and stained with the PD-L1 antibody (Bio Legend; #124308) at a 1:200 dilution for 15 minutes. The cells were once again washed using the same wash buffer and fixed using 1% paraformaldehyde (PFA). The samples were stored in the dark at 4°C overnight and data was acquired the following day using the BD LSR Fortessa flow cytometry machine. The FlowJo program was used to determine the geometric mean fluorescence intensity (gMFI) of each sample.

2.3 *In Vivo* Treatment

2.3.1 Mouse Models of Ovarian Cancer

To assess the response of ovarian tumours to therapy, three different syngeneic models of intraperitoneal (IP) tumours were used and information regarding each model can be found in **Table 1**. C57BL/6 mice (The Jackson Laboratory; #664) were used for syngeneic model development for all cell lines. All the animals were housed in the Animal Care and Veterinary Services (ACVS) facilities at the University of Ottawa. The experimental protocols adhered to the standards defined by the guidelines of the Canadian Council on Animal Care and were approved by the University of Ottawa Animal Care Committee. The animals were provided with the standard chow diet and monitored on a daily basis. To induce tumour development, 8-week-old mice were given IP injections of 5.0 x 10^6 cells diluted in 100 µL of PBS. The treatments started 25% into the predicted length of survival of each tumour model which was established based on previous studies in the Vanderhyden lab (**Table 1**).

Table 1. Development timelines for various ID8 syngeneic models of HGSOC. The mice were each injected with 5.0x10^6 cells at a similar passage number (<10) by intraperitoneal injection. Survival periods were calculated based on the mean survival of 8 mice bearing the same syngeneic tumour type in previous studies.

Tumour Model	Predicted survival (days post cancer cell injection)	Start of treatment (days post cancer cell injection)
ID8 *Trp53*$^{-/-}$	65	16
ID8 *Trp53*$^{-/-}$ *Brca1*$^{-/-}$	46	12
ID8 *Trp53*$^{-/-}$ *Brca2*$^{-/-}$	57	14

2.3.2 The First *In Vivo* Study: Impact of Olaparib Monotherapy on Survival

The three syngeneic tumour models listed in **Table 1** were used to determine whether olaparib monotherapy can improve the survival of tumour-bearing mice. The treatment started when the mice reached 25% of the predicted length of their survival. The experimental groups (n=8) received daily doses of 50mg/kg olaparib which was initially dissolved in DMSO and later

in a mixture of PBS containing Captisol (MedChemExpress; HY-17031). The final concentrations of DMSO and Captisol were 5% and 20%, respectively. The drug was administered as a 100 µL IP injection daily for 18 consecutive days. The control group received PBS containing only DMSO and Captisol. During the period of treatment and seven days after the last injection, the mice were housed in the designated Level-1 cytotoxic chemical room of the ACVS facilities at the University of Ottawa and were later returned to general housing.

Following the end of the treatment period, the mice were monitored on a daily basis. The development of ascites evident by abdominal distension; piloerection, reduced mobility, and impaired blood flow to the limbs were used as additional indicators of loss of wellness at which time the mice were euthanized. The euthanasia was carried out by a short period of CO_2 exposure followed by cervical dislocation. The mice were weighed, and necropsies were carried out to determine ascites volume, tumour mass and spleen mass. The collected ascites was centrifuged at 2000 revolutions per minute (RPM) for 15 minutes and the supernatant was flash frozen. A portion of the tumours were flash frozen for RNA collection. Other portions were either embedded in optimal cutting temperature compound (OCT; Fisher Scientific; 23-730-571) and stored at -80^{o}C, or fixed in 10% PFA and later transferred to 70% ethanol.

2.3.3 The Second *In Vivo* Study: Olaparib, PD-L1 Monoclonal Antibody and Their Combination

The two *Brca*-mutated ID8 cells listed in **Table 1** were used to induce tumour development in mice to study the effects of therapy on survival and TME composition. The three treatments in this study included olaparib and anti-PD-L1 monotherapies, and their combination (**Figure 3**). Olaparib was prepared as described in section **2.3.1** and the monoclonal antibodies were diluted in sterile PBS to produce the desired concentrations. The antibodies were administered through five

consecutive, 100 µL IP injections containing 200 µg of antibody. The animals then received 100 µg doses of antibody every four days, for a total of 11 antibody injections (**Figure 3**).

The study animals in the study were assigned to four groups for each of the two *Brca*-mutant cell lines: (1) olaparib, (2) anti-PD-L1, (3) combination and (4) the control group. All treatments began 25% into the expected survival period of the animals. The animals in the olaparib group received 18 daily of 50 mg/kg/day of olaparib, as well as the appropriate dose of isotype control monoclonal antibody. The anti-PD-L1 group received 18 doses of the vehicle control for olaparib, which contained PBS, 20% captisol and 5% DMSO; as well as the appropriate dose of the PD-L1 monoclonal antibody, depending on the day. The combination group received 18 daily of 50 mg/kg/day of olaparib and the appropriate dose of anti-PD-L1 monoclonal antibody. Finally, the control group received the vehicle control of olaparib as well as the isotype control antibody. The animals in this study were collected at two different time points. In order to determine the effects of treatment on TME composition, 40 mice collected approximately 36 hours after the last olaparib injections. To determine the effects of treatment on animal survival, the remaining 64 mice (8 animals/group) were monitored on a daily basis and euthanized at the humane endpoint, at which time tissues such as tumours and ascites were collected and flash frozen. Similar to the first study, the mice were housed in the designated Level-1 cytotoxic chemical room of the ACVS facilities at the University of Ottawa throughout the treatment period and were returned to general housing seven days later.

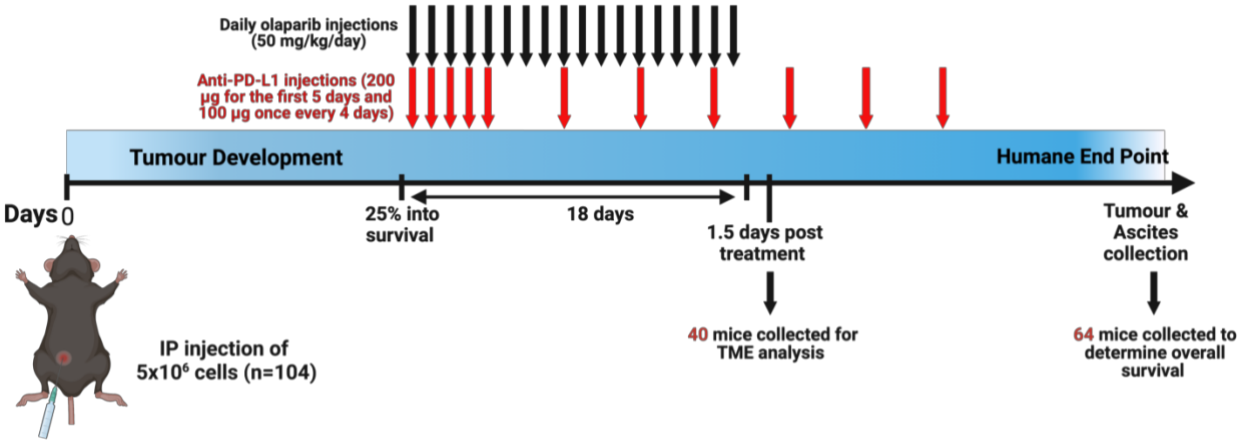

Figure 3. Treatment regimen in the second *in vivo* study. The mice were all injected with $5.0x10^6$ cells with a similar passage number (<10) by intraperitoneal injections on day zero. The treatments began 25% into the predicted survival period of each model. All treatments were provided using 100 µL intraperitoneal injections. All drugs were dissolved in sterile PBS. On days that the mice received both drugs (olaparib and the monoclonal antibody, or their controls), the drugs were administered using one 200 µL injection to reduce stress. In order to analyze the TME composition in response to treatment, 40 mice were collected 36 hours after the end treatment. The rest of the animals (n=64) which belonged to the survival group were collected at the humane endpoint to assess the impact of treatment on the survival of tumour bearing mice.

2.4 Assessment of the TME

2.4.1 Flow Cytometry TME Analysis

Approximately 36 hours after the last olaparib injection on day 18, five mice from each group were collected for TME analysis. Euthanasia was carried out as described in section 2.3.1. Peritoneal washes (PW) were collected following an intraperitoneal injection of 5 mL PBS containing 2mM ethylenediaminetetraacetic acid (EDTA) and a 5-minute abdominal massage. To generate single cell suspensions of the PW, the washes were filtered using 70 µm filters. Spleen tissue was also collected and dissociated using glass slides over a petri-dish containing PBS and was later filtered using 70 µm filters. Ammonium chloride potassium (ACK) lysis buffer (VWR, #10128-802) was used to induce blood lysis in all samples and cells were later counted using Trypan blue exclusion. To assess viability, the cells were stained using a viability stain at a 1:500 dilution (BD Biosciences, BV510) and incubated for 15 minutes at room temperature. Fc blocking was carried out for 5 minutes using 3.33 µl or 6.66 µl of the fragment crystallizable (Fc)-blocking antibody (BD Biosciences, #553142) for 2.0 x 10^7 spleen or PW cells, respectively. The cells were divided for staining using two separate antibody master mixes for different panels. The cells were then washed in PBS + 2% FBS, fixed using 1% PFA solution and stored at 4^{o}C in the dark until flow cytometry was performed. The cells that received intracellular staining were also incubated in fixation/permeabilization buffer (eBioscience) at room temperature for 45 minutes and were later washed twice using the permeabilization buffer (eBioscience). The CD206 antibody was diluted in the permeabilization buffer and was used to stain the samples for approximately 40 minutes at room temperature in the dark. Details regarding all antibodies used for flow cytometry staining are presented in **Table 2**. The data analysis for the flow cytometry was carried out using the FlowJo software.

Table 2. Fluorophore conjugated flow cytometry antibodies used to analyze the composition of the ovarian tumour microenvironment. All antibodies, with the exception of BV510 were diluted in PBS + 2% FBS. The viability BV510 stain was diluted in PBS only.

Panel	Target	Fluorochrome	Dilution	Company and Catalogue #
1	FVS510	BV510	1:200	BD Biosciences Cat# 564406
	CD3e	BUV496	1:200	BD Biosciences Cat# 564378
	CD45	PerCP-Cy5.5	1:200	BD Biosciences Cat# 561869
	CD4	APC-H7	1:200	BD Biosciences Cat# 561828
	CD8	BUV615	1:200	BD Biosciences Cat# 552877
	CD25	BV421	1:200	BD Biosciences Cat# 564370
	LAG3	BV605	1:200	BioLegend Cat# 135225
	PD-1	BV785	1:200	BD Biosciences Cat# 552380
	CD62L	PECY7	1:200	BD Biosciences Cat# 560516
	DX5	FITC	1:200	BD Biosciences Cat# 553857
	CD44	BV711	1:200	BD Biosciences Cat# 743924
	NKG2D	APC	1:200	BD Biosciences Cat# 562347
	TIGIT	APC-R700	1:200	BD Biosciences Cat# 565474
	CD19	PE-CF594	1:400	BD Biosciences Cat# 562291
2	FVS510	BV510	1:200	BD Biosciences Cat# 564406
	CD3e	BUV496	1:200	BD Biosciences Cat# 564378
	CD45	PerCP-Cy5.5	1:200	BD Biosciences Cat# 561869
	CD11c	PE-CY7	1:200	BD Biosciences Cat# 563048
	CD11b	BV786	1:400	BD Biosciences Cat# 740861
	CD86	APC-R700	1:200	BD Bioscience Cat#565479
	I-A/I-E	AF488	1:200	BD Bioscience Cat#562352
	PD-L1	PE	1:200	BD Biosciences Cat# 558091
	CD103	BV711	1:200	BioLegend Cat# 121435
	Ly6G	APC-H7	1:200	BD Biosciences Cat# 560618
	Ly6c	BV605	1:200	BD Biosciences Cat# 560618
	F4/80	BV421	1:150	BD Biosciences Cat# 565411
	CD206	AF647	1:200	BioLegend Cat# 141720

2.4.2 Reverse Transcription Polymerase Chain Reactions

To conduct reverse transcription and quantitative real-time polymerase chain reaction (RT-qPCR) analysis on tumours collected at end point, flash frozen tumours were homogenized in the RLT Plus Lysis Buffer (Qiagen, #1053393) using a syringe and needle. RNA concentrations and quality were assessed using a NanoDrop spectrometry and iScript Reverse Transcription Master

mix (Bio-Rad, #1708841) was used for cDNA synthesis. The relative expression of the genes of interest was assessed by qPCR using the Taq-polymerase-based PrimeTime Gene Expression Master Mix kit (Integrated DNA Technologies; #1055772) and a 7500 Fast Real-Time PCR machine. The expression of each gene was determined as a fold change in relation to the house-keeping gene, *Hprt*. The names of each probe assay primer are listed in **Table 3**.

Table 3. The qPCR probe assays used to analyze ovarian tumours collected at humane endpoint.

Gene name	IDT qPCR Probe Assay
Hprt	Mm.PT.39a 22214828
Cd274	Mm. PT.58.11921659
Cd8a	Mm.PT.58.43535544

2.4.3 Immunofluorescent Staining

Immunofluorescent staining of tissues was carried out using 7 µM sections of OCT embedded tumours. The sections were fixed using 2% PFA at room temperature for 20 minutes. The tissues were then washed twice using 1X PBS for 1 minute and incubated using a blocking solution containing 10% goat serum and 0.2% Triton X-100 in PBS for 1 hour at room temperature. A 10% goat serum in PBS solution was used to dilute the primary antibodies listed in **Table 5** and the tissues were incubated with the antibodies in the dark at 4° C overnight. The next day, the primary antibodies were aspirated, and tissues were washed in PBS 3 times. The secondary antibodies (**Table 5**) were diluted in the same diluent and incubated on the tissue for 1 hour at room temperature in the dark. The tissues were then washed one last time, mounted using Immuno-Mount (Themo Fisher Scientific, #9990402) and imaged the next day using the AxioSkop 2 MOT Zeiss microscope at 40X magnification.

Table 4. List of primary and secondary antibodies used for immunofluorescent staining. All antibodies were diluted in PBS containing 10% goat serum.

Antibody	Company and Catalogue #	Dilution
Anti-MHC Class II	ThermoFisher, Cat# 14-5321-82	1:250
Rat Anti-Mouse CD45	BD Pharmigen, Cat#550539	1:200
AF488 Goat Anti-Rat	ThermoFisher, Cat# A-11006	1:400
AF594 Goat Anti-Rabbit	ThermoFisher, Cat# A-11012	1:400

2.4.4 Flow-Based Cytokine Array

Ascites fluid was collected from mice at endpoint and centrifuged at 2000 RPM for 15 minutes, after which the supernatant was collected, flash frozen and stored at -80^{o} C. For the assay, ascites supernatant was diluted in the LEGENDplex^{TM} Cytokine Release Syndrome Panel assay buffer (BioLegend, #741024). The staining was then carried out using the manufacturer's protocol and flow cytometry was carried out using the BD LSR Fortessa flow cytometer on the same day. The data was then analyzed using the LEGENDplex Quognit software (BioLegend).

2.5 Bulk RNA Sequencing Data Analysis

RNA-seq data from ID8 cell lines and IP tumours which were previously processed by the Vanderhyden lab[90] were used to assess transcriptomes related to PARP activity and differential TME gene expression. The cell lines were all of a similar passage number (<20) and the IP tumours were collected at the humane endpoint. The R Studio program was used to create a normal distribution of the log-normalized RNA-seq values and the various sets of data were visualized using the pheatmap function in R.

2.6 Statistical Analysis

All statistical analyses were performed with Prism 9.0 (GraphPad Software Inc.) The Prism 9.0 software and R Studio were used to generate all the figures. Comparisons between two groups were performed using the student's *t* test, and the one-way analysis of variance (ANOVA) and Tukey's multiple comparisons were used to compare three or more groups. The Log-Rank test was used to determine any significant differences in the survival data shown using Kaplan-Meier plots. All histogram data sets are presented as the means ± standard deviation (SD). Statistical significance was set at $p \leq 0.05$ (*p ≤ 0.05; **p < 0.01; ***p < 0.001; ****p < 0.0001).

Results

3.1 Assessing the Response of *Brca*-Mutated Ovarian Cancer Cells to PARPi *In Vitro*

3.1.1 Olaparib Reduces the *In Vitro* Viability of *Brca*-Mutated Cancer Cells

The assessment of the loss of viability in response to *in vitro* olaparib therapy was carried out using the AlamarBlue assay on the ID8 cell lines listed in **Table 1**. Following the 24-hour treatment, viability of the ID8 *Trp53*$^{-/-}$ group did not change in response to any dose of olaparib therapy (**Figure 4**). Cells with double knockout of *Trp53*$^{-/-}$ *Brca1*$^{-/-}$ modestly responded to olaparib toxicity and the highest dose of olaparib (10 µM) resulted in a significant 25% reduction in viability ($p<0.05$). Conversely, the viability of the ID8 *Trp53*$^{-/-}$ *Brca2*$^{-/-}$ cells was reduced significantly at every dose of olaparib, making it the most olaparib-sensitive cell line. Thus, within the ID8 model, mutations in the *Brca* genes are associated with reduced cell viability in response to olaparib treatment.

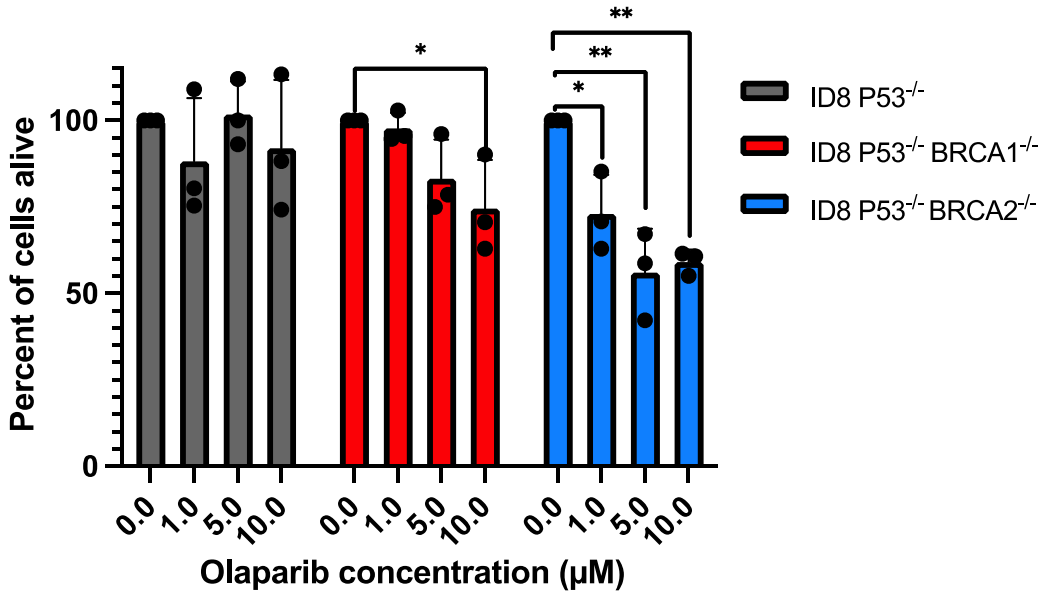

Figure 4. Olaparib sensitivity of ID8 cell lines after a 24-hour *in vitro* treatment. ID8 cell lines were treated with 0, 1.0, 5.0 and 10 µM olaparib for 24 hours, after which AlamarBlue assays were used to measure viability. Viability at each dose was compared to the 0 µM (negative control) group. Analysis was done using a one-way ANOVA followed by a Tukey's multiple comparison (n=3). Each dot represents the average data of 3 technical replicates from a unique experiment, and error bars indicate SD. *$p<0.05$, **$p<0.01$.

3.1.2 *In Vitro* Olaparib Treatment Results in Enhanced PD-L1 Expression in Ovarian Cancer Cells

Expression of immune checkpoint molecules plays an important role in creating an immunosuppressive TME which is often a phenotype present in ovarian tumours. In breast cancer models, treatment of cancer cells with olaparib results in upregulation of PD-L1 expression[91]. Expression of checkpoint molecules is also associated with PARPi resistance both *in vitro* and *in vivo.* To assess whether treatment with olaparib enhances the expression of PD-L1 in ID8 cells as well, we treated the cells with 10 µM olaparib for 24 hours and assessed PD-L1 expression by flow cytometry (**Figure 5**). Treatment with olaparib enhanced the expression of PD-L1 in all three cell lines (**Figure 5A)**. However, the largest increase occurred in the *Brca1*$^{-/-}$ group (**Figure 5B)**. Thus, the results of this experiment are analogous with the data found in the literature and identify PD-L1 as a target for combination therapy *in vivo.*

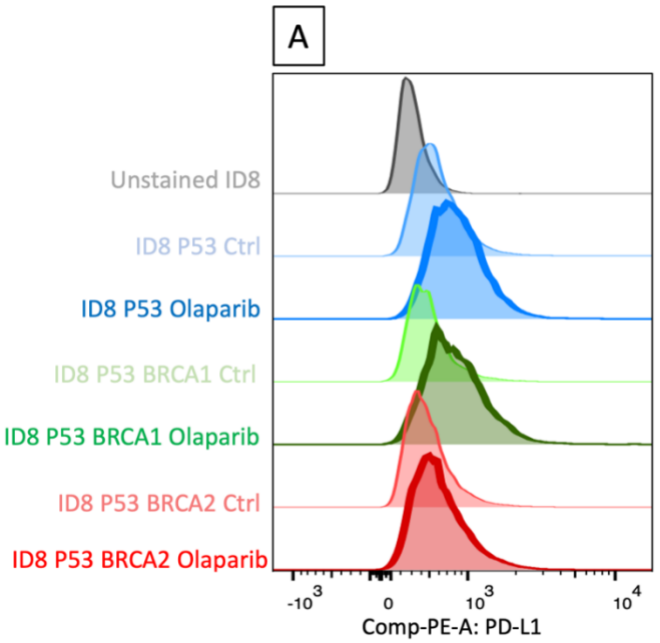

B

Sample	Geometric Mean: Comp-PE-A
Unstained ID8	329
ID8 *Trp53*$^{-/-}$ Control	681
ID8 *Trp53*$^{-/-}$ Olaparib	882
ID8 *Trp53*$^{-/-}$ *Brca1*$^{-/-}$ Control	539
ID8 *Trp53*$^{-/-}$ *Brca1*$^{-/-}$ Olaparib	863
ID8 *Trp53*$^{-/-}$ *Brca2*$^{-/-}$ Control	517
ID8 *Trp53*$^{-/-}$ *Brca2*$^{-/-}$ Olaparib	648

Figure 5. *In vitro* treatment of ID8 cells with olaparib enhances PD-L1 expression. ID8 cell lines were incubated with 10 µM olaparib for 24 hours and stained for PD-L1, for which the geometric mean fluorescence intensity was determined using flow cytometry. (A) indicates the visual representations of the peaks and (B) demonstrates the quantified values. Enhancement of PD-L1 expression occurred in all three cell lines, regardless of genotype.

3.2 Assessing the Influence of Olaparib Monotherapy on the Survival of Tumour-Bearing Mice and Their TME Composition in the First Animal Study

3.2.1 Assessing the Effects of Olaparib Therapy on the Survival of Tumour-Bearing Mice

In vivo treatment of the ID8 model with olaparib was performed to determine whether intraperitoneal delivery of the drug can prolong the survival of tumour-bearing mice. In this study, treatment with olaparib did not significantly prolong the survival of the *Trp53*$^{-/-}$ model, and the median length of survival of the control (48 days) and olaparib (52 days) were similar (**Figure 6A**). However, *in vivo* treatment of the *Trp53*$^{-/-}$*Brca1*$^{-/-}$ tumour model significantly improved survival, with the median survival of the olaparib-treated mice being 32% longer than the isotype control (**Figure 6B**). Lastly, olaparib therapy tended to improve the median survival of the *Trp53*$^{-/-}$*Brca2*$^{-/-}$ model, however this difference did not reach significance (**Figure 6C**). It should be noted that one mouse in the control group of this model unexpectedly survived to 100 days, which is double the predicted median survival. The absence of any improvements in the *Trp53*$^{-/-}$ model resulted in the exclusion of this group from the next *in vivo* study.

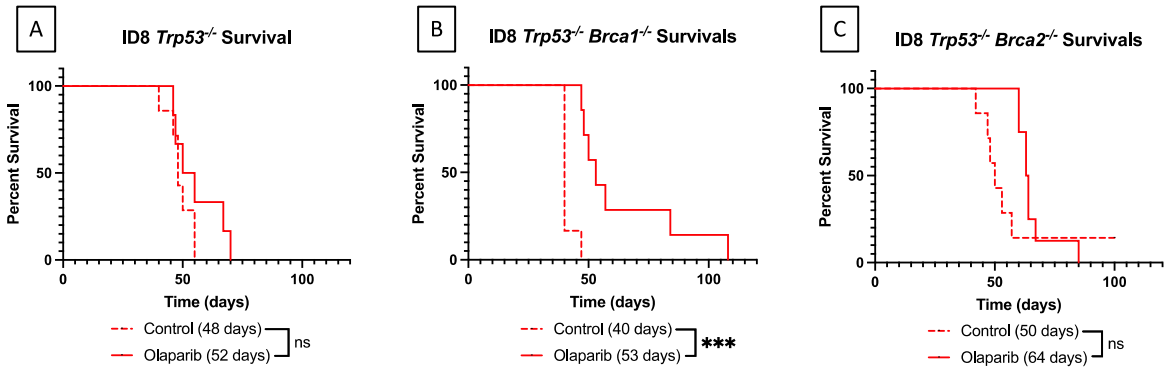

Figure 6. Kaplan-Meier plots showing survival of ID8 tumour-bearing mice. 5x10^6 cancer cells were injected IP on day zero (n=8 per group). The olaparib therapy began at 25% into the average survival timeline for that model (12-16 days post cell injection). The therapy regimen included 18 consecutive, daily IP injections at a dose of 50mg/kg/day or vehicle control. All mice were euthanized at humane endpoint. Analysis was carried out using the Log-rank (Mantel-Cox) test. ns: not significant, ***p<0.001.

3.2.2 Analysis of the Composition of the ID8 TME at Humane Endpoint

For all tumour models, tissues were collected at the humane endpoint. It is generally expected that tumour progression which takes place for weeks after the end of therapy may dilute any differences between control and treated groups at humane endpoint. Nevertheless, the tumours of the *Brca1*-mutated group were analyzed to detect any potential differences and to provide directions for analysis in the next study (**Figure 7**). Immunofluorescence staining of OCT embedded tissues did not result in any differences in the percentage of CD45-positive (**Figure 7A-B)** or MHC II-positive cells in the *Brca1*-null TME (**Figure 7A-C**). RT-qPCR from the tumour RNA collected at endpoint was analyzed for the expression of CD8 and PD-L1. The expression of CD8 was highly variable between the biological replicates and the difference from control tumours was not statistically significant (**Figure 7D)**. Similarly, expression of PD-L1 was similar between the treated and untreated tumours at humane endpoint (**Figure 7E)**. As the composition of the TMEs were not different at the humane endpoint, the tissues used to analyze the ovarian TME were collected immediately after the end of treatment in the next *in vivo* study.

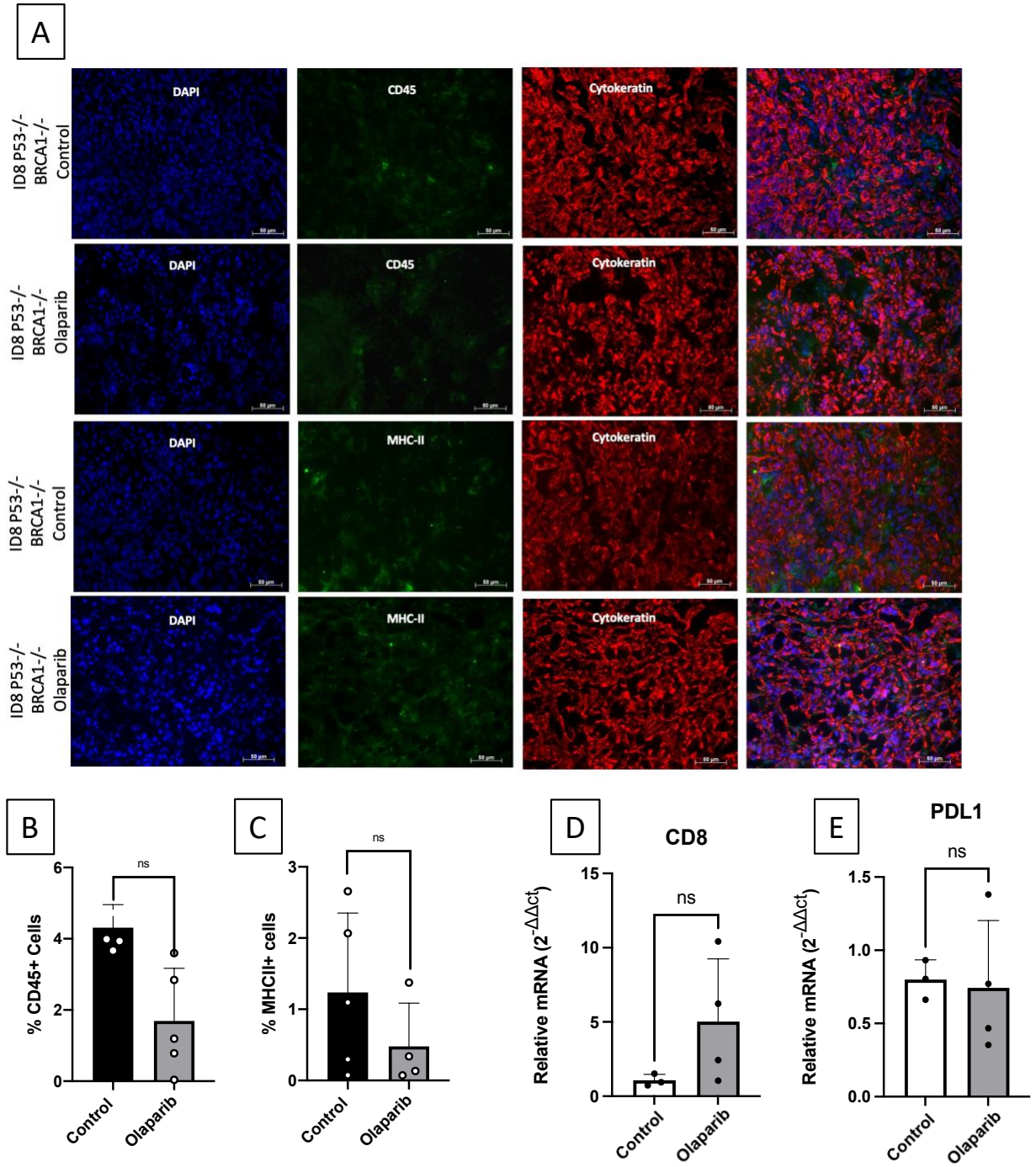

Figure 7. Tumour microenvironment expression of CD45, MHC II, CD8 and PD-L1 at endpoint in the ID8 *Trp53*$^{-/-}$ *Brca1*$^{-/-}$ model. Tumours collected at humane end point of the ID8 *P53*$^{-/-}$ *Brca1*$^{-/-}$ model were analyzed using immunofluorescent staining (n=4-5 per group) and RT-qPCR (n=3 per group). Immunofluorescent analysis of the tumours did not result in any significant differences in the expression of MHC II and CD45 between the control and olaparib-treated groups (A-C). RT-PCR analysis of CD8 and PD-L1 expression did not indicate any significant differences between the two groups. Histograms indicate the mean +/- SD. ns: not significant.

3.3 Assessing the Influence of Monotherapies and Their Combination on the Composition of the ID8 TME and Animal Survival in the Second Animal Study

3.3.1 The Effects of Olaparib, PD-L1 Monoclonal Antibody and Their Combination on Survival

Olaparib and PD-L1 antibodies, alone and in combination, differently influenced the survival of *Brca*-mutated ID8 models **(Figure 8**). In the *Trp53*$^{-/-}$ *Brca1*$^{-/-}$ model, the anti-PD-L1 monotherapy nearly doubled the median survival of tumour-bearing mice (75 days) compared to the isotype control (38 days), making it the most beneficial overall treatment in terms of survival (**Figure 8A**). The survival of mice given olaparib monotherapy (50 days) and combination therapy (52 days) groups were very similar and were both significantly longer than the isotype control (**Figure 8A**).

In the *Trp53*$^{-/-}$ *Brca2*$^{-/-}$ model, the anti-PD-L1 monotherapy did not improve the survival and the median survival was very similar to the isotype control (**Figure 8B**). Unlike the first *in vivo* study however, the olaparib monotherapy did significantly improve the survival of the mice harbouring *Brca2*-null tumours (**Figure 8B**). Similar to the *Brca1*-null group, the outcomes from the combination therapy heavily resembled the survival of the olaparib monotherapy group (**Figure 8B**). Overall, the olaparib and combination therapy similarly improved the survival of both models. However, the anti-PD-L1 monotherapy was only successful in lengthening the survival of the *Trp53*$^{-/-}$ *Brca1*$^{-/-}$ mice.

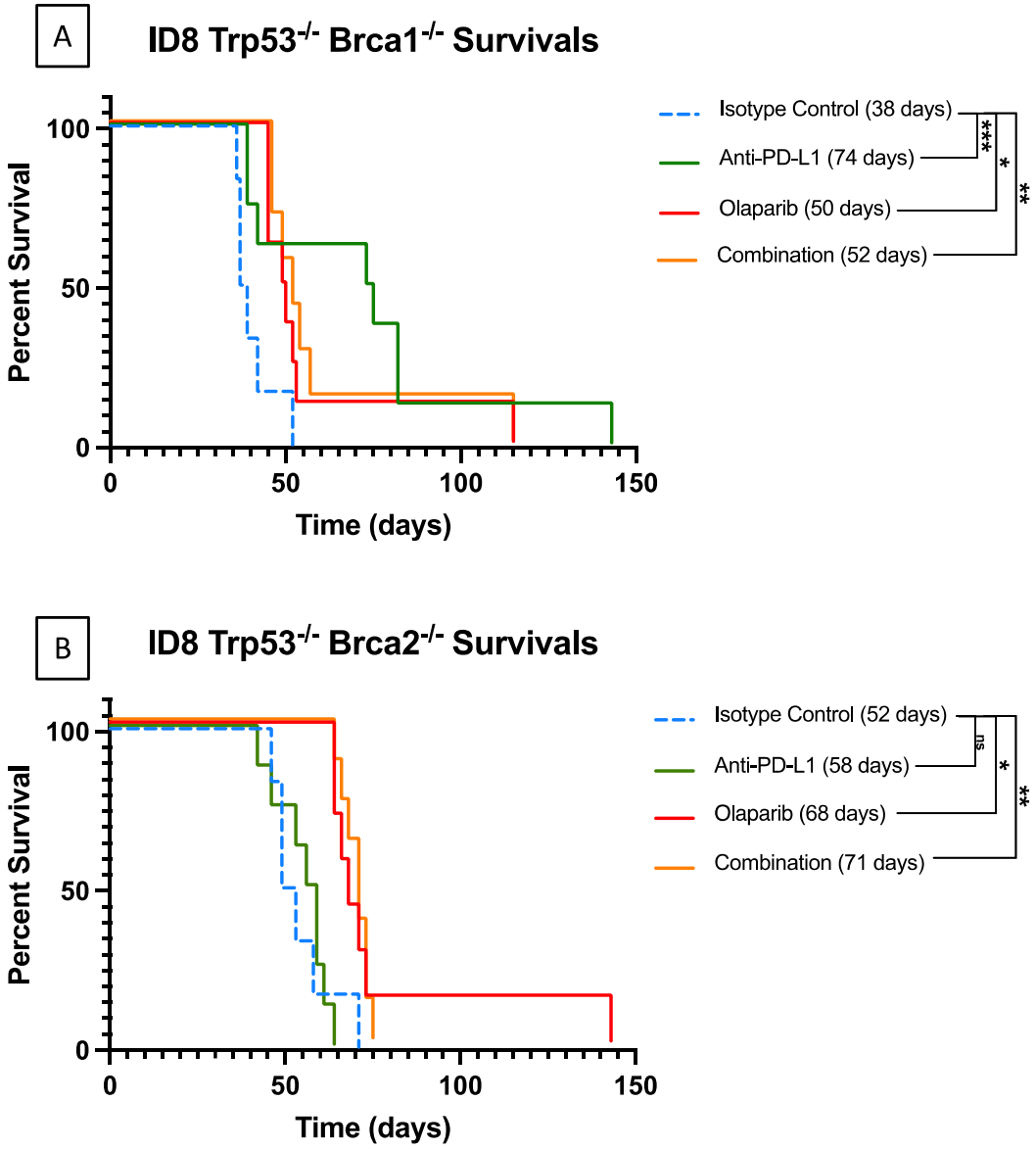

Figure 8. Survival Kaplan-Meier plots of ID8 tumour-bearing mice. 5x10^6 cancer cells were injected IP on day zero (n=8 per group). All therapies began at 25% into the average survival timeline of that model (12-16 days post cell injection). The olaparib monotherapy regimen included 18 daily IP injections at a dose of 50mg/kg/day; the anti-PDL1 monotherapy regimen included five daily IP injections of 200 µg anti-PD-L1 monoclonal antibody followed by one 100 µg injections every four days for a total of 11 doses. The combination group received both drugs as outlined for the monotherapies. All mice were euthanized at humane endpoint. (A) presents the survival of ID8 *Trp53*$^{-/-}$ *Brca1*$^{-/-}$ tumour-bearing mice, while (B) outlines the survival mice with ID8 *Trp53*$^{-/-}$ *Brca2*$^{-/-}$ tumours. Analysis was carried out using the Log-rank (Mantel-Cox) test. ns: not significant, *p<0.05, **p<0.01, ***p<0.001.

3.3.2 Effects of Therapy on the Immune Composition of the ID8 TME and Spleen Tissue

The effects of PARPi treatment on the composition of the ovarian TME have not been studied extensively. As such, we set out to characterize the immune composition of PARPi-treated tumours immediately after the end of therapy. However, as we had also detected enhanced expression of PD-L1 in response to *in vitro* olaparib therapy, we also added anti-PD-L1 as a monotherapy and in combination with olaparib. This addition provided us with a more sophisticated and complete image of the TME composition in response to novel therapeutics. Using flow-cytometric analysis, we analyzed the TME and spleen composition (**Figure 9**) from mice 36 hours after the end of the olaparib treatment, at which time the mice had also received 8 doses of anti-PD-L1. The analysis was done using two panels; the first panel focused on the adaptive immune system while the second panel analyzed the composition of the innate immune cells.

The analysis of the TME and spleen immune compositions yielded over 300 unique correlations for each tissue. To narrow down the analysis, the changes that were significantly different from the isotype control or the combination therapy were identified and are presented as histograms. Any significant changes in <1% of cells have been excluded here as well. In our analysis, we measured TME changes both in terms of the percentage of cells in that population and also changes in expression levels which were demonstrated by the gMFI values.

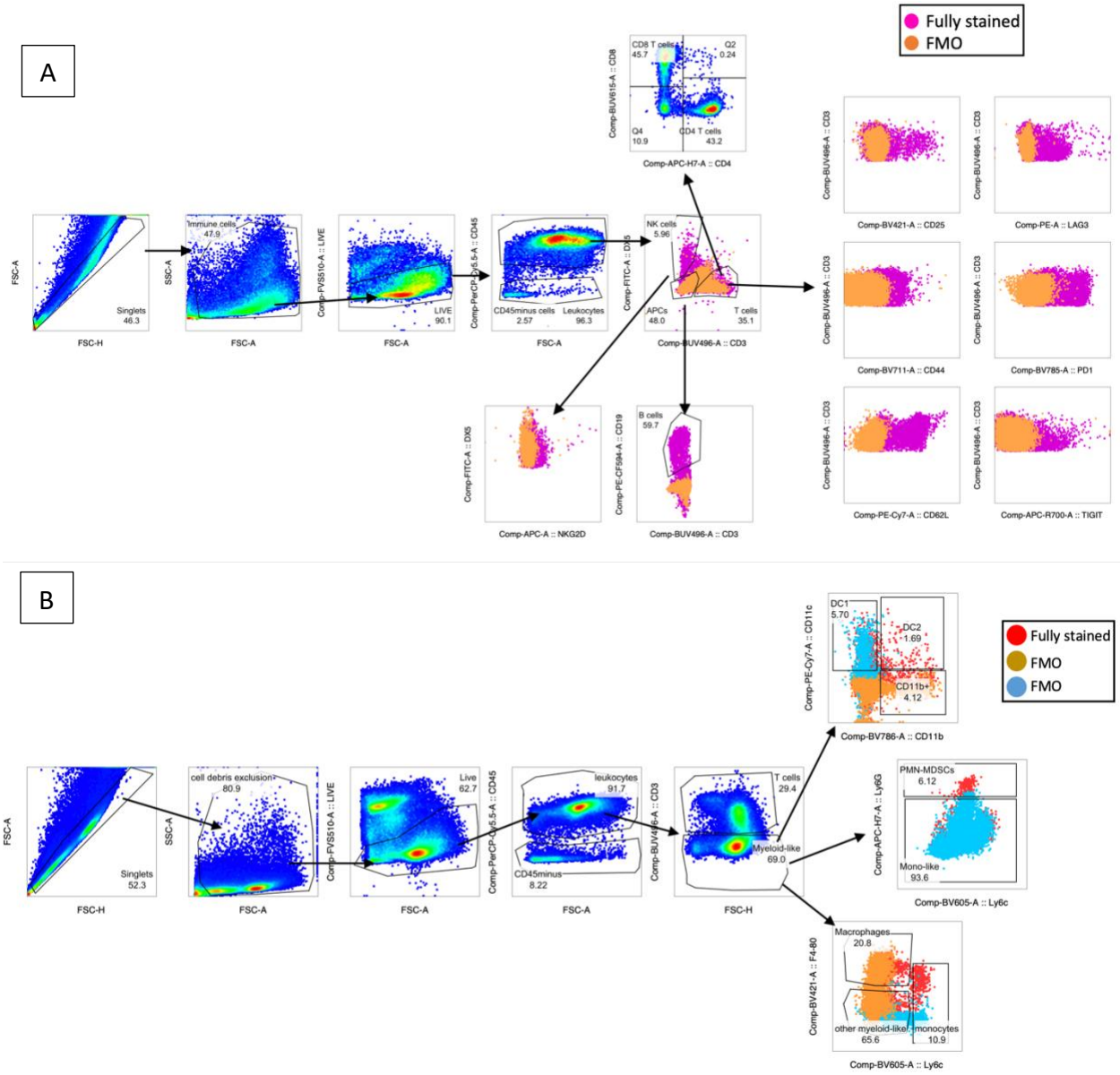

Figure 9. Gating strategy for the analysis of flow cytometry data. Peritoneal washes and spleens were collected and analyzed by flow cytometry approximately 36 hours after the end of therapy. (A) The gating strategy used to analyze the first flow cytometry panel is as follows: singlet, cell debris exclusion, live cell exclusion, leukocytes (CD45+), CD3+ (T cells), CD3- (B cells), DX5+ (natural killer cells). The T cell panel was further assessed using markers such as CD4, CD8, PD-1, LAG3, CD44, CD25, CD62L and TIGIT. (B) The gating strategy for the second panel included selection of singlets, cell debris exclusion, live cell exclusion, leukocytes (CD45+), CD3+ (T cells) and CD3- (Myeloid-like cells). The myeloid-like panel was further assessed by using markers for dendritic cells (DCs), myeloid-derived suppressor cells (MSDCs), monocytes, macrophages, and other myeloid-like cells. Fluorescence minus one (FMOs) represent the counter plots shown in each figure.

3.3.3 Changes in the Composition of the *Trp53*$^{-/-}$ *Brca1*$^{-/-}$ TME in Response to Therapy

As the influence of treatment on the composition of the ovarian TME remains largely unknown, we set out to determine how the treatments used in this study can influence various innate and adaptive immune cell populations in the ID8 TME. We further specified this analysis by examining the tissues from *Brca*-mutated tumour individually. All three treatments uniquely transformed the *Trp53*$^{-/-}$ *Brca1*$^{-/-}$ TME (**Figure 10**). The administration of monotherapies and their combination was associated with higher percentages of multiple different cell types as seen in the positive z-scores in the heatmap rows which represent treatment groups (**Figure 10**). The cell number changes which are significantly different from isotype control and/or the combination therapy are outlined in **Figure 11**. In term of T cell populations, the combination therapy resulted in an 8% increase in overall T cell numbers compared to the isotype control (**Figure 11A**). The olaparib monotherapy increased the total number of CD8 T cells and activated, CD44 expressing CD4 T cells by approximately 5% (**Figure 11B-C**). Notably however, the combination therapy resulted in a reduced number of activated CD4 T cells to near zero levels compared to the monotherapies (**Figure 11B**). Similarly, the combination therapy resulted in a consistent 14% reduction of activated, CD44+ CD8 T cells compared to all other groups, which once again reduced the percentage of these cells to near zero levels (**Figure 11D**). The olaparib monotherapy also reduced the CD4/CD8 T cell ratio compared to all groups by approximately 50% (**Figure 11E**).

The therapies also uniquely influenced the composition of NK cell populations. The olaparib monotherapy resulted in a 5% reduction in overall NK cell numbers (**Figure 11F**) while the combination therapy enhanced CD25+ NK populations by 5% (**Figure 11G**). The anti-PD-L1 and olaparib monotherapies both increased the number of CD44+ NK cells (3-4%) while the combination therapy reduced this population to nearly zero (**Figure 11H**). Lastly, the

monotherapies distinctively influenced NK cell exhaustion, with olaparib and anti-PD-L1 doubling the population of PD-1 and LAG3 positive cells, respectively (**Figure 11I-J**).

PD-L1 expressing cell populations were all highly influenced, and their numbers were increased by all therapies, but particularly when the anti-PDL1 was administered. All three therapies increased the number of PD-L1 expressing CD3 T cells by 30 to 40% (**Figure 11K**). The increases in the percentage of PD-L1 expressing cell types were similar in the anti-PD-L1 monotherapy and combination groups, and they increased the percent of PD-L1+ cells by approximately 30% in macrophages (**Figure 11L**), dendritic cell 1s (DC1) (**Figure 11N**), DC2s (**Figure 11O**) and myeloid-like cells (**Figure 11P**). However, the combination therapy was the only treatment that uniquely increased the proportion of PD-L1+ monocytes by about 30%, doubling the population of this cell type (**Figure 11M**). Lastly, the proportion of macrophages expressing class II major histocompatibility complex molecule (MHC II) was influenced by all treatments. The anti-PD-L1 treatment resulted in relatively small (<10%) reduction in MHC II+ macrophages (**Figure 11R**). The olaparib monotherapy reduced this population more drastically (27.5%), to nearly half the number of cells in the isotype control (**Figure 11R**). However, there appeared to a synergetic reduction in this cell population as the combination of the two therapies resulted in a 42% reduction in the population of antigen-presenting macrophages (**Figure 11R**).

Aside from the changes in cell numbers, the expression levels of various markers measured by gMFI changed as well (**Figure 12**). The combination therapy enhanced the expression of CD25 on both CD4 and CD8 T cell subtypes (**Figure 12A-B**). Conversely, however, the combination therapy also drastically reduced the expression of CD44 in those cell types, similar to the change observed in cell percentages (**Figure 12C-D**). In T cells, the combination therapy also enhanced PD-L1 expression (**Figure 12G**), while olaparib monotherapy enhanced the expression of

exhaustion markers such as PD-1 and LAG3 in cytotoxic T cells when compared to the anti-PD-L1 treated groups (**Figure 12E-F**).

Expression of exhaustion markers was highly influenced by olaparib and combination therapy in NK cells as well. The olaparib monotherapy slightly enhanced the expression of PD-1 while the combination therapy significantly reduced the expression of this marker (**Figure 12H**). However, the combination therapy doubled the expression of TIGIT on NK cells, and both the anti-PD-L1 and combination therapy enhanced LAG3 expression on these cells (**Figure 12I-J**). All therapies enhanced the expression of CD25 on NK cells while the combination therapy drastically reduced CD44, an effect also observed in the percentage of CD44+ NK cells (**Figure 12K-L**). Analysis of the second panel revealed that the combination therapy drastically reduced MHC II expression on macrophages, a reduction which was also observed on MHCII+ macrophage numbers (**Figure 12M**). Lastly, anti-PD-L1 treatment both as a monotherapy and in combination with olaparib, yielded a generalized enhancement in PD-L1 expression (**Figure 12N-R**). In summary, all treatments uniquely transformed the ID8 *Trp53*$^{-/-}$ *Brca1*$^{-/-}$ TME, both in terms of cell numbers and marker expression levels. Evaluation by flow cytometry revealed that compared to all tissues analyzed in this study, the ID8 *Trp53*$^{-/-}$ *Brca1*$^{-/-}$ TME was the most transformed entity in response to all therapies.

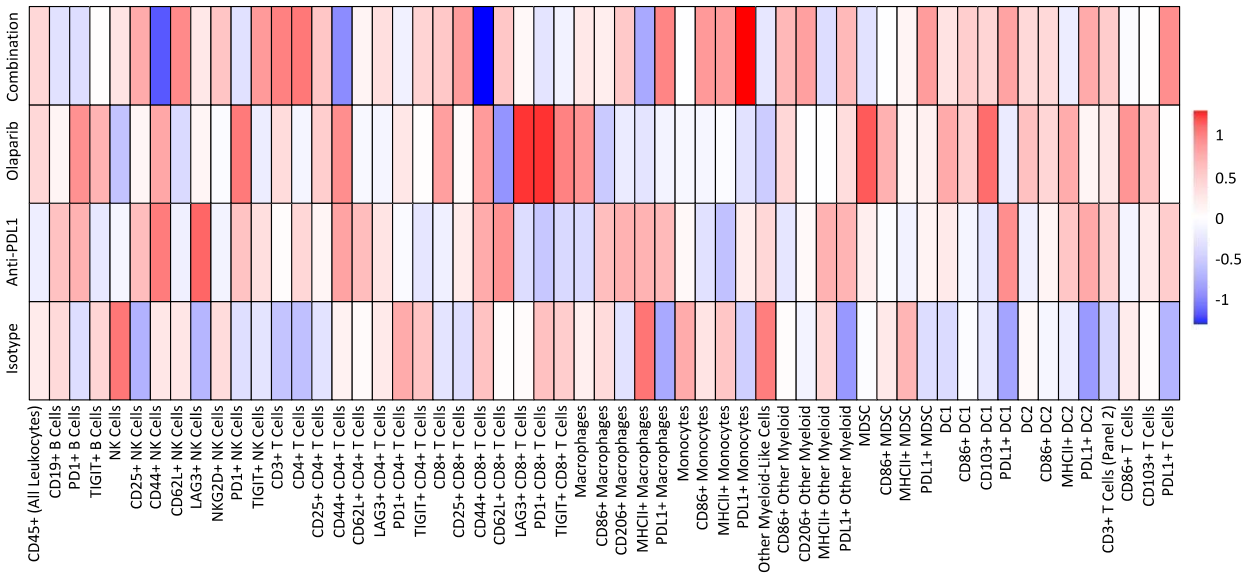

Figure 10. Heatmap presenting the abundance of various immune cell types within the ID8 *Trp53*$^{-/-}$ *BRCA1*$^{-/-}$ tumour microenvironment. Peritoneal washes (n=5 mice per group) were collected from tumour-bearing mice injected with $5x10^6$ cells which were treated with olaparib, anti-PD-L1 or their combination, and analyzed by flow cytometry approximately 36 hours after the end of treatment. For each cell type, the value was calculated as the percent in all leukocytes. The percentages were normalized, and each box represents the mean of the 5 biological replicates.

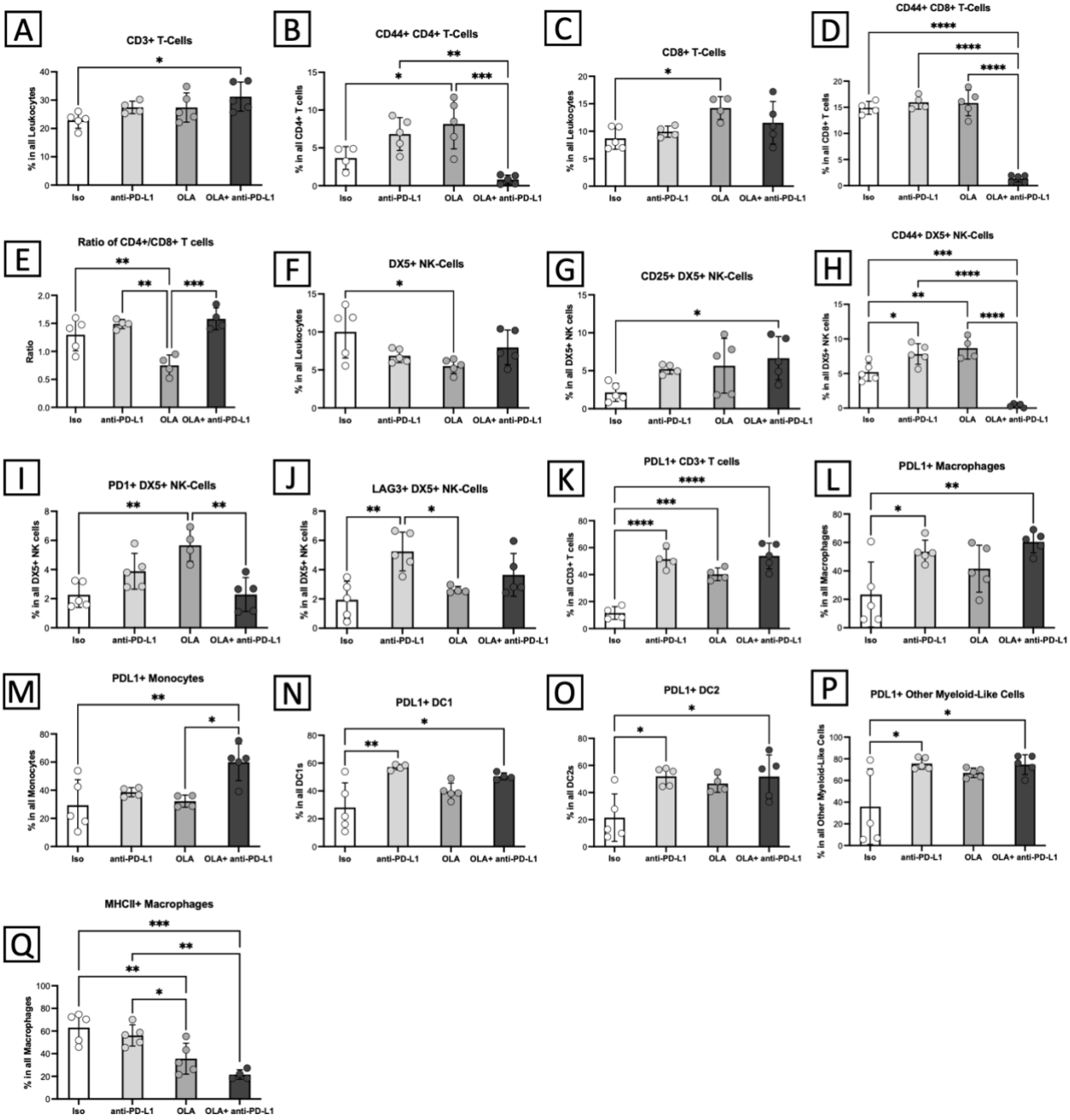

Figure 11. Abundance of innate and adaptive immune cells within the ID8 *Trp53*$^{-/-}$ *BRCA1*$^{-/-}$ tumour microenvironment. Peritoneal washes (n=5 mice per group) were collected from tumour-bearing mice injected with $5x10^6$ cells which were treated with olaparib, anti-PD-L1 or their combination, and analyzed by flow cytometry approximately 36 hours after the end of treatment. Only the immune populations which are significantly different from isotype control or the combination therapy are shown. Each dot represents one biological replicate. Mean values with SD are shown. ISO indicates the isotype control group and OLA indicates the olaparib treated group. Analysis was done using a one-way ANOVA followed by a Tukey's multiple comparison test. *p<0.05, **p<0.01, ***p<0.001, ****p<0.0001.

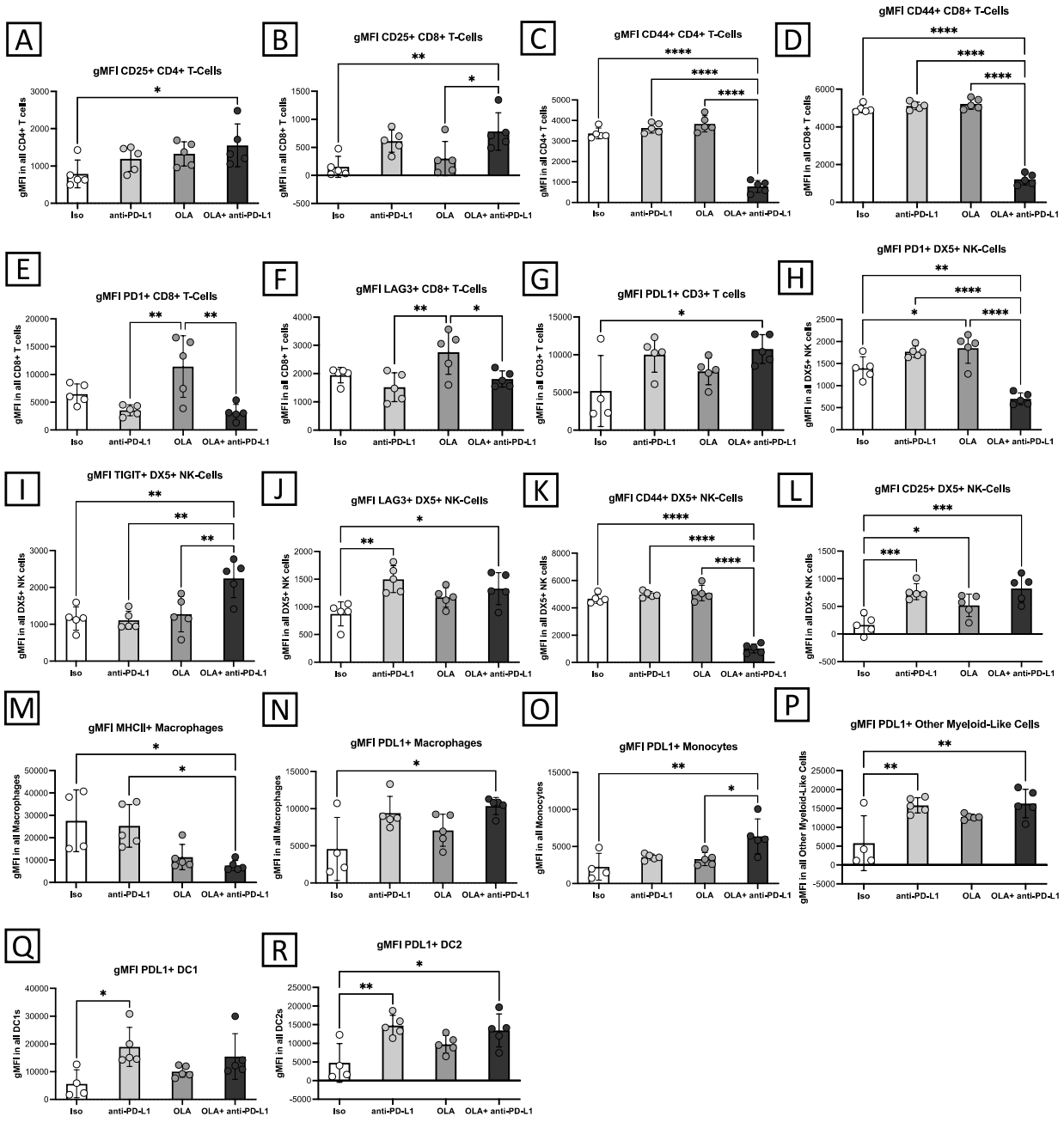

Figure 12. Mean fluorescence intensity of various markers expressed by immune cells within the ID8 *Trp53*$^{-/-}$ *BRCA1*$^{-/-}$ tumour microenvironment. Peritoneal washes (n=5 mice per group) were collected from tumour-bearing mice injected with $5x10^6$ cells which were treated with olaparib, anti-PD-L1 or their combination, and analyzed by flow cytometry approximately 36 hours after the end of treatment. Only the immune populations which are significantly different from isotype control or the combination therapy are shown. Each dot represents one biological replicate. Mean values with SD are shown. ISO indicates the isotype control group and OLA indicates the olaparib treated group. Analysis was done using a one-way ANOVA followed by a Tukey's multiple comparison test. *p<0.05, **p<0.01, ***p<0.001, ****p<0.0001.

3.3.4 Changes in the Composition of the *Trp53*$^{-/-}$ *Brca2*$^{-/-}$ TME in Response to Therapy

Following the analysis of the *Brca1*-null TME, we proceeded to investigate how the treatments would influence the same cell populations within the *Brca2*-null tumours. As seen in the heatmap in **Figure 13**, the administration of monotherapies and combination therapies differentially influenced *Brca2*-null TME composition (**Figure 13**). However, compared to the *Brca1*-null group, there appears to be more negative z-scores present in this tissue, especially in response to olaparib monotherapy (**Figure 13**). While the vast majority of immune cell populations appear to be lowest in the TME of the olaparib group, some cell types are also present at higher proportions, namely those expressing LAG3, PD-1 and TIGIT, all of which are markers of exhaustion and/or inhibition **(Figure 13**). Although these changes which took place within the olaparib treated TME were not statically different from the isotype control, it is noteworthy that this TME appears to be distinctively immunosuppressive.

Statistical analysis of the various cell types revealed a small number of significant differences between the isotype control and treatment groups (**Figure 14-15**). Interestingly, there were no statistically significant changes in the percentage of CD4+ and CD8+ T cells, which are critical components of the TME. The percent of LAG3+ NK cells was reduced by about 3% in the combination group, thereby reducing this population by half compared to the isotype control (**Figure 14A**). Administration of anti-PDL1 as a monotherapy or in combination with olaparib enhanced the population of PD-1+ B cells by approximately 3%, which nearly doubled this population compared to the isotype controls (**Figure 14B**). Furthermore, the anti-PD-L1 monotherapy reduced the CD4+ T cell population by about 5% (**Figure 14C**). The olaparib monotherapy augmented the population of CD86+ macrophages by 10%, which doubled this population compared to the control (**Figure 14D**). Analogous to the *Brca1*-null TME, treatment

with anti-PD-L1 both as a monotherapy and in combination with PARPi resulted in greater percentages of PD-L1+ cells in multiple cell types. The populations of cells expressing this marker was elevated in CD3+ T cells (~20%), macrophages (~30%), DC1s (~13%), and other myeloid cells (11%) (**Figures 14E-I**). However, PD-L1 enhancement in monocytes were only seen when anti-PD-L1 was provided as a monotherapy and not in combination with olaparib (**Figure 14F**). This could potentially be caused by the greater amount of variability associated with PD-L1+ cells in the anti-PD-L1 monotherapy compared to the combination group, where there is much less variability between the biological replicates.

Analysis of expression levels of various markers revealed a small number of trends that were similar to the changes in cell numbers (**Figure 15**). For instance, similar to the effects of the anti-PD-L1 therapy on the number of PD-1+ B cells, the expression of PD-1 was also increased in B cells with the administration of the antibody as a monotherapy or in combination with olaparib (**Figure 15A**). A similar trend was observed in NK cells, with the combination group having the highest PD-1 expression (**Figure 15B**). Lastly, the CD3+ T cells were the only cell type in which PD-L1 expression was enhanced by anti-PD-L1 treatment (**Figure 15C**). Overall, the immune cell composition of the *Brca2*-null TME revealed notable modifications albeit not as extensive as those seen in the *Brca1*-null model, suggesting that the response to therapy varies between these models.

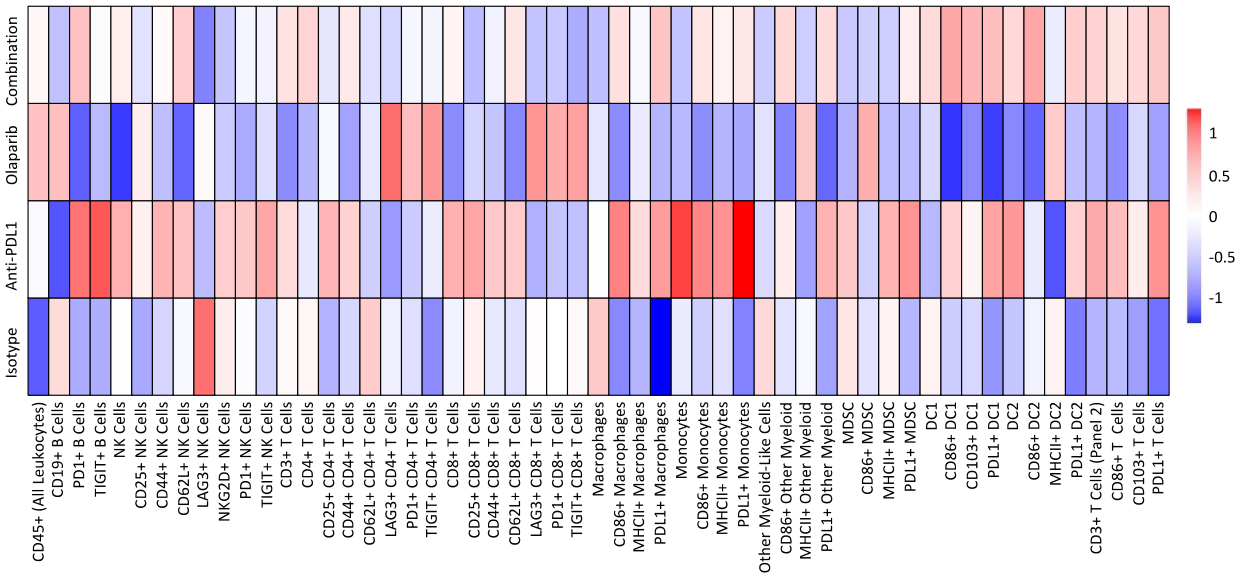

Figure 13. Heatmap presenting the abundance of various immune cell types within the ID8 *Trp53*$^{-/-}$ *BRCA2*$^{-/-}$ tumour microenvironment. Peritoneal washes (n=5 mice per group) were collected from tumour-bearing mice injected with $5x10^6$ cells which were treated with olaparib, anti-PD-L1 or their combination, and analyzed by flow cytometry approximately 36 hours after the end of treatment. For each cell type, the value was calculated as the percent in all leukocytes. The percentages were normalized, and each box represents the mean of the 5 biological replicates.

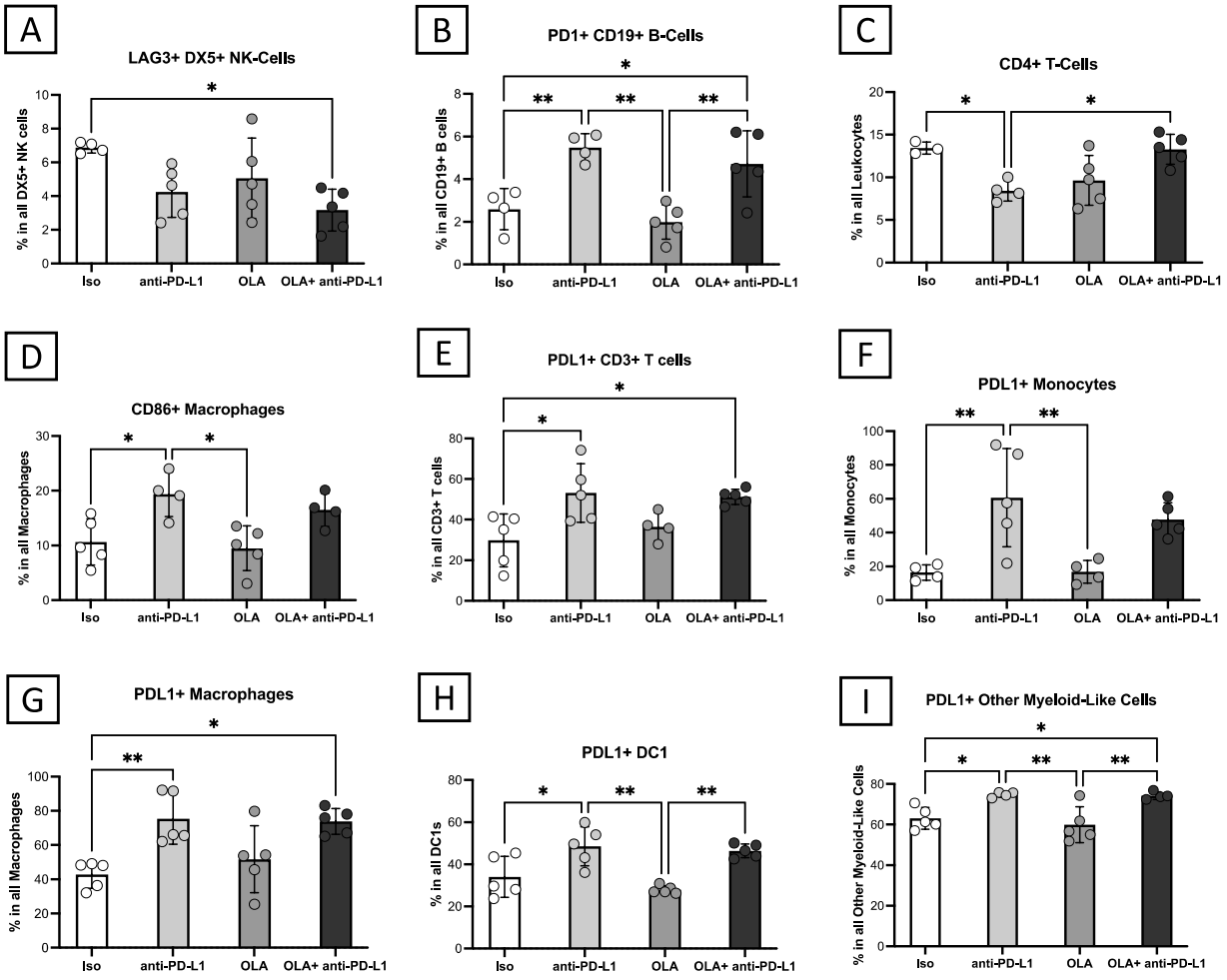

Figure 14. Abundance of innate and adaptive immune cells within the ID8 *Trp53*$^{-/-}$ *BRCA2*$^{-/-}$ tumour microenvironment. Peritoneal washes (n=5 mice per group) were collected from tumour-bearing mice injected with $5x10^6$ cells which were treated with olaparib, anti-PD-L1 or their combination, and analyzed by flow cytometry approximately 36 hours after the end of treatment. Only the immune populations which are significantly different from isotype control or the combination therapy are shown. Each dot represents one biological replicate. Mean values with SD are shown. ISO indicates the isotype control group and OLA indicates the olaparib treated group. Analysis was done using a one-way ANOVA followed by a Tukey's multiple comparison test. *$p<0.05$, **$p<0.01$.

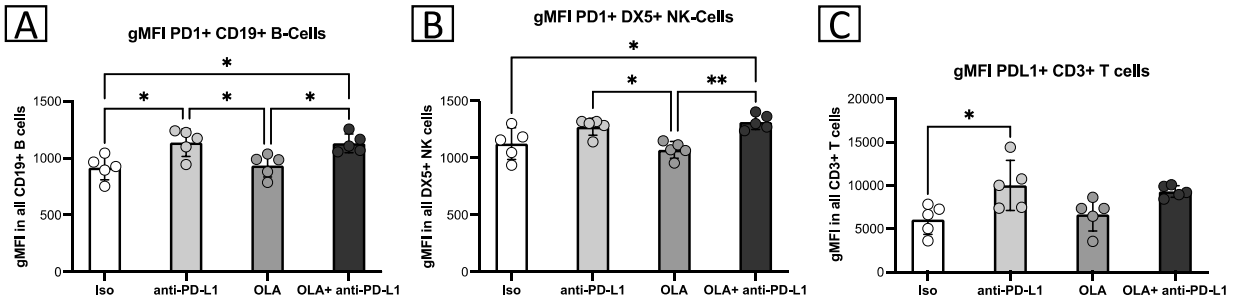

Figure 15. Mean fluorescence intensity of various markers expressed by immune cells within the ID8 *Trp53*$^{-/-}$ *BRCA2*$^{-/-}$ tumour microenvironment. Peritoneal washes (n=5 mice per group) were collected from tumour-bearing mice injected with $5x10^6$ cells which were treated with olaparib, anti-PD-L1 or their combination, and analyzed by flow cytometry approximately 36 hours after the end of treatment. Only the immune populations which are significantly different from isotype control or the combination therapy are shown. Each dot represents one biological replicate. Mean values with SD are shown. ISO indicates the isotype control group and OLA indicates the olaparib treated group. Analysis was done using a one-way ANOVA followed by a Tukey's multiple comparison test. *p<0.05, **p<0.01.

3.3.5 Systemic Effects of Therapy on the Immune System of ID8 *Trp53*$^{-/-}$ *Brca1*$^{-/-}$ Tumour-Bearing Mice

Spleen tissues collected from the mice were analyzed to get an understanding of the systemic effects of therapy on the animal's immune system. As shown in the heatmap in **Figure 16**, the therapies both increased and decreased the proportions of various cell populations in the spleen of the *Trp53*$^{-/-}$ *Brca1*$^{-/-}$ group. Notably, the spleen tissue from the isotype control group exhibits comparatively lower levels of innate immune cell types in contrast to the spleen of animals in the treatment groups (**Figure 16**).

All of the statistically significant changes in the spleens of the *Brca1*-null mice were observed in the second panel of flow cytometry, which mostly looked at the innate arm of the immune system (**Figure 17-18**). The olaparib monotherapy enhanced the population of MHC II+ monocytes (6%) and macrophages (20%), and in both cases nearly doubled these cell populations compared to the control group (**Figure 17A-B**). The proportion of CD86+ monocytes was reduced by both monotherapies, but the change was only significant in the combination group which

resulted in the biggest (~6%) reduction in CD86 expression (**Figure 17C**). In macrophages however, both monotherapies significantly reduced the percentage of CD86+ cells (7-8%) (**Figure 17D**).

Changes in PD-L1+ populations resembled that of the *Brca1*-null TME, with the anti-PD-L1 increasing the proportions of PD-L1 expressing cell types both as a monotherapy and in combination with olaparib (**Figure 17E-K**). In the spleen tissue, the changes in PD-L1+ populations were nearly identical for both the monotherapy and combination in all cell types. However, unlike the *Brca1*-null TME the percent change was not similar across the various cell types. In the CD3+ T cells, the percentage of PD-L1+ T cells was increased by about 15% (**Figure 17E**). In monocytes and macrophages, the percentages of PD-L1+ cells were increased by 3% and ~50%, respectively (**Figure 17F-G**). In both subtypes of DCs, the increase in the PD-L1+ cells were similar and in the 20-30% range (**Figure 17H-I**). The increase in the other myeloid-like cells was also about 20% in both the combination and monotherapy groups (**Figure 17J**). Lastly, the percentage of PD-L1+ cells was also increased in MDSCs (~4%), a change which was not present in the TME of either model (**Figure 17K**).

Changes in fluorescence intensity were similar and less abundant than the changes in cell percentages but followed similar trends (**Figure 18**). For instance, the olaparib monotherapy reduced the expression of CD86 in macrophages (**Figure 18A**). Moreover, the expression of MHC II was increased in DC2s in response to olaparib monotherapy (**Figure 18B**). Similar to the increase in the population of cells which were PD-L1+, the expression levels of this marker were also enhanced in macrophages, DC1s, DC2s and CD3+ T cells in response to both anti-PD-L1 and combination therapies (**Figure 18D-I**). In summary, the modifications observed in the splenic tissue of the animals in the *Trp53*$^{-/-}$ *Brca1*$^{-/-}$ model were predominantly limited to innate immune

cell populations. Additionally, the systemic rise in PD-L1 observed in the TME was also detected in this tissue, indicating that the effects of therapeutics are not confined to the TME but can extend to systemic immune responses.

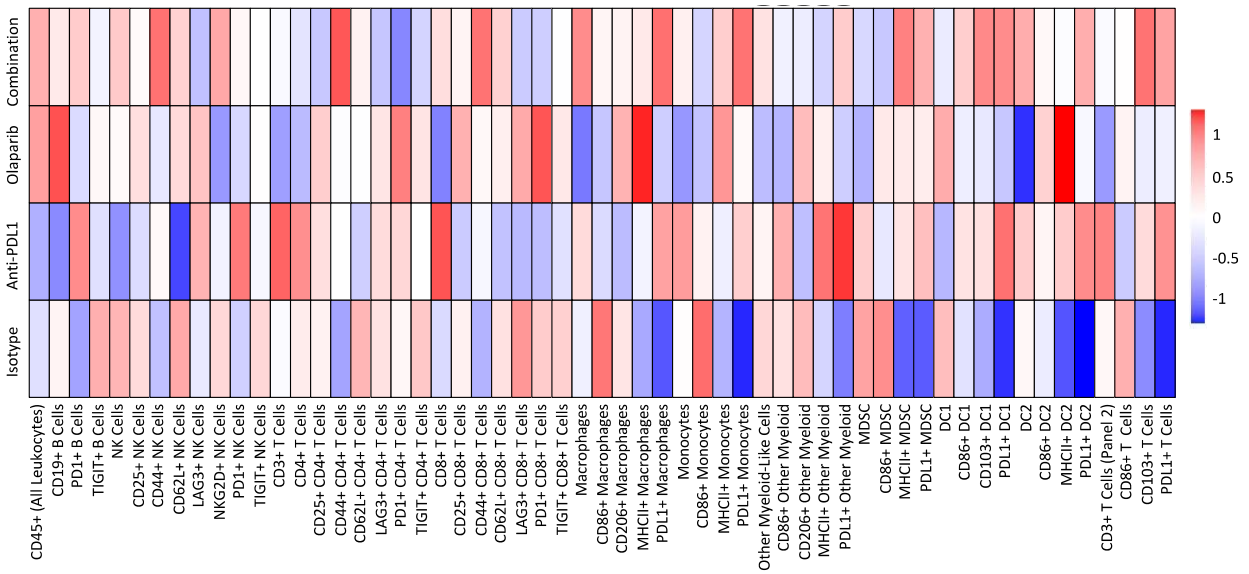

Figure 16. Heatmap presenting the abundance of various immune cell types present in the spleens of ID8 *Trp53*$^{-/-}$ *BRCA1*$^{-/-}$ mice. Spleens (n=5 mice per group) were collected from tumour-bearing mice which were treated with olaparib, anti-PD-L1 or their combination, and analyzed by flow cytometry approximately 36 hours after the end of treatment. For each cell type, the value was calculated as the percent in all leukocytes. The percentages were normalized, and each box represents the mean of the 5 biological replicates

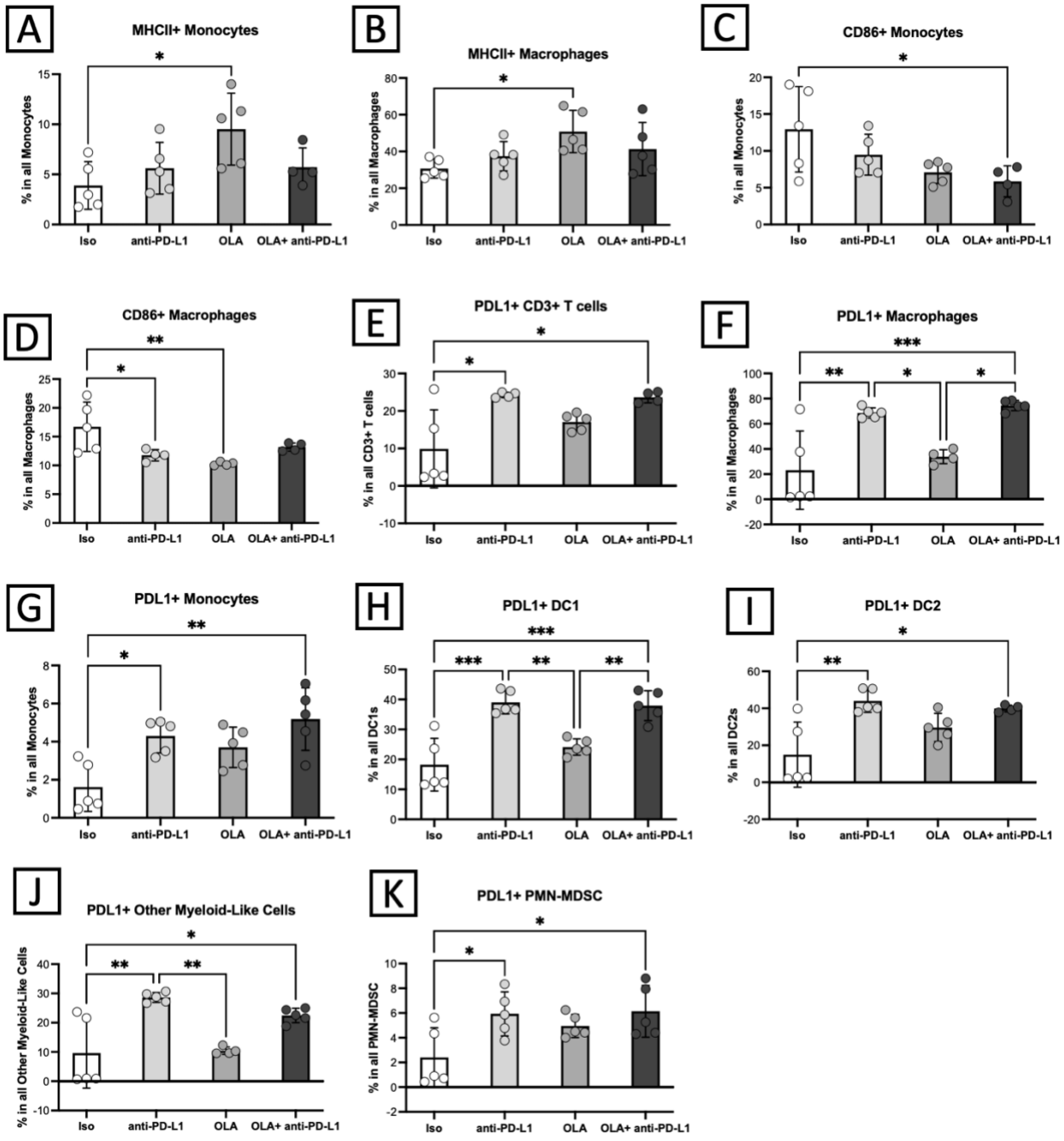

Figure 17. Abundance of innate and adaptive immune cells within the ID8 *Trp53*$^{-/-}$ *BRCA1*$^{-/-}$ spleens. Spleen tissues (n=5 mice per group) were collected from tumour-bearing mice injected with 5x10^6 cells which were treated with olaparib, anti-PD-L1 or their combination, and analyzed by flow cytometry approximately 36 hours after the end of treatment. Only the immune populations which are significantly different from isotype control or the combination therapy are shown. Each dot represents one biological replicate. Mean values with SD are shown. ISO indicates the isotype control group and OLA indicates the olaparib treated group. Analysis was done using a one-way ANOVA followed by a Tukey's multiple comparison test. *p<0.05, **p<0.01, ***p<0.001.

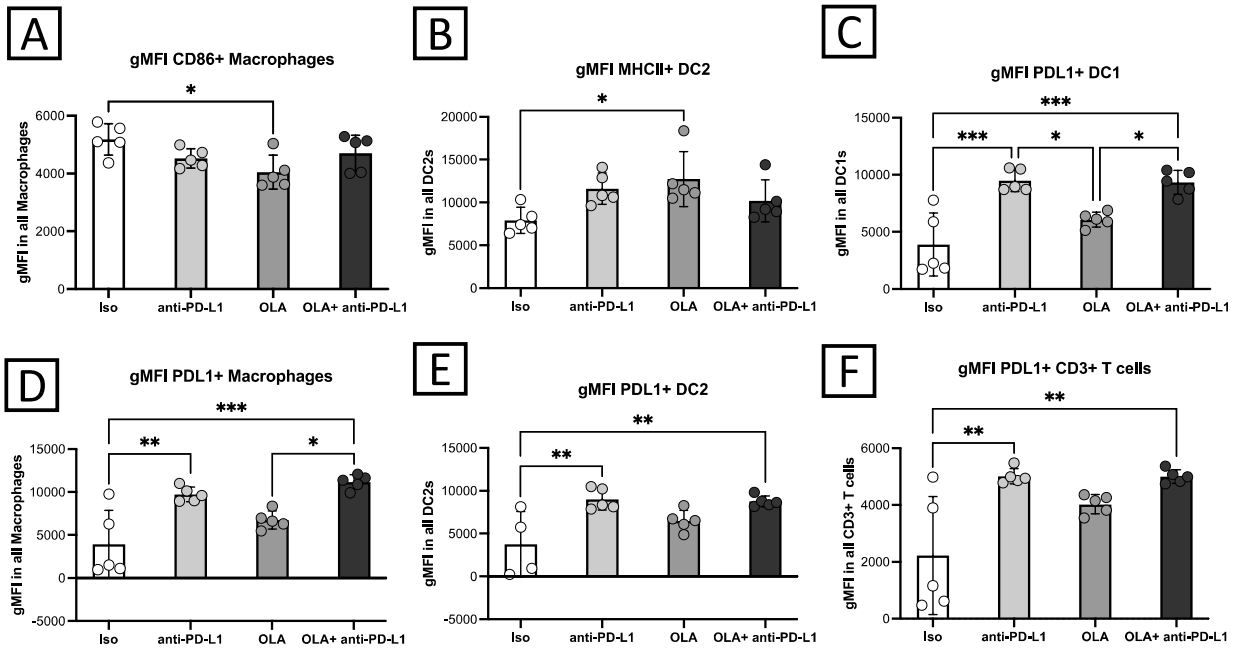

Figure 18. Mean fluorescence intensity of various markers expressed by immune cells within the ID8 *Trp53*$^{-/-}$ *BRCA1*$^{-/-}$ spleens. Spleen tissues (n=5 mice per group) were collected from tumour-bearing mice injected with $5x10^6$ cells which were treated with olaparib, anti-PD-L1 or their combination, and analyzed by flow cytometry approximately 36 hours after the end of treatment. Only the immune populations which are significantly different from isotype control or the combination therapy are shown. Each dot represents one biological replicate. Mean values with SD are shown. ISO indicates the isotype control group and OLA indicates the olaparib treated group. Analysis was done using a one-way ANOVA followed by a Tukey's multiple comparison test. *p<0.05, **p<0.01, ***p<0.001.

3.3.6 Systemic Effects of Therapy on the Immune System of ID8 *Trp53*$^{-/-}$ *Brca2*$^{-/-}$ Tumour-Bearing Mice

Upon the detection of several changes in the splenic tissue of the *Brca1*-null model following therapy, we further investigated how the same treatments would affect the cell populations within the spleens of mice harbouring *Brca2*-null tumors. Similar to the TME of the *Brca2*-null model which had fewer cells compared to the *Brca*1- null TME, the spleens of this model appeared to have fewer cells as well (**Figure 19**). This is especially true of the isotype control group which has the lowest overall number of leukocytes (**Figure 19**).

Compared to the spleen of the *Trp53*$^{-/-}$ *Brca1*$^{-/-}$ model, there is a more diverse range of significant changes taking place in the spleens of this model; significant changes were detected in both innate and adaptive immune cell populations (**Figure 20**). The olaparib monotherapy resulted in an 8% increase in the population of PD-1+ CD4+ T cells, which was significantly different from all other groups (**Figure 20A**). The olaparib monotherapy also uniquely reduced CD62L expression in CD8+ and CD4+ T cells by 20 and 26 percent, respectively (**Figure 20B-C**). These reductions were significant compared to all other groups. However, a significant reduction of 2-12% CD62L+ NK cells was seen in all treatments, with the olaparib monotherapy group having the highest reduction (**Figure 20D**).

Akin to all other tissues, administration of anti-PD-L1 enhanced the population of PD-L1+ cell types in the spleens of this model (**figure 20E-K**). However, unlike other tissues the olaparib monotherapy resulted in various PD-L1 related changes in multiple cell types as well. Both the antibody monotherapy and the combination therapy increased the percentage of PD-L1+ cells by approximately 10% in CD3+T cells (**Figure 20E**). In monocytes, macrophages and MDSCs, the anti-PD-L1 monotherapy was the only treatment that changed PD-L1 expressing populations and the changes were 2, 21 and 5 precent, respectively (**Figure 20F-H**). In both DC1s and DC2s, the anti-PD-L1 monotherapy enhanced the PD-L1+ population by 13%, while the olaparib monotherapy reduced it by 4% in DC1s and 12% in DC2s (**Figure 20I-J**). In other myeloid-like cells, the anti-PD-L1 monotherapy and combination therapies increased the PD-L1+ populations by 11.5% and 4.2% respectively, while the olaparib monotherapy reduced it by 14.3% (**Figure 20K**).

Analysis of gMFI values revealed changes in both PD-1 and PD-L1 (**Figure 21**). The combinaiton therapy enhanced PD-1 expression in both B cells and NK cells present in the spleen

of this model (**Figure 21A-B**). Replicating the expression levels in the spleen of the *Brca1*-null model, anti-PD-L1 both alone and in combination with olaparib enhanced PD-L1 expression in macrophages, DC1s, DC2s and T cell (**Figure 21C-F**). In summary, the modifications observed in the splenic tissue of the animals in the *Trp53*$^{-/-}$ *Brca2*$^{-/-}$ model were more extensive than the *Trp53*$^{-/-}$ *Brca1*$^{-/-}$ model, with modifications occurring in both innate and adaptive immune populations. Additionally, the systemic increase in PD-L1 previously observed in all analyses, was detected in this tissue as well. Thus, the differences in response to therapy between the *Brca1*- and *Brca2*-null model were not limited to the TME, and the systemic effects of treatment diverged between these models as well.

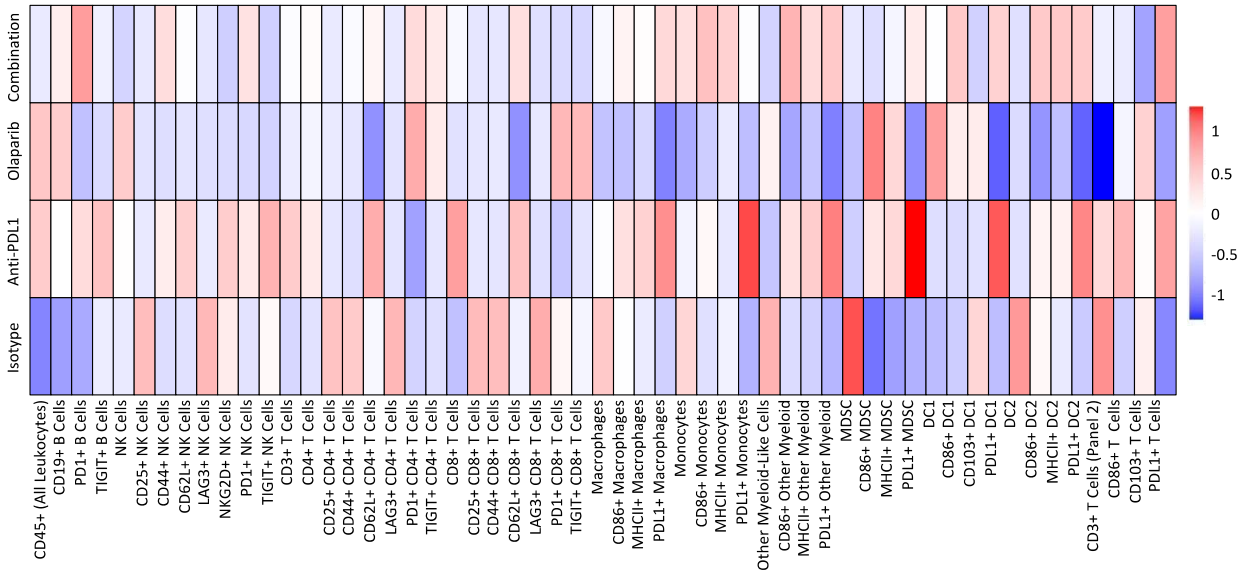

Figure 19. Heatmap presenting the abundance of various immune cell types in the ID8 *Trp53*$^{-/-}$ *BRCA2*$^{-/-}$ spleen tissue. Spleens (n=5 mice per group) were collected from tumour-bearing mice which were treated with olaparib, anti-PD-L1 or their combination, and analyzed by flow cytometry approximately 36 hours after the end of treatment. For each cell type, the value was calculated as the percent in all leukocytes. The percentages were normalized, and each box represents the mean of the 5 biological replicates

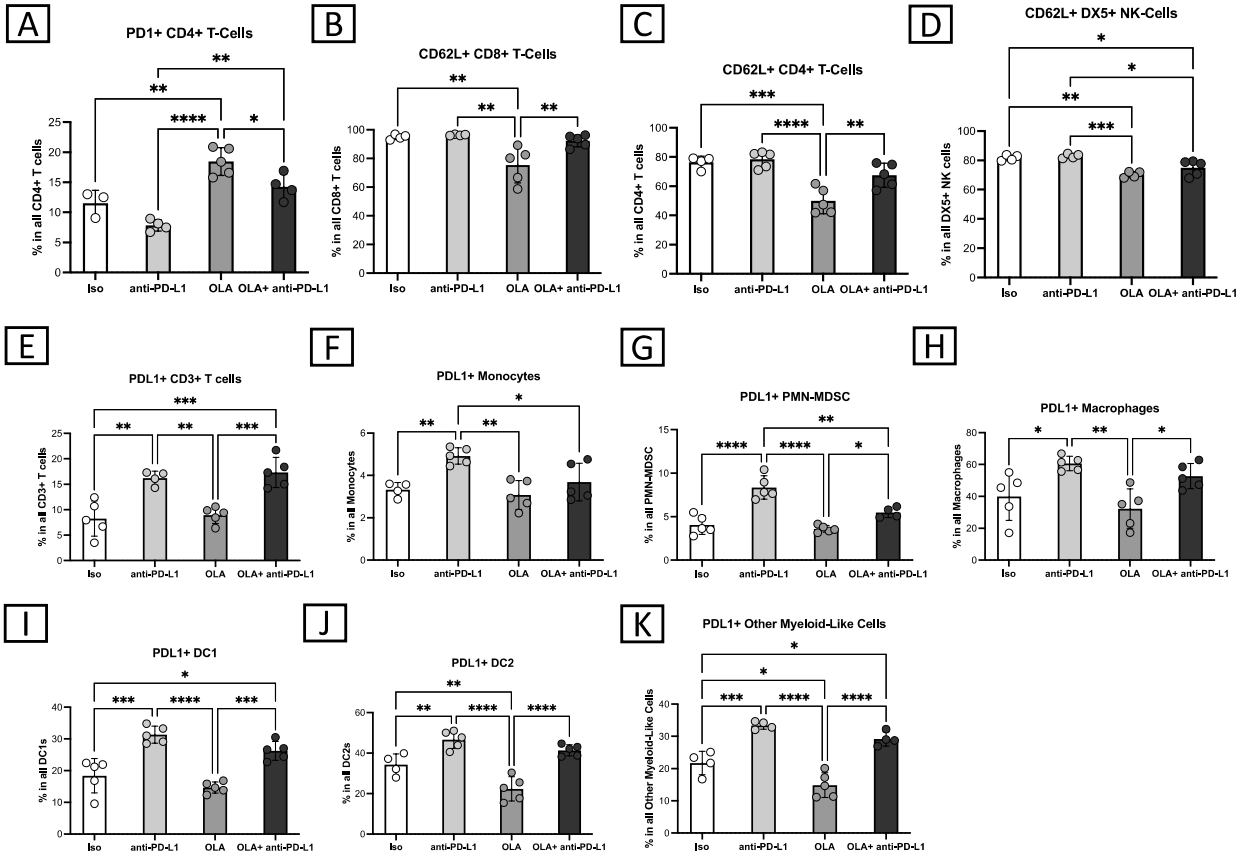

Figure 20. Abundance of innate and adaptive immune cells within the ID8 *Trp53*$^{-/-}$ *BRCA2*$^{-/-}$ spleen. Spleen tissues (n=5 mice per group) were collected from tumour-bearing mice injected with 5x10^6 cells which were treated with olaparib, anti-PD-L1 or their combination, and analyzed by flow cytometry approximately 36 hours after the end of treatment. Only the immune populations which are significantly different from isotype control or the combination therapy are shown. Each dot represents one biological replicate. Mean values with SD are shown. ISO indicates the isotype control group and OLA indicates the olaparib treated group. Analysis was done using a one-way ANOVA followed by a Tukey's multiple comparison test. *p<0.05, **p<0.01, ***p<0.001, ****p<0.0001.

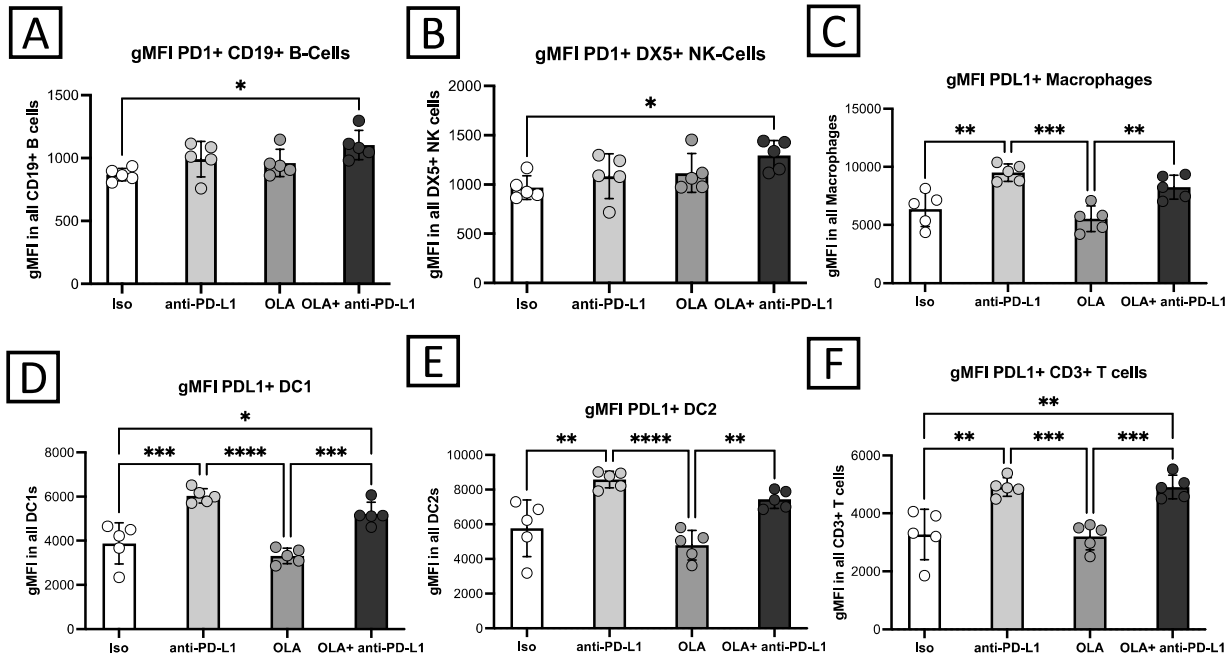

Figure 21. Mean fluorescence intensity of various markers expressed by immune cells within the spleens of mice with ID8 *Trp53*$^{-/-}$ *BRCA2*$^{-/-}$ tumours. Spleen tissues (n=5 mice per group) were collected from tumour-bearing mice injected with $5x10^6$ cells which were treated with olaparib, anti-PD-L1 or their combination, and analyzed by flow cytometry approximately 36 hours after the end of treatment. Only the immune populations which are significantly different from isotype control or the combination therapy are shown. Each dot represents one biological replicate. Mean values with SD are shown. ISO indicates the isotype control group and OLA indicates the olaparib treated group. Analysis was done using a one-way ANOVA followed by a Tukey's multiple comparison test. *p<0.05, **p<0.01, ***p<0.001, ****p<0.0001.

3.4 The Influence of Therapy on Cytokine Production

The effect of PARPi and monoclonal antibody therapy on cytokine production in ovarian tumours remains largely unknown. As such, we set out to determine the effects of these treatments on the concentrations of 13 cytokines and chemokines. Analysis of the cytokine array which was conducted on ascites fluid collected at the humane endpoint resulted in over 100 individual changes, as shown in the heatmap in **Figure 22A**. Of those, changes that were significant in either the *Brca1* or *Brca2*-null models are individually presented in **Figures 22B-K**.

As presented in the heatmap, the anti-PDL1 monotherapy resulted in a general reduction in cytokine production in the ID8 *Trp53*$^{-/-}$ *Brca1*$^{-/-}$ model compared to the isotype control (**Figure 21A**). The combination therapy appeared to have the same reductive effect, which was even greater for certain cytokines, such as chemokine CC motif ligand 4 (CCL4) (**Figure 22A**). The olaparib monotherapy, on the other hand, resulted in cytokine concentrations that were either similar to or higher than the isotype control (**Figure 22A**). Changes in cytokine production in the ID8 *Trp53*$^{-/-}$ *Brca2*$^{-/-}$ model were similar to those in the *Brca1*$^{-/-}$mice, although the antibody-mediated reduction was more substantial in this model (**Figure 22A**). Unlike the *Trp53*$^{-/-}$ *Brca1*$^{-/-}$ model, olaparib monotherapy had both suppressive and enhancing effects on cytokine production in the *Brca2*$^{-/-}$ model (**Figure 22A**). The combination therapy had similar effects, with both increases and decreases in cytokine production that followed the same trends as the olaparib monotherapy. It should be noted however, that certain increases and decreases appeared to be greater in magnitude in the combination group (**Figure 22A**).

With regards to significant changes, some changes were consistent across both models, while others were only present in one model (**Figure 22B-K**). Within the ID8 *Trp53*$^{-/-}$ *Brca1*$^{-/-}$ model, the concentration of CCL4 was significantly reduced by 50% in the combination therapy compared to the isotype control and olaparib monotherapy (**Figure 22B**). Conversely, there were no statistically significant changes in CCL4 levels in the ID8 *Trp53*$^{-/-}$ *Brca2*$^{-/-}$ model and in fact, the combination therapy had the highest CCL4 concentration (**Figure 22C**). Similarly, in the *Brca1*-null group, chemokine (C-X-C motif) ligand 1 (CXCL10) concentrations were lowest in the combination group and this reduction was significant compared to olaparib monotherapy (**Figure 22D**). However, no change was seen in CXCL10 concentrations in the *Brca2*-null model (**Figure 22E**).

Compared to all other cytokines in the *Brca1*-null TME, IFN-*a* production was significantly higher in the olaparib monotherapy (**Figure 22F**). Remarkably however, presence of anti-PD-L1 on its own or in combination with olaparib drastically reduced IFN-*a* concentrations to near zero levels (**Figure 22F**) This trend was also seen in the *Brca2*-null model (**Figure 22G**). Expression of granulocyte-macrophage colony-stimulating factor (GM-CSF) closely resembled that of IFN-*a*, as the presence of anti-PD-L1 antibody completely diminished GM-CSF production in both models (**Figure 22H-I**), however the changes were only significant in the *Brca1*-null group (**Figure 22H**). Lastly, a synergistic effect of both monotherapies resulted in the highest VEGF concentration in the combination therapy in the *Brca2*-null model (**Figure 22K**). The enhanced concentrations of VEGF were more than 4 times greater than the isotype control (**Figure 22K**). Conversely, there were no changes VEGF concentrations of the *Brca1*-null TMEs (**Figure 22J**). In short, the impact of therapy on cytokine concentrations within the ovarian TME was found to vary between treatments, with anti-PD-L1 exhibiting a unique reductive effect. The cytokine concentrations in the olaparib treated group, however, were generally similar or higher than the isotype control, albeit not always significantly different. Furthermore, akin to the variations in the cellular composition of the TME, the alterations in the cytokine profiles were found to differ greatly between the *Brca1*- and *Brca2*-null models.

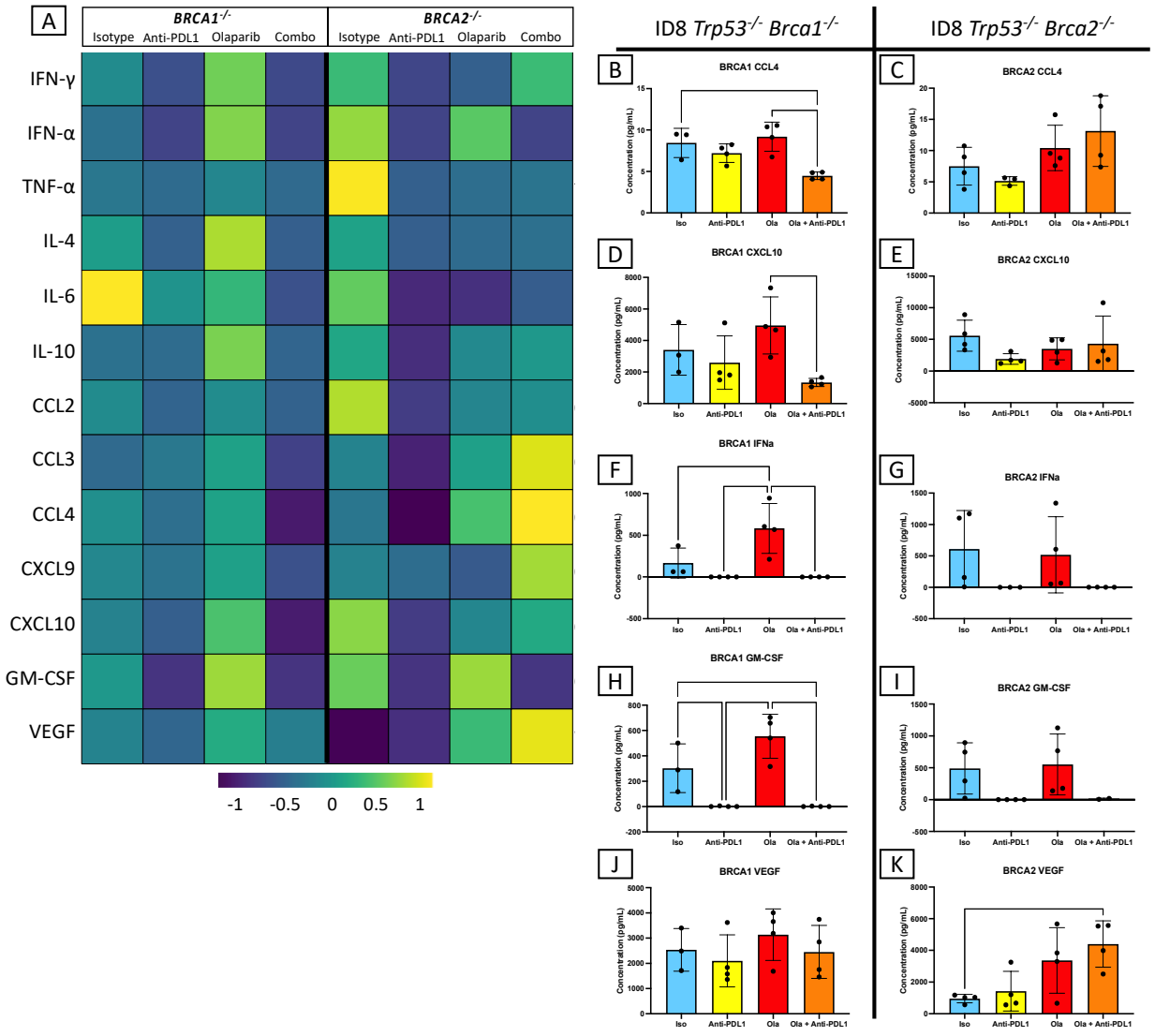

Figure 22. The ascites cytokine concentrations indicate the influence of therapy on cytokine/chemokine production. Ascites fluids were collected from peritoneal washes at humane endpoint (n = 4 per group). Cytokines were quantified using the LEGENDplex Mouse Cytokine Release Syndrome flow-based assay. (A) Heatmap showing the normalized concentrations of cytokines in the ID8 *Trp53*$^{-/-}$ *Brca1*$^{-/-}$ and ID8 *Trp53*$^{-/-}$ *Brca2*$^{-/-}$ models. Each box represents the mean of 4 replicates. (B-K) Histograms indicating the concentrations which are significantly different from isotype control or the combination. Each dot represents the ascites supernatant from one biological replicate. Mean values with SD are shown. Analysis was done using a one-way ANOVA followed by a Tukey's multiple comparison. *p<0.05, **p<0.01, ***p<0.001.

3.5 *In Silico* Analysis of Bulk RNA Sequencing data From the ID8 Model

3.5.1 Mutations *Brca1* and *Brca2* Differentially Influence the Expression of Genes Involved in the PARP Pathway Both *In Vitro* and *In Vivo*

The ID8 cell lines and IP tumours responded differently to olaparib monotherapy. *In vitro*, the *Brca2*-null group was more sensitive to olaparib induced toxicity (**Figure 4**). *In vivo* however, the survival of the mice harbouring *Trp53*$^{-/-}$ *Brca2*$^{-/-}$ tumours was improved in only one of the two studies, while the survival of the *Brca1*-null model was improved in both studies. As such, we set out to study the expression of PARP pathway associated genes in both models.

Bulk RNA-seq analysis of the ID8 *Trp53*$^{-/-}$ *Brca2*$^{-/-}$ cells growing *in vitro* demonstrated a higher expression of both PARP1 and PARP2 compared to the *Brca1*$^{-/-}$ model (**Figure 23A**). Furthermore, expression levels of the DNA repair gene XRCC1 were highest in the *Brca2*-null model (**Figure 23A**). Interestingly, nearly all PARP pathway associated genes were highest in the ID8 *Trp53*$^{-/-}$ model without mutations in *Brca*. Analysis of RNA expression from IP tumours developing *in vivo* however, indicated a reversal in PARP pathway gene expression between the *Brca1* and *Brca2*-mutated models (**Figure 23B**). In IP tumours, nearly all the genes involved in this pathway were highest in the ID8 *Trp53*$^{-/-}$ *Brca1*$^{-/-}$ tumours (**Figure 23B**).

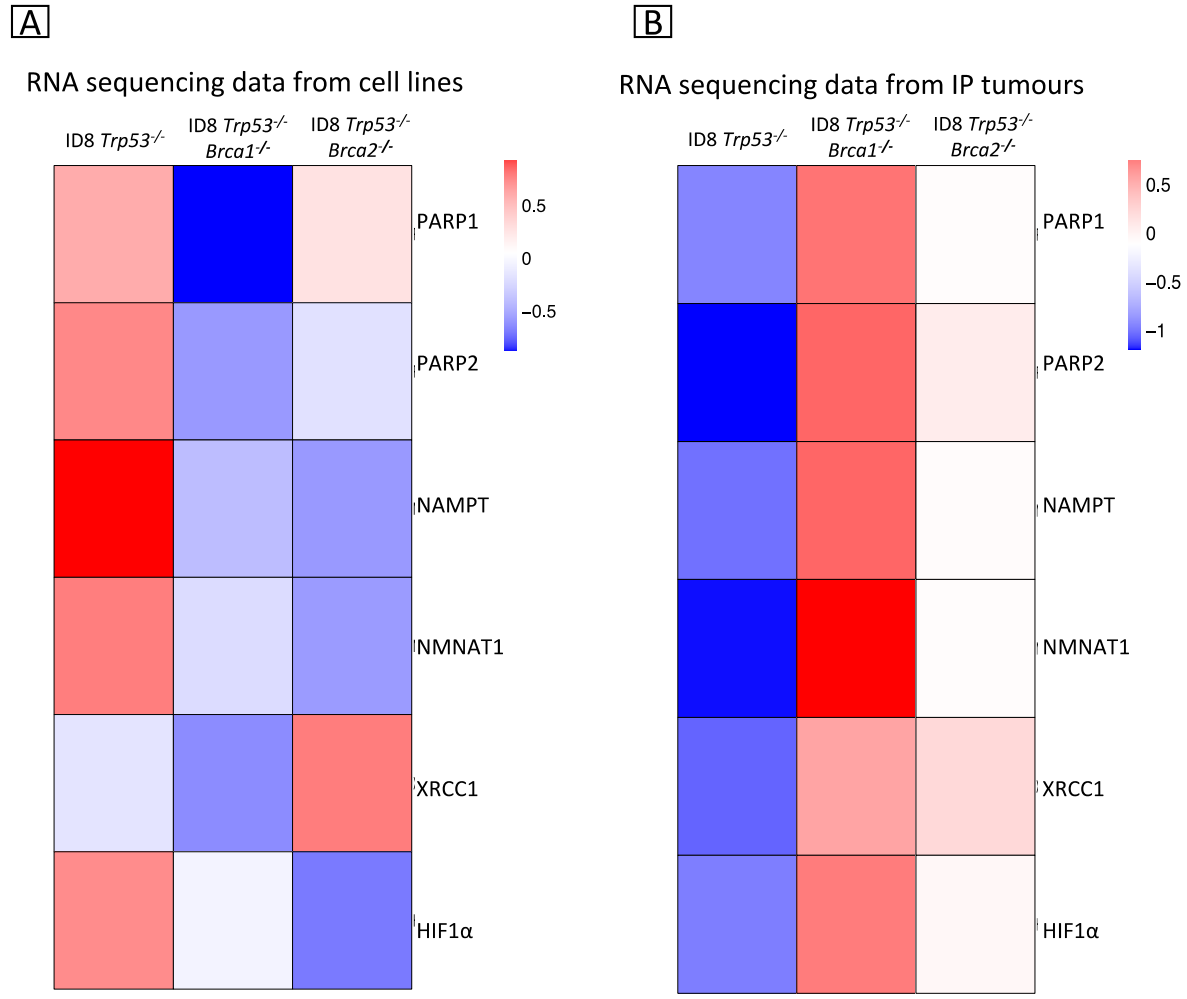

Figure 23. Mutations in *Trp53* and *Brca1/2* can influence the expression of genes involved in the PARP pathway. Bulk RNA-seq data was collected from cell lines growing *in vitro* (n=3) and as intraperitoneal tumours (n=4). (A) presents the relative expression of PARP pathway genes in cell lines. (B) presents the relative expression of PARP pathway related genes in intraperitoneal tumours. Each box represents the mean value of log-normalized RNA seq data.

3.5.2 Mutations *Brca1* and *Brca2* Differentially Influence the Expression of Various Genes Involved in Shaping the TME

As the TME analysis from the two models revealed differences in various cell populations and cytokines, we analyzed bulk RNA sequencing data from both tumour models to further investigate the differences between them. The analysis revealed notable differences in the RNA levels of various cell type markers between tumour models. Expression of CD45 was higher in the *Trp53*$^{-/-}$ *Brca1*$^{-/-}$ model compared to both the *Trp53*$^{-/-}$ and *Trp53*$^{-/-}$ *Brca2*$^{-/-}$ models (**Figure 24A**). Flow cytometry data from the TME also revealed that, at least in part, this difference translates to the protein level. As shown in **Figure 24B**, the *Brca1*-null TMEs have a consistently high percentage of CD45+ cells, while the *Brca2*-null TME has a highly variable range with a mean value that is approximately 20% lower. However, this difference is not statistically significant ($p=0.11$) (**Figure 24B**).

Similarly, expression levels for CD3 and other major T cell markers such as CD4 and CD8 were highest in the *Brca1*-null model. However, the major B cell marker, CD19, was similar across the three tumour models. Expression of genes associated with immune cell function also varied between the three models. For instance, expression of PD-L1 was higher in the *Brca1*-null model, while PD-1 expression was equally high in both *Brca*-mutated tumours (**Figure 24A**). Once again, the RNA seq data is similar to the flow cytometry data which revealed that the percentage of PD-L1+ cells appear to be lower in the *Brca2*-null TME, with the exception of one biological replicate (**Figure 24C**). Furthermore, markers of both leukocyte activation (CD44) and exhaustion (LAG3) were also higher levels in the *Brca1*-null model (**Figure 24A**).

Aside from markers of cell types, the expression of genes encoding cytokines differed between the models as well. For pro-inflammatory cytokines for such as TNF-*a* and interlukin-1 alpha (IL-1*a*), expression levels were greatest the ID8 *Trp53*$^{-/-}$ *Brca1*$^{-/-}$ tumour model while the

anti-inflammatory cytokine IL-10 was expressed at a lower level. However, it must be noted that expression levels of IL-11, a potent anti-inflammatory cytokine, were also higher in the *Brca1*-null model (**Figure 24A**). Lastly, genes associated with angiogenesis and tumour vascularity such as vascular endothelial growth factor (*Vegf*), VEGF receptor (*Vegfr1*) and hypoxia induced factor alpha (*Hif1a*) were all expressed at higher levels in the *Brca1*-null model (**Figure 24A**). This increase was at least in part translated to the protein level as concentrations of VEGF were higher in the ascites fluid of the *Brca1*-null model compared to the *Brca2*-null model (**Figure 24D**).

Given the large number of differences detected between the immune composition of the *Brca*-mutated TMEs, we set out to further investigate the expression level of a key inflammatory mediator, nuclear factor kappa-light-chain-enhancer of activated B cells (NF-*k*B) between these models. This was achieved by measuring the expression levels of a set of 60 genes that are known to be downstream of this transcription factor. NK-kB, in addition to being a primary driver of inflammation, is a key downstream constituent of one of the major driving forces in TME composition: cyclic GMP-AMP synthase-stimulator of interferon genes (cGAS-STING) signaling. Therefore, analysis of NF-*k*B signaling could be used as one of the indicators of potential a change in cGAS-STING activity. Examination of this data revealed that NF-*k*B activity was highest in the *Trp53*$^{-/-}$ *Brca1*$^{-/-}$ model, modest in the *Trp53*$^{-/-}$ *Brca2*$^{-/-}$ tumours and lowest in the *Trp53*$^{-/-}$ group (**Figure 24E**). Taken together, the RNA sequencing data point to the fact that, compared to the *Brca2*-null model, ID8 *Trp53*$^{-/-}$ *Brca1*$^{-/-}$ tumours have a more "inflamed" TME with higher expression of leukocytes, inflammatory cytokines, and angiogenesis. Nevertheless, this phenotype is not completely consistent, as certain anti-inflammatory regulators such as IL-11 and tumour growth factor-beta (TGFβ) are also expressed at a higher level in the *Brca1*-null TME.

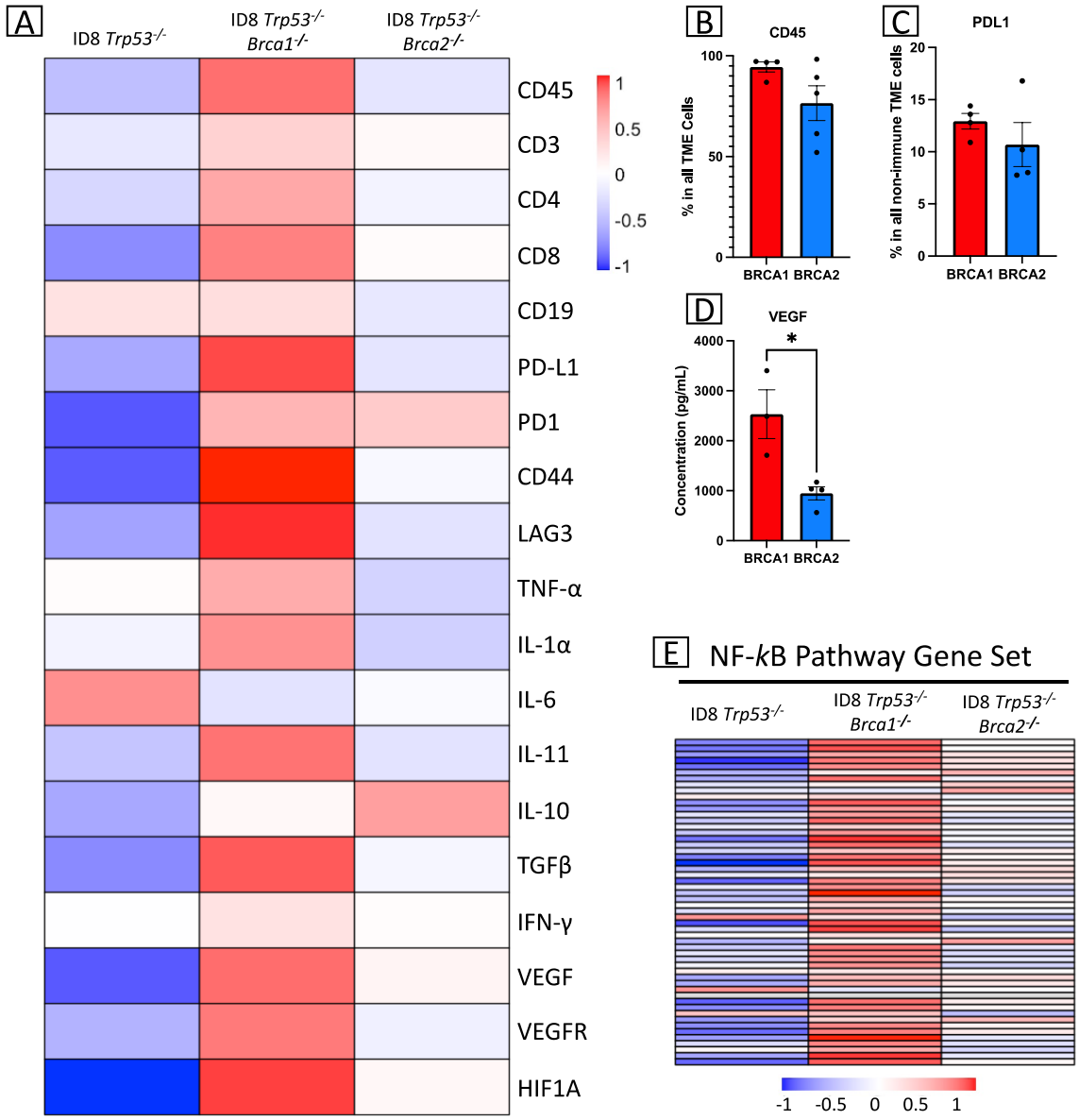

Figure 24. Mutations in *Brca1* and *Brca2* differently influence the expression of immune-related constituents in the ovarian tumour microenvironment. (A) Relative expression of immune-related genes in intraperitoneal tumours. Each box represents the mean value of log-normalized bulk RNA-seq data from 4-6 biological replicates. Gene names were replaced by the corresponding protein name. (B-C) Percentage of CD45+ and PDL1+ immune cells in the ID8 tumour microenvironment. Peritoneal washes (n=5 mice per group) were collected from tumour-bearing mice injected with $5x10^6$ cells and analyzed by flow cytometry approximately 36 hours after the end of therapy. These animals belonged to the isotype control group. (D) Concentrations of VEGF in the ascites fluid collected at humane endpoint (n=4 mice per group). Cytokines were quantified using the LEGENDplex Mouse Cytokine Release Syndrome flow-based assay. (E) Analysis of a gene set which demonstrates NF-*k*B pathway activity. Each dot in the histograms represents one biological replicate. Mean values with SD are shown. Analysis was done using the student's t-test. *$p<0.05$.

Discussion

Despite the fact that they've been studied extensively, the effects of PARPi and PD-L1 monoclonal antibodies on the composition of the ovarian TME remain unknown. In this thesis, we used syngeneic models of ovarian cancer to investigate the effects of therapy on the immune and cytokine profile of the ovarian TME. Furthermore, we studied the role of mutation of the *BRCA1/2* DNA repair genes in TME composition, response to therapy, and expression of genes involved in various pathways.

4.1 *In Vitro* Analysis of Response to Olaparib Therapy in Ovarian Cancer Cell Lines

4.1.1 *In Vitro* Olaparib Therapy Reduced the Survival of *Brca* Mutated ID8 Cell Lines

It has been previously established that *Brca*-mutated ovarian cancer cells which are heavily reliant on the PARP repair pathway are sensitive to PARPi therapy[88,89]. As such, various concentrations of olaparib were tested to determine whether the ID8 cell lines with *Brca1/2* mutations have the same PARPi sensitivity as the cell lines in the published literature. The *Trp*53-null model was not sensitive to olaparib-induced toxicity. This was expected as the intact HR pathway would repair the DNA of this model, and the blockage of the less frequently used PARP repair pathway should not be detrimental to cell survival. The *Brca*-mutated cell lines, however, were sensitive to olaparib-induced toxicity; the *Trp53*$^{-/-}$ *Brca1*$^{-/-}$ model was sensitive to the highest concentration of the drug while the *Trp53*$^{-/-}$ *Brca2*$^{-/-}$ model was sensitive to olaparib toxicity at all concentrations. This dissimilarity in drug sensitivity between the *Brca1*- and *Brca2*-mutated cells may in part be explained by the expression of the PARP-pathway associated genes. Analysis of the RNA-seq data from the ID8 cell lines revealed that the expression of PARP1 and PARP2 which are the major targets of olaparib[48], are higher in the ID8 *Trp53*$^{-/-}$ *Brca2*$^{-/-}$ cells compared to the

Brca1-null cells. Thus, the ID8 *Trp53*$^{-/-}$ *Brca2*$^{-/-}$ cell line may be more dependent on the PARP pathway and more sensitive to PARPi-induced toxicity. The expression of XRCC1, the major SSB repair protein was highest in these cells as well, which provides further support for the potential of over reliance of the *Brca2*-null cells on SSB repair activity. It should be noted that the ID8 *Trp53*$^{-/-}$ cell line had even higher levels PARP pathway expression in the RNA seq data. As mentioned previously, however, the less error-prone HR is functional in this model, and it is unlikely that the cells are frequently employing the PARP pathway to repair the DNA. Instead, the intact BRCA pathway is likely at play, thus eliminating, or at least reducing, the need for PARP activity. The low expression of XRCC1 in the *Trp53*$^{-/-}$ cells further indicates that, although the cells may express the enzymes involved in the PARP pathway at higher levels, SSB repair is not necessarily taking place. Additionally, the pathways which induce the expression of PARP enzymes are not completely understood. As such, it is alternatively possible that enzymes in unrelated pathways enhance the expression PARP, and the upregulation of this pathway in the ID8 *Trp53*$^{-/-}$ model in unrelated to DNA repair.

4.1.2 *In Vitro* Olaparib Treatment Enhances PD-L1 Expression in the ID8 Model

Treatment of the ID8 cells with olaparib also enhanced the expression of PD-L1, and this phenomenon was not limited to the *Brca*-mutated cell lines. Previous studies have noted that the treatment of breast and ovarian cancer cell lines with PARPi such as niraparib can induce the expression of PD-L1 through the phosphorylation of glycogen synthase kinase-3 beta (GSK3β)[91,92]. Under normal conditions, GSK3β activity results in phosphorylation-dependent degradation of PD-L1[93]. Treatment of cancer cells with PARPi has been shown to phosphorylate GSK3β at Ser 9 and Ser 21, which inhibits the activity of this enzyme and thus, PD-L1 expression

can take place continuously[91]. The enhanced levels of PD-L1 expression in response to olaparib therapy in this experiment allowed us to identify a target for the *in vivo* combination therapy.

4.1.3 Limitations of the *In Vitro* Experiments and Future Directions

To determine the effects of olaparib therapy on cell survival, we used a 3-(4,5-dimethylthiazol-2-yl)-2,5-diphenyl-2H-tetrazolium bromide (MTT) AlamarBlue assay. Such MTT assays merely detect the metabolic activity of cells through the reduction of its active ingredient, Resazurin, which works as an intermediate electron acceptor of the electron transport chain[94]. If presence of olaparib in the cytoplasm results in compromised oxidative phosphorylation or impaired mitochondrial permeability, the data produced by this assay may suffer from a type I error. In fact, recent evidence has demonstrated that olaparib can inhibit the activity of the mitochondria complex I.[179] Thus, determining drug sensitivity using another assay which directly measures cell death (i.e., apoptosis assays) could provide a more accurate measure of PARPi-induced toxicity. Another possible limitation associated with this study is the fact that the ID8 cell lines are single cell clones generated via CRISPR-Cas9 mediated gene deletions[88,89]. Although hypothetically the CRISPR-Cas9 system is supposed to induce precise DNA deletions, it can also influence multiple various pathways through off-target effects. As such, the phenotypes observed in this study could, at least in part, be the influenced by off-target effects of CRISPR-Cas9 treatment. The ID8 model also suffers from potential issues associated with clonal variation. As the cell lines are generated from single cell clones, it is plausible that the unique properties attributed to the original cell can bias the entire model. This concern was in part addressed by Walton *et al.,* where they established that the various ID8 single cell clones which they generated have identical IC50 values in response to rucaparib treatment[88,89]. Additionally, the survival

periods of mice harbouring tumours which were made of the various ID8 clones were extremely similar[88]. The similarities in PARPi sensitivity and survival period suggest that these clones are comparable, and the probability of a single-cell clone bias is minimal.

4.2 Assessing the Effects of *In Vivo* Olaparib Therapy on the Survival of ID8 Tumour-Bearing Mice

4.2.1 Olaparib Monotherapy Improved the Survival of Mice Harbouring *Trp53*$^{-/-}$ *Brca1*$^{-/-}$ Tumour

Prior to assessing how olaparib therapy influences the composition of the ovarian TME, we first set out to determine if this monotherapy can enhance the survival of tumour-bearing mice. As expected, the olaparib treatment regimen did not improve the survival of the mice harbouring ID8 *Trp53*$^{-/-}$ tumours. The underlying reasons for this lack of improvement are likely similar to that of the unresponsive *Trp53*$^{-/-}$ cell lines which were treated *in vitro*. The proficient HR pathway is likely repairing the DNA, which prevents the accumulation of DNA damage in tumour cells and thus, renders them unresponsible to PARPi treatment. Consequently, any potential immunomodulatory effects of PARPi therapy were likely absent or insignificant, and therefore unable to result in any significant reductions in tumour progression. As such, this model was excluded from the next animal study where the TME of the ID8 models was studied in detail. The prolonged survival of the *Trp53*$^{-/-}$ *Brca2*$^{-/-}$ tumour-bearing was also not significant. However, the median survival of the olaparib treated mice was 28% higher compared to the control group. With high potential for survival improvement, as well as the remarkable sensitivity of this model to *in vitro* olaparib treatment, it was deemed appropriate to study the effects of therapy on the composition of the *Brca2*-null TME in the next study. The group of mice harbouring the ID8

Trp53$^{-/-}$ *Brca1*$^{-/-}$ tumours were the only group for which survival was improved significantly. The 33% improvement in survival in this model was also the largest change observed in all groups.

The difference in response to olaparib therapy between the *Brca1*$^{-/-}$ and *Brca2*$^{-/-}$ models may in part be due to the differences in the expression of the PARP pathways in these IP tumours. As shown in the RNA-seq data, the ID8 *Trp53*$^{-/-}$ *Brca1*$^{-/-}$ IP tumours have the highest expression of all the known genes which are involved in the PARP pathway when compared to the other tumour models. These higher levels of expression may be indicative of a potentially higher reliance on the PARP pathway, making these *in vivo* tumours more sensitive to the PARP-induced toxicity.

The drastic change in the expression of the PARP-associated genes between the cell lines and tumours should also be noted. The literature on cancer research often points to the differences between cells growing *in vitro* compared to those developing *in vivo* tumours. These changes are often caused by the presence of the plethora of other biological systems, cell types and factors present in living organisms. When examining the PARP pathway, we noted a complete reversal in the expression of genes involved in the PARP pathway in cell lines and the IP tumours which develop from those cell lines. In future studies using syngeneic models, it will be critical to evaluate the behaviour of cancer cells in both environments in detail.

4.2.2 At the Humane Endpoint, TMEs of Treated and Untreated Tumours Are Not Different

Analysis of tumours collected at the humane endpoint did not reveal any changes in the expression of CD45, MHC I, CD8 or PD-L1. This observation was anticipated as treated and untreated tumours collected humane endpoint are frequently similar. This is likely due to the fact that the treatment regimen ended weeks prior to the humane endpoint of these syngeneic models.

As such, the effects of the drug on the TME were likely diluted as tumour progression continued and the drug was eliminated from the body.

4.2.3 Study Limitations and Future Directions

The potential limitations arising from the differences between single cell clones which were discussed in **4.1.3** also pose a risk in biasing the result of *in vivo* studies. However, there are also a number of other limitations which impact the outcomes associated with this *in vivo* model. First of all, the ID8 model is developed from the cells of the ovarian surface epithelium, as this used to be the presumed origin of most HGSOCs. The rationale behind this proposition was the "incessant-ovulation hypothesis"[95], which associated the high rates of ovarian surface rupture during ovulation as the major cause of cell proliferation which increased risk of neoplasia in these rapidly dividing cells. More recently, however, the fallopian tube has been identified as the tissue of origin of most low- and high-grade ovarian carcinomas[96,97]. Therefore, the ID8 model is not a perfect representation of most ovarian tumours due to the difference in the tissue of origin.

Secondly, the IP injected tumour cells form several small metastases as they spread around the peritoneal cavitary and therefore, there is a lack of a large primary tumour which is present in patients. As such, the peritoneal wash collected in this study is only partially representative of the solid TME of most ovarian cancer patients. The third limitation associated with the *in vivo* tumours of the ID8 model is the complete deletion of the genes of interest. Most patients have specific mutations in the *BRCA* genes, and the exact location of these mutations can greatly influence patient outcomes[98]. However, the *Brca* genes of the ID8 model have been completely deleted and as such their genotype is not a prefect representation of the human disease.

The IP route of drug administration in this model was also not a perfect representation of treatment in women. PARPi are usually administered as an orally ingested pill and as such, oral gavage would have been a more representative mode of drug delivery[21]. However, the large number of animals and the high frequency of drug administration made oral gavage nearly impossible. Lastly, the time point at which the TME was analyzed was major limitation in this initial study, as our analysis failed to detect any differences in the treated and untreated tissued at humane endpoint. To address this limitation in the next animal study, the TME was analyzed immediately after the end of treatment.

4.3 Assessing the Effects of Treatment on the Composition of the Ovarian TME

4.3.1 Monotherapies and Combination Treatment Differentially Influence the Survival of Mice Harbouring Tumours with *Brca1/2* Mutations

Unlike the previous study, the olaparib monotherapy in the second study significantly increased the median survival of both *Brca*-mutated tumour models and the improvements were very similar. Clinical studies have demonstrated that patients with mutations in either *BRCA* gene can benefit from the survival improvements associated with olaparib therapy, and the results of this animal study compliment the data found in the literature[99,100]. Unexpectedly, however, the response to anti-PD-L1 treatment was completely different between the two models, as it doubled the survival of mice with *Trp53*$^{-/-}$ *Brca1*$^{-/-}$ tumours but had no effect on the survival of mice harbouring *Trp53*$^{-/-}$ *Brca2*$^{-/-}$ tumours. The exceptional survival improvement in the *Trp53*$^{-/-}$ *Brca1*$^{-/-}$ model may be due to a variety of different factors that make this tumour model more susceptible to PD-L1 blockage. First of all, RNA-seq analysis revealed that *Trp53*$^{-/-}$ *Brca1*$^{-/-}$ tumours have higher levels of PD-L1 expression. Data from the literature also point to higher expression of this marker in *BRCA1*-mutated tumours of breast and ovarian cancer patients[81,101]. This specific

increase in the *Brca1*-mutated models may be due to the intracellular role that PD-L1 plays in DNA repair. Recent evidence has emerged which identified PD-L1 as a translocator of BRCA1 from the cytoplasm into the nucleus[102]. As such, homologous recombination is heavily dependent on the activity of this protein. *Brca1*-deficient cells may be upregulating PD-L1 in an attempt to increase translocation of absent BRCA1 from the cytoplasm into the nuclei. The higher expression of PD-L1 provides more targets for the anti-PD-L1 to bind to and therefore, increase the likelihood of the drug to improve outcomes by reducing immune cell exhaustion.

Secondly, data from the flow cytometry study, as well as the recent literature indicate that the *Trp53*$^{-/-}$ *Brca1*$^{-/-}$ TME is more infiltrated by immune cells and is more immunogenic than the *Trp53*$^{-/-}$ *Brca2*$^{-/-}$ TME[81,103]. The higher expression of neoantigens as a result of greater TMB in *BRCA*1-mutated tumours may in part account for this immune cell attraction and infiltarion[81]. The greater abundance of immune cells within the *Trp53*$^{-/-}$ *Brca1*$^{-/-}$ TME makes this tumour model ideal for anti-PD-L1 treatment, as the highly abundant immune cells will be able to continuously eliminate cancer cells without being inhibited[75,104]. Overall, greater TMB, neoantigen presentation, PD-L1 expression and immune cells infiltration may all combine to make the *Trp53*$^{-/-}$ *Brca1*$^{-/-}$ model more responsive to anti-PD-L1 treatment.

The survival of mice treated with the combination therapy was nearly identical to the olaparib monotherapy in both models. This observation is reasonable for the *Trp53*$^{-/-}$ *Brca2*$^{-/-}$ tumour-bearing mice as this group did not respond to anti-PD-L1 treatment. As such, olaparib was hypothetically the only effective tumour suppressive agent in the combination mixture for this specific model. However, the *Trp53*$^{-/-}$ *Brca1*$^{-/-}$ tumour-bearing mice responded remarkably well to both treatments and it was expected that there would be a synergistic increase in survival in the combination group. One plausible explanation for the lack of this observation could be the

surprising reduction in CD44 expression in NK, CD4+, and CD8+ cells in the TME of the *Trp53*$^{-/-}$ *Brca1*$^{-/-}$ combination group. Although the molecular mechanisms underlying this reduction are unclear, it is possible that the combination of the two monotherapies simply prohibited the activation of these immune cells which in turn prevented their immune-mediated cancer cell elimination. As such, the only functional tumour-suppressive agent in this mixture would have been the olaparib which results in direct HRD cancer cell death. A list of the changes in immune cell populations of the *Brca*-mutated tumor microenvironments that potentially contributed to improvements in survival is outlined in **Table 5.** Data from the ongoing clinical trials which are currently testing the combination of these therapeutics in women would be useful in better understanding this lack of synergy.

Table 5. List of the changes in immune cell populations of the *Brca*-mutated tumor microenvironments that potentially contributed to improvements in survival.

	Olaparib	Anti-PD-L1
ID8 *Trp53*$^{-/-}$ *Brca1*$^{-/-}$	• ↑ in CD44+ CD4+ T cell number • ↑ in CD8+ T cell number • ↓ in CD4/CD8 T cell ratio	• ↑ in LAG3+ NK cell number • ↑ expression of LAG3 on NK cells • ↑ expression of CD25 on NK cells
ID8 *Trp53*$^{-/-}$ *Brca2*$^{-/-}$	• N/A	• ↑ in CD86+ macrophage number

4.3.2 Olaparib Monotherapy Differently Influences the Composition of *Brca*-Mutated TMEs and the Spleen of Tumour-Bearing Mice

Olaparib treatment transformed the TME of *Brca1*- and *Brca2*-null mice differently. In the *Trp53*$^{-/-}$ *Brca1*$^{-/-}$ TME, the changes were in the percentage of cells expressing various markers as well as the expression levels of the markers themselves. Treatment with PARPi increased the percentage of activated, CD44+ CD4 T cells. Expression of CD44 can be used a means to discriminate between naïve helper T cells and those that are activated, which can be subdivided

into effector and memory CD4+ T cells[105]. The activated CD4+ helper T cells can drive the direct activation of anti-tumour cytotoxic CD8 T lymphocytes (CTL) through the secretion of IL-2, a cytokine which can also help induce proliferation of these cells[106–108]. Indirectly, CD4 T cells also produce cytokines such as TNF-*a* and IFN-γ that can further attract, activate, and help with the differentiation of other immune cells in the TME[109,110]. Furthermore, through CD40 and CD40 ligand (CD40L) interaction, CD4+ helper T cells can stimulate antibody production in B cells, which in turn assist with tumour antigen recognition and destruction by CTLs[111–114].

The olaparib monotherapy also enhanced the proportion of CD8+ T cells in the ovarian TME. Upon activation by T helper cells or DCs, effector CD8+ CTLs can kill cancer cells through two major pathways: exocytosis of granule[115,116] and Fas ligand (FasL)-induced[117] apoptosis. Due to their extraordinary tumour suppressive abilities, CD8+ CTLs are the favoured adaptive immune cell for antitumour immunity. In fact, increased infiltration of TME by CD8+ CTL has been associated with better prognosis and survival in ovarian cancer patients[118–120]. The olaparib monotherapy also reduced the ratio of CD4/CD8 T cells in the ID8 *Trp53*$^{-/-}$ *Brca1*$^{-/-}$ TME. In clinical studies, a lower CD4/CD8 ratio has been associated with better outcomes in ovarian cancer patients[121,122]. Together, the olaparib driven changes in the T lymphocytes populations within the *Trp53*$^{-/-}$ *Brca1*$^{-/-}$ TME are all associated with improved anti-tumour activity and superior prognosis.

In terms of NK cell populations, the olaparib monotherapy was mostly immunosuppressive and the total population of NK cells was decreased. Similarly, the expression of the inhibitory marker PD-1, as well the percentage of cells which expressed this marker significantly increased upon olaparib therapy. NK cells directly contribute to the killing of cancer cells through the secretion of granzymes and perforin[74,123]. Increased expression of PD-1 on NK cells has been

associated with dysfunction, exhaustion, and poor outcomes[124], while the blockage of this ligand has been shown to restore NK cell activity[125]. As such, it is expected that reduced NK cell numbers as well as enhanced inhibition of this cell type reduced NK-mediated cancer cell death in the *Brca1*-null model.

Finally, olaparib monotherapy reduced the percentage of MHC II+ macrophages in the *Trp53*$^{-/-}$ *Brca1*$^{-/-}$ TME. Expression of MHC II in macrophages is linked with enhanced expression proinflammatory genes which are often correlated with a M1 phenotype[126]. Generally, M1 macrophages are associated with anti-tumour activity not only because they can be directly cytotoxic to tumour cells[127,128], but also because they secrete factors (i.e., IFN-γ) which stimulate the tumour suppressive NK and T cells[129].

Taken together, analysis of the effects of olaparib on the *Trp53*$^{-/-}$ *Brca1*$^{-/-}$ TME revealed several potential mechanisms through which this PARPi could both augment and suppress the functions of the immune system. Within the *Trp53*$^{-/-}$ *Brca2*$^{-/-}$ TME, however, olaparib monotherapy did not result in any significant changes in immune cell populations. In fact, based on the heatmap shown in Figure 13, the olaparib-treated *Brca2*-null TME appears to be the "coldest". This extreme difference in TME response to treatment is one of many results in this study that defines the differences between *Brca1*- and *Brca2*-mutated TMEs. Based on these results, mutations in *Brca* do not only influence DNA replication and TME composition, but also response to PARPi therapy.

The spleens of treated mice were collected and studied as they represent the "systemic" effects of treatment on the immune system. Yet again, the tissues of *Brca1*- and *Brca2*-mutated models underwent completely diverse transformations in response to therapy. In the spleens of the *Trp53*$^{-/-}$ *Brca1*$^{-/-}$ model, the changes were associated with MHC II expression on monocytes and

macrophages. However, unlike the TME, the percentage of these MHC II+ mononuclear phagocytes increased in the splenic tissue. A reduction of these cells in the TME and an increase in the spleens may be a result of poor tumour infiltration as a result of olaparib therapy. It is possible that olaparib may be impairing the expression or function of adhesions molecules that are required for the trafficking circulating immune to the TME. Immunohistochemical analysis of tumours collected shortly after treatment would be helpful in determining whether or not this hypothesis is correct. Alternatively, olaparib treatment may be reducing MHC II expression on the phagocytes which enter the TME after they depart from the spleen. As IFN-γ is the main driver of MHC II expression in macrophages and monocytes, analyzing the concentration of this cytokine in the TME immediately following treatment would also be useful in understanding this observation[130]. The expression levels of MHC II were also increased in DC2s present in the spleen of the *Trp53*$^{-/-}$ *Brca1*$^{-/-}$ model. Within the TME, DC2s can help to both initiate and support anti-tumour activity through antigen presentation[131]. More specifically DCs use the MHC II molecule for naïve CD4+ T cell recognition which results in T cell priming[132]. It is possible that the systemic increase in MHC II+ DC2s is one of the factors contributing to the enhanced levels of activated CD4+ T cells in the *Brca1*-null TME. Although not statistically significant, the levels of MHC II+ DC2s were also highest in the *Trp53*$^{-/-}$ *Brca1*$^{-/-}$ tumours (**Figure 10**). It is possible that MHC II+ DC2s are leaving the spleen and infiltrating the TME following olaparib exposure. Analysis of olaparib treated spleen and TME at various time points throughout the treatment period would be needed to confirm this postulation. The last olaparib induced change in the spleen of the *Trp53*$^{-/-}$ *Brca1*$^{-/-}$ model was a reduction in CD86 expression on macrophages. The expression of this marker on macrophages provides a co-stimulatory signal for T cell activation through CD86-CD28 signaling and its reduction may reduce T cell priming[133]. In short, the olaparib induced changes in

the spleens of the *Brca1*-deficient model were all in various APC populations which have both immunosuppressive and immunomodulating effects, with the vast majority of the changes biasing towards a tumour suppressive phenotype.

In splenic tissue of the *Trp53*$^{-/-}$ *Brca2*$^{-/-}$ model the effects of olaparib monotherapy were almost exclusively immunosuppressive. For instance, this treatment significantly increased the percentage of PD-1+ CD4+ T cells. PD-1 expression on T cells is generally a marker of exhaustion and inhibition, due to a variety of downstream pathways that are inhibited upon PD-1 activity. PD-1 activity results in recruitment of phosphatases such as Src homology 2 (SH2) domain-containing tyrosine phosphatase-2(SHP2)[134]. This phosphatase can inhibit signalling pathways that are downstream of the TCR, such as phosphatidylinositol 3-kinase (PI3K)/protein kinase B (Akt) pathway, which plays a role in T cell activation and proliferation[135,136]. As such, it is likely that the highly abundant PD-1+ CD4+ T cells in the olaparib-treated mice are unable to perform functions such as CTL activation and proinflammatory cytokine release[137]. Likewise, the olaparib monotherapy reduced CD62L expression in NK cells, CD8 and CD4 T cells. CD62L, or L-selectin, is a cell adhesion molecule that controls the infiltration of immune cells into various tissues such as lymph nodes and TME[138]. A reduction of CD62L within the TME would be indicative of an effector phenotype within the T cell populations, which would be considered a tumour suppressive phenotype[139]. However, the reduction of this marker in spleen cells may reduce the ability of circulating NK and T cells to infiltrate the tumour and kill the cells within the TME. In this situation, the analysis of triple positive groups (i.e., CD44+ CD62L+ CD8+) cells would provide more information on the acquired phenotype of these cells. However, in our analysis these cell types were extremely rare (<1%) and reliable analysis of these populations was not possible.

In summary, the olaparib monotherapy resulted in augmented CD4 T cell exhaustion and systemic reduction of CD62L expression in the spleens of the *Trp53*$^{-/-}$ *Brca2*$^{-/-}$ model. This is in contrast to the generally tumour suppressive changes in the innate immune cells of the *Trp53*$^{-/-}$ *Brca1*$^{-/-}$ spleen which once again points out the vast difference in treatment response in these models. Based on these data, the type of *BRCA* status in ovarian tumours should be considered when determining the optimal treatment regimen for ovarian cancer patients.

4.3.3 Anti-PD-L1 Monotherapy Differently Influences the Composition of *Brca*-Mutated TMEs and the Spleen of Tumour-Bearing Mice

The remarkable difference in survival timelines of the anti-PD-L1 treated mice harbouring *Brca1*- and *Brca2*-null tumours was an early indicator of the fact that the treatment likely had different effects on the composition of these TMEs. Upon further analysis, however, we found that these TMEs were parallel in many ways. In the *Trp53*$^{-/-}$ *Brca1*$^{-/-}$ TME, the anti-PD-L1 monotherapy increased the number of LAG3+ NK and the level of expression of this marker. In NK cells, LAG3 is an inhibitory marker that can impair cytokine production[140]. Aside from this immunosuppressive change, the anti-PD-L1 monotherapy resulted in a universal increase in PD-L1, both in expression levels and the number of cells which expressed this marker. Surprisingly, the anti-PD-L1 was more transformative in the *Trp53*$^{-/-}$ *Brca2*$^{-/-}$ TME and affected the population B cells, T cells and macrophages, as well as a systemic increase in the percentage of PD-L1+ cells which was also noted in the previous tumour model. This monoclonal antibody enhanced PD-1 expression on a large percentage of B cells, a phenotype which is generally associated with reduced B cell function, likely as a result of a similar inhibition noted in T cells[141]. B cells play a diverse and critical role in the TME through direct cytotoxicity to tumour cells and priming of CD4+ and CD8+ T cells[142]. In ovarian cancer, low B cell counts have been associated with unfavourable prognostic impact[143].

As such, inhibition of B cell activity may be limiting the potential immunomodulatory influences of anti-PD-L1 therapy in the *Trp53*$^{-/-}$ *Brca2*$^{-/-}$ TME.

Another outcome of anti-PD-L1 monotherapy which may hinder its anti-tumour functions is a reduction in CD4+ T cell numbers. As described previously, the helper T cell is a central mediator of anti-tumour immunity and a reduction in this cell type may limit the immunomodulatory effects of immunotherapy. On the other hand, the monoclonal antibody therapy enhanced the percent of CD86+ macrophages in the *Brca2*-null TME which is associated with improved T cell priming[133].

One significant effect which was shared by both tumour models was a universal increase in PD-L1+ cells in the treated TME. In the *Trp53*$^{-/-}$ *Brca1*$^{-/-}$ TME the expression of PD-L1 was also upregulated in all cell types. However, in the *Trp53*$^{-/-}$ *Brca2*$^{-/-}$ model the change was only in the percent of cells and not expression levels, with the exception of CD3+ T cells. This systemic increase in PD-L1 positivity in both models in likely a compensatory reaction to anti-PD-L1 blockade. A similar compensatory upregulation of alternative immune checkpoint molecules has been noted in various other studies[144–146]. However, none of the studies reported an upregulation in the very target which they inhibited and rather focused on alternative checkpoint molecules. Here, we demonstrate that ovarian cancer cells can upregulate the expression of PD-L1 in response to anti-PD-L1 blockage. It is possible that this upregulation is a result of increased IFN-γ production in antibody treated cells, as IFN-γ signaling is the main driver of PD-L1 signaling[147]. Blocking of PD-L1 could result in hyperactivity and eventually exhaustion of lymphocytes. The overworked lymphocytes such as CD8+ T cells will upregulate IFN-γ, as the upregulation of this marker is a marker of CTL exhaustion. Ultimately, the over expression of IFN-γ could drive the expression of PD-L1 in the antibody treated cells. Although both the *Trp53*$^{-/-}$ *Brca1*$^{-/-}$ and *Trp53*$^{-/-}$

Brca2$^{-/-}$ TME models share the increase in PD-L1+ cells, the expression of this protein is only upregulated in the *Trp53*$^{-/-}$ *Brca1*$^{-/-}$ TME. Yet again, this finding points to differences in these tumour models. Since the baseline expression levels of PD-L1 are already higher in the *Trp53*$^{-/-}$ *Brca1*$^{-/-}$ model, as discussed previously, this may be one of the factors which contributes to the difference in the compensatory PD-L1 expression of these two models. Overall, the findings from the analysis of anti-PD-L1 treated TMEs signified that this monotherapy resulted in generally immunosuppressive effects in the ovarian TME. Furthermore, the compensatory and systemic increase in PD-L1+ cells was present in both models was likely IFN-γ driven.

The effects of anti-PD-L1 therapy were similar in the spleens of *Trp53*$^{-/-}$ *Brca1*$^{-/-}$ and *Trp53*$^{-/-}$ *Brca2*$^{-/-}$ tumour-harboring mice. The only difference between these two models was in the percentage of CD86+ macrophages, which was reduced in the *Trp53*$^{-/-}$ *Brca1*$^{-/-}$ model. A similar reduction was seen as a result of the olaparib monotherapy, which indicates that both monotherapies impair the activity of macrophages to systemically activate and prime T cells. However, the more drastic change that occurred in the spleen was the universal increase in PD-L1. It is possible that the compensatory upregulation of PD-L1 both systemically and within the TME is limiting the ability of this monotherapy to have a prolonged immunomodulatory effect. Future studies which test the combination of various ICIs would be useful in addressing this limitation.

4.3.4 The Combination Therapy Differently Influenced the Composition of *Brca*-Mutated TMEs and the Spleen of Tumour-Bearing Mice

In the TME of the two *Brca*-mutated models, some of the effects of the combination therapy were as a result of a synergistic influence of both components, while the majority of changes were driven by one monotherapy. The largest change that was present in both models and

was the antibody-driven systemic upregulation of PD-L1 which was also noted in the anti-PD-L1 monotherapy. The vast majority of other differences in each TME were different as a result of the tumour *Brca* status.

In the *Trp53*$^{-/-}$ *Brca1*$^{-/-}$ TME, a large of number of changes were caused by the synergy of the monotherapies. For instance, although both monotherapies yielded insignificant increases in total CD3+ cell percentages, their combination significantly increased the percent of T cells present in the TME. A similar effect was present with regards to the expression of CD25 in NK cells, where the cooperative influence of both drugs significantly upregulated the expression of this marker on these cells and also enhanced the percentage of CD25+ NK cells within the TME. CD25, a high affinity receptor for IL-2, is a marker expressed on active NK cells and allows for the proliferation of these cells within the TME[148]. Increased expression of CD25 and the consequent IL-2 attraction augments the production of cytolytic effectors and improves the NK cell's efficacy to eliminate target cells[149,150]. The synergistic effects were not all immunomodulatory however, as the combination therapy treated *Trp53*$^{-/-}$ *Brca1*$^{-/-}$ TMEs also had the lowest expression levels and cell number of MHC II+ macrophages. As described previously, MHC II^{high} macrophages acquire an anti-tumour, M1 phenotype and the reduction in MHC II is indicative of weaker innate immunity within the TME[126]. Furthermore, the combination of the two drugs resulted in a collective increase in expression of CD25 in CD4 and CD8 T cells. Unlike its effects in NK cell populations, CD25 plays a regulatory role in T cells; and CD25+ CD4+ and CD25+ CD8+ T cells are often regarded as regulatory T cells (Tregs)[151]. Although the expression of the prominent Treg marker FOX3 is also required to confirm the Tregs status of these T cells with certainty, the recent literature has indicated improved antitumour activity in CD8+ CTLs following CD25 blockade within the TME[152].

Aside from the harmonious effects of the monotherapies, several outcomes of the combination therapy were driven by the individual monotherapies. In addition to the universal upregulation of PD-L1, the monoclonal antibody was the main driver of many significant changes in the combination group. For instance, the olaparib monotherapy significantly increased the percentage of inhibited PD-1+ NK cells. Within the combination group however, the addition of anti-PD-L1 monotherapy prevented this increase and reduced the percent of PD-1+ NK cells back to basal levels. Similarly, the presence of anti-PD-L1 in this combination was responsible for preventing the olaparib driven increases of LAG3 and PD-1 which were observed in the TME of the olaparib monotherapy. Thereby, treatment with anti-PD-L1 prevented olaparib-induced T cell exhaustion and inhibition in the combination group[153]. However, the influence of anti-PD-L1 in the combination group was not exclusively immunomodulatory, as the upregulated levels of LAG3 which were seen in the NK cells of the anti-PD-L1 monotherapy were also present in the combination group.

In addition to the influence of complementary and individual effects of the monotherapies within the *Trp53*$^{-/-}$ *Brca1*$^{-/-}$ model, the combination therapy also resulted in some unique and unexpected changes in this TME. For instance, this treatment resulted in a universal downregulation of CD44, a marker that is often associated with immune cell activation[105]. Furthermore, although the monotherapies resulted in slight increases in PD-1 expression in NK cells, the combination therapy reduced the expression of this marker to below basal levels. On the contrary, however, the combination therapy also enhanced the expression of TIGIT on NK cells. This effect was unexpected as neither monotherapy had any impact on NK cell LAG3 expression within the *Brca1*-null TME. One plausible explanation for the paradoxical change in PD-1 and TIGIT expression within the NK populations would be a compensatory reaction. As PD-1

functionally blocks NK cell activity, it is expected that reduced expression of this inhibitory molecule would result in prolonged and uninterrupted NK cell activity[154]. However, this continuous activity may eventually lead to NK cell exhaustion, reflected by the expression of TIGIT[155,156].

In summary, the composition of the *Trp53*$^{-/-}$ *Brca1*$^{-/-}$ TME was heavily altered by the combination therapy, with effects from both monotherapies and their synergy. The combination therapy in this TME also resulted in unique and unexpected changes that can in part be explained by continued immune cell stimulation and eventual exhaustion. The numerous changes in response to the combination therapy were exclusive to *Brca1*-null TME, as the mixture of these drugs resulted in little to no change in other tissues analyzed in this study. The immunogenicity of the *Brca1* mutation which can result in exceptional immune diversity of this TME model are likely the underlying causes behind these various transformations[103].

The combination therapy was far less transformative in the *Trp53*$^{-/-}$ *Brca2*$^{-/-}$ TME, although there were a small number of both immunomodulatory and immunosuppressive changes. The percentage of LAG3+ NK cells were reduced in what appears to be a synergistic effect of both combination therapies. Similarly, olaparib monotherapy prevented the anti-PD-L1 driven decrease in the total number CD4+ T cells. On the other hand, the presence of anti-PD-L1 yielded a tumour promoting increase of PD-1 in both B and NK cells, which assisted with impaired function in both cell types[141,153]. The comparatively small number of changes in the *Brca2*-null tumour model are yet another indication that the difference in *Brca* status can greatly impact the response to therapy.

The study of the systemic effects of the combination therapy by spleen tissue analysis revealed one main similarity between this tissue and the TME: systemic upregulation of PD-L1 as a result of treatment with anti-PD-L1. In the *Trp53*$^{-/-}$ *Brca1*$^{-/-}$ model, the individual potential of

both monotherapies also resulted in a synergistic reduction of CD86+ monocytes in this model. Aside from this singular change, the spleens of the *Brca1*-null model were unreactive to the combination therapy. In the *Trp53*$^{-/-}$ *Brca2*$^{-/-}$ model, the olaparib reduction in CD62L in various cell types was rescued by the anti-PD-L1. Furthermore, similar to the changes seen in the TME of this model, the combination therapy enhanced the expression of PD-1 in B cells and NK cells of the spleen tissue, making this one of the few observations that were similar in both tissues.

Nevertheless, mutations in *Brca1* and *Brca2* radically changed the response to combination therapy. The moderately "hot" TME of the *Brca1*-null model was transformed drastically while the relatively cold *Brca2*-null TME was hardly responsive. The clinical trials which are testing the efficacy of the combination of olaparib and anti-PD-L1 in patients harbouring *BRCA* mutations started patient recruitment in 2016[157]. As of now, no results have been published on the effects of this combination therapy in patients. These results would be imperative in determining the level to which the outcomes of this animal study are replicated in patients.

4.3.5 Limitations and Future Directions

All limitations discussed in **4.2.3** directly apply to this animal study as well. However, this combination study was also faced with another limitation: the clonal variability of the anti-PD-L1 antibody. The anti-PD-L1 used in this study was just one of many clones used for *in vivo* blocking of this ligand. Depending on their binding epitope, however, anti-PD-L1 antibodies can have both blocking and agonistic effects[158]. Although the published literature does not indicate any agonistic effects associated with the 10F.9G2 clone used in this study, it would be valuable to test the blocking potential of multiple anti-PD-L1 clones from various manufacturers to identify any potential differences in TME composition in future studies.

4.4 Cytokine Secretion in the Ovarian TME

4.4.1 Monotherapies and Their Combination Differentially Effect Cytokine Production in *Brca*-Mutated TMEs

The TME changes induced by the various treatments continued for weeks after the end of therapies, which may have minimized any differences in cytokine expression observed at the humane endpoint. For the most part, the *Brca*-mutated models had similar cytokine secretions. For instance, in both tumour models anti-PD-L1 treatment resulted in a universal reduction of cytokine secretion, although this reduction was more severe in the *Trp53*$^{-/-}$ *Brca2*$^{-/-}$ model. Similarly, the combination therapy resulted in a general reduction of most cytokine concentrations in both models, which in this case, was more severe in the *Brca1*-null model. One noteworthy reduction observed in both models was the complete diminution of IFN-*a* and GM-CSF concentrations as a result of anti-PD-L1 treatment, both as a monotherapy or in combination with olaparib. It should be noted, however, that the reductions were only statistically significant in the *Trp53*$^{-/-}$ *Brca1*$^{-/-}$ model. The reduction in IFN-*a* may be a result of the universal upregulation of PD-L1 in both tumour models. A recent study by Hodgins *et al*., demonstrated that intracellular PD-L1 activity can reduce type 1 interferon production through metabolic alterations that increase glycolysis and reduce oxidative phosphorylation[158]. PD-L1 drives the upregulation of the glycolytic pathway and results in the accumulation of pyruvate, which is converted into lactate, and cytoplasmic lactate buildup negatively regulates the production of type I interferons[158]. The pathway through which lactate buildup negatively regulates type I interferon expression is not completely understood. One possible explanation could be the lactate-induced inhibition of cGAS-STING signaling. This pathway is a major driver of both type I interferons and NF-*k*B (**Figure 25**). It is plausible that

lactate build up results in impaired cGAS-STING activity which in turns inhibits IFN-*a* transcription[159,160].

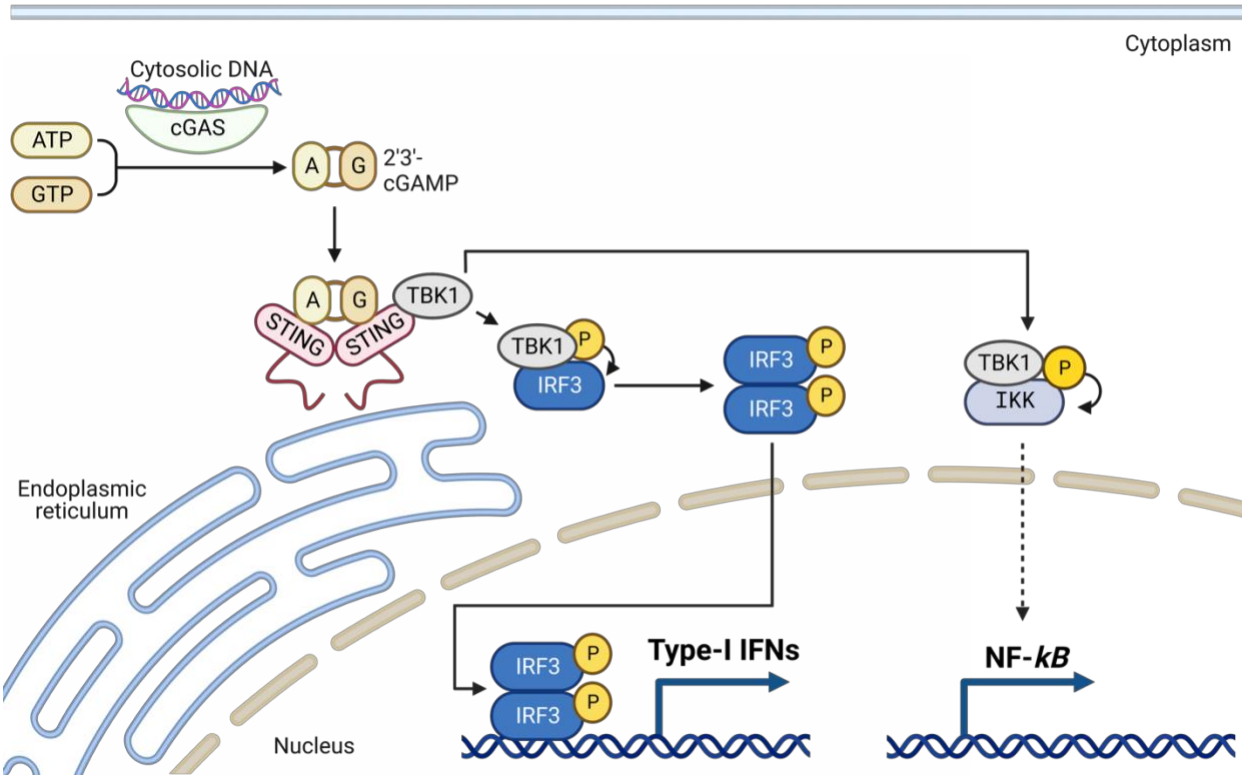

Figure 25. Overview of the cGAS-STING signaling pathway. Presence of cytoplasmic DNA can result in the dimerization of GTP and ATP by cyclic GMP-AMP synthase (cGAS), producing 2'3'-cyclic GMP-AMP (2,3-cGMAP). The 2,3-cGMAP then binds the endoplasmic reticulum transmembrane protein stimulator of interferon genes (STING), which becomes activated and translocates to the intermediate compartments between the endoplasmic reticulum and the Golgi apparatus. During translocation, cGAMP recruits TANK-binding kinase-1 (TBK1), which phosphorylates STING, leading to recruitment of interferon regulatory factor-3 (IRF3). TBK1 phosphorylates IRF3, causing it to dimerize and move into the nucleus, where it induces transcription of genes such as type-I interferons. The TBK1 can also recruit and phosphorylate IκB kinase (IKK), and pathways downstream of the activated IKK can drive the expression of NF-*k*B. Created using *BioRender*.

The possible lactate-driven decrease in cGAS-STING could also be associated with reductions in GM-CSF in anti-PD-L1 treated models. Aside from type I interferon transcription, cGAS-STING signaling induces the activity of NF-*k*B which can increase GM-CSF production in 2 ways. Firstly, NF-*k*B directly drives the transcription of GM-CSF as the promoter for this gene

has a Kappa B binding site[161]. As such, inhibition of NF-*k*B signaling would reduce the downstream transcription of GM-CSF. Similarly, enhanced expression of NF-*k*B can recruit GM-CSF producing immune cells into the TME[162]. Chronic impairments in the transcription of NF-*k*B in anti-PD-L1 treated TMEs may reduce the number of infiltrated TILs at humane endpoint and thus, it may be one of the reasons behind the low levels of GM-CSF. It should be noted that clustering of protein concentrations in the R software revealed a close relationship between the levels of these two cytokines across all biological replicates, which further supports a common underlying mechanism for their similar reduction. Aside from changes in GM-CSF and IFN-*a* concentrations, all statistically significant changes were dissimilar in the *Brca1*- and *Brca2*-mutated TMEs indicating that these mutations continue to play a role in TME composition long after the end of therapy.

The combination therapy resulted in a significant reduction in both CCL4 and CXCL10 only in the *Trp53*$^{-/-}$ *Brca1*$^{-/-}$ model. Within the TME, CCL4 can enhance vascularization[163], metastasis[164], and overall cancer progression[165,166]. Similarly, CXCL10 within the TME has been associated with enhanced tumour progression and increased infiltration of regulatory T cells[167]. The reductions in CCL4 and CXCL10 in the combination group were surprising as neither monotherapy independently reduced their concentrations. This unexpected reduction was akin to the reduced levels of CD44 expression, which was unique to the combination therapy treated *Trp53*$^{-/-}$ *Brca1*$^{-/-}$ tumour. There is some evidence that expression of both CCL4 and CXCL10 is associated with the expression of CD44. CCL4 is primarily produced by the immune cells within the TME, and blocking CD44 has been linked with reduced levels of this protein[168]. As such, it is plausible that the reduced expression of this activation marker within the *Brca1*-null TME caused the impairments in CCL4 secretion. Similarly, CXCL10 expression is driven by leukocytes in the

TME and in mouse models of vitiligo, tissues with the lowest levels of CXCL10 also had highest ratio of $CD44^{low}$ to $CD44^{high}$ CD8+ T cells[169]. As such, the reduction of one variable, either CXCL10 or CD44, may be driving the reduction of the other.

The last significant difference in the cytokine levels of the *Trp53*$^{-/-}$ *Brca1*$^{-/-}$ tumour model was an increase in the concentrations of IFN-*a* in the olaparib treated mice. As discussed previously, the cGAS-STING pathway is a major driver of type 1 interferon expression (**Figure 25**). The major driver of cGAS-STING signalling is the detection of cytosolic DNA. Upon detection of DNA within the cytoplasm, the cGAS enzyme drives the dimerization of GTP and ATP, which produced 2'3'-cyclic GMP-AMP (2,3-cGMAP). The 2,3-cGMAP binds to STING on the endoplasmic reticulum and sets off a cascade of reactions that result in IFN-*a* expression[170]. The accumulation of DNA damage as a result of olaparib activity in HRD cells results in transmission of DNA damage into the stages of mitosis, and the P53 protein is not present to control the quality of the DNA[171]. This causes formation of mitotic bridges from the fusion of sister chromatids and these bridges result in the formation of micronuclei, small DNA-containing structures surrounded by a lipid bilayer. The weak structural integrity of the micronuclei lamina results in frequent rupture within the cytoplasm, which results in the release of the DNA fragments in the cytosol[172]. The cGAS senses the presence of cytosolic DNA, which results in overactivation of the cGAS-STING pathway and yields higher levels of IFN-*a* in PARPi treated tissues[173]. In fact, RNA-seq analysis of *Brca*-mutated ID8 tumours also indicated higher levels of NF-*k*B, which provides further support for the greater activity of cGAS-STING in cells with greater levels of DNA damage.

4.4.2 Limitations and Future Directions

One limitation associated with this cytokine array was the fact that it was limited to 13 protein targets. In future studies, analysis of a larger number of cytokines can address this limitation and provide us with better understanding of how various therapies and *Brca* mutations influence the cytokine profile of the ID8 TME. Another limitation associated with this array was the fact that the cytokines could have been produced by any cell type present within the TME. In order to assess the change in the cytokine production of the tumour cells specifically, it would also be valuable to collect media from the cells treated *in vitro* and repeat this experiment. This will allow us to determine the extent to which *Brca* mutations in the cancer cells themselves can influence cytokine production.

4.5 Mutations in *Brca1* and *Brca2* Result in Differential TME Composition

Nearly every experiment in this thesis indicated that both TME composition and response to therapy are different in the *Brca*-mutated models of ovarian cancer. As such, we set out to determine the expression levels of various pathways through RNA-seq analysis which resulted a plethora of differences between these models. Aside from the PARP pathway and expression of PD-L1 discussed earlier, absence of *Brca1* resulted in greater expression CD45, as well as other major immune cell indicators much as CD4, CD8, CD19 etc. Similarly, markers of exhaustion such as PD-1, LAG3 and PD-L1 were also highest in the *Trp53*$^{-/-}$ *Brca1*$^{-/-}$ model. Lastly, the expression of various genes involved in angiogenesis such as *VEGF*, *VEGFR*, and *HIF1a* were all highest within the *Brca1*-null TME. The expression levels of some of these genes such as CD45, PDL1 and VEGF were also higher at the protein level, although these differences were not all

statistically significant. Rather, these trends indicate that at least in part, the changes at the RNA levels translate to the protein level and the recent literature supports these observations. For instance, a study by Dai *et al.,* identified *BRCA1* as a marker of immunogenicity in ovarian cancer as the mutations in this gene associated with greater immune infiltration and expression of immune check-point molecules[103]. Furthermore, similar to the findings of this thesis, their study indicated that patients harbouring *BRCA1* mutations are more responsive to immunotherapy[103]. Analogously, a study by George *et al.,* indicated that both mutations and hypermethylation of *BRCA1* but not *BRCA2* are associated with greater T cell infiltration within the ovarian TME and overall created a more "immunoreactive" environment[174].

One notable difference between the *Brca1*- and *Brca2*-mutated models which was detected in our analysis and is discussed in length in the literature, was the increase in angiogenic markers. At the RNA level, *Trp53*$^{-/-}$ *Brca1*$^{-/-}$ IP tumours had greater expression *VEGF*, *VEGFR*, and *HIF1a* and at the protein level, expression of VEGF was significantly higher in this model compared to the *Brca2*-null TME. Bruand *et al.,* also found that loss of *Brca1* was associated with upregulation of VEGF within tumours, which supported the observations in our analysis[175]. Interestingly, results of PAOLA-1 which is a recent clinical trial that tested the efficacy of combining olaparib with a VEGF inhibitor (bevacizumab), noted that this combination therapy was most beneficial for ovarian cancer patients harbouring *BRCA1*-mutated tumours[98]. These results confirm that absence *BRCA1* or *BRCA2* does not result in the same phenotype, and that these proteins have functions that beyond DNA repair. For instance, expression of *BRCA1* can negatively regulate the expression of *VEGFA*, and in its absence, this *VEGFA* is upregulated. This is likely as a result of the interaction between *BRCA1* and estrogen receptor alpha (ER-*a*)[176]. Two specific domains on BRCA1 are capable of binding to the active function-2 domain of ER-*a*, thereby preventing its

dimerization with estradiol (E2)[176]. The dimerized complex of ER-*a* and E2 can induce the transcription of many genes, including *VEGFA*[177]. As such, in the absence of BRCA, the ER-*a*-E2 complex can continually induce the expression of this protein. Given the overabundance of data that point to differences between tumours harbouring *BRCA* mutations, new studies have been exploring the influence of these mutations in response to therapy and TME composition, although not yet in ovarian cancer. A recent study by Samstein *et al.,* found that in mouse models of breast cancer, a deficiency in *Brca2* was associated with greater immunogenicity, unlike the ovarian cancer models[178]. Furthermore, in near perfect contrast to the findings of this thesis and the ovarian cancer literature, ICI treatment significantly improved the survival of mice harbouring *Brca2*-null breast cancer tumours, but not mice with *Brca1*-null tumours[178].

In summary, analysis of the RNA-seq data complemented the results of the *in vivo* studies and points out the significant impacts of *Brca* mutations on the composition of the ovarian TME. These findings, along with recent evidence from the literature indicate that BRCA proteins likely have functions beyond DNA repair and that personalized treatments are required based on the specific patient genotypes. Future studies investigating the various influences of *BRCA* mutations are key in improving our understanding of ovarian cancer and its treatment.

4.6 Conclusion

This thesis aimed to elucidate the effects of PARPi, immunotherapies and their combination on the immune composition of the ovarian TME. Additionally, we sought to investigate how the presence of *Brca1* and *Brca2* mutations can alter the results of therapy. To achieve these objectives, we first analyzed the *in vitro* response of ovarian cancer cell PARPi-induced toxicity. Our results indicate that the presence of *Brca1* and *Brca2* mutations confer varying degrees of sensitivity to olaparib, likely due to differential expression of the PARP pathway between these models. We also established that *in vitro* olaparib treatment upregulates the expression of PD-L1 on ovarian cancer cells, independent of their genotype.

In vivo olaparib treatment of mice harbouring *Brca1*- and *Brca2*-mutated tumours significantly increased the survival rate. Interestingly, only the *Brca1*$^{-/-}$ TME underwent significant transformation following this monotherapy, exhibiting pro- and anti-inflammatory changes in CD8+ and CD4+ T cells, as well as NK cells. The anti-PD-L1 monotherapy improved the survival of mice with *Brca1*-null tumours but not *Brca2*-null tumours. This treatment induced several significant changes in both tumour models, with the systemic increase in PD-L1 being the most prominent alteration in all tissues. This novel observation was likely a compensatory reaction in response to the prolonged immune activation. Additionally, the anti-PD-L1 treatment led to a substantial reduction in cytokine concentrations, namely IFN-*a* and GM-CSF. Lastly, the improvements in survival produced by the combination therapy heavily resembled the olaparib monotherapy. The TME changes produced by this treatment were generally attributed to one or both of the monotherapies. However, this therapy also led to an unexpected reduction of CD44 among multiple cell types on the *Brca1*-null TME. Furthermore, the TME of combination treated mice exhibited the same significant upregulation of PD-L1 as seen in the anti-PD-L1 group.

Through a detailed *in silico* analysis of RNA-seq data from *Brca*-mutated tumours, we found that these mutations have differential effects on the ovarian TME. Specifically, *Brca1*-null tumours exhibited an inflamed phenotype, with enhanced expression of various adaptive and innate immune markers, cytokines, vascularity, as well as the PARP and NF-*k*B pathways.

Clinically, *BRCA1*- and *BRCA2*-mutated ovarian cancers have been treated as the same disease. However, it is clear that these mutations can have significant impacts on patient outcomes. The findings of this study, as well as the ongoing clinical trials, can help to shed light on the influence of *BRCA* mutations in the treatment of ovarian cancer. Further study of the non-HR roles of the BRCA proteins is crucial for understanding the exact role that their absence plays in clinical outcomes. By considering the *BRCA* status of the tumour, clinicians may be able to provide treatments that are personalized to the needs of patients with various genotypes.

References:

1. Brett M. R, Jennifer B. P, Thomas A. S, Brett M. R, Jennifer B. P, Thomas A. S. Epidemiology of ovarian cancer: a review. Cancer Biol Med 2017;14(1):9–32.

2. PDQ Adult Treatment Editorial Board. Ovarian Epithelial, Fallopian Tube, and Primary Peritoneal Cancer Treatment (PDQ®): Health Professional Version. 2023. Accessed March 1, 2023. https://www.cancer.gov/types/ovarian/hp/ovarian-epithelial-treatment-pdq

3. Canadian Cancer Statistic. Ovarian Cancer Statistics: Canadian Cancer Statistics Advisory Committee. 2022. Accessed March 1, 2023. https://cancer.ca/en/cancer-information/cancer-types/ovarian/statistics

4. Timmermans M, Sonke GS, Van de Vijver KK, van der Aa MA, Kruitwagen RFPM. No improvement in long-term survival for epithelial ovarian cancer patients: A population-based study between 1989 and 2014 in the Netherlands. Eur J Cancer 2018;88:31–7.

5. Radziszewska AU, Karczmarek-Borowska B, Wójcik S, Kluz T. Survival rates among women with ovarian cancers diagnosed in the area of Podkarpacie province in the years 1990–2015. Współczesna Onkologia 2018;22(3):151–7.

6. Kuroki L, Guntupalli SR. Treatment of epithelial ovarian cancer. BMJ 2020;m3773.

7. Rosen DG. Ovarian cancer: pathology, biology, and disease models. Frontiers in Bioscience 2009;Volume(14):2089.

8. Ciucci A, Buttarelli M, Fagotti A, Scambia G, Gallo D. Preclinical models of epithelial ovarian cancer: practical considerations and challenges for a meaningful application. Cellular and Molecular Life Sciences 2022;79(7):364.

9. Köbel M, Kang EY. The Evolution of ovarian carcinoma subclassification. Cancers (Basel) 2022;14(2):416.

10. Terada KY, Ahn HJ, Kessel B. Differences in risk for type 1 and type 2 ovarian cancer in a large cancer screening trial. J Gynecol Oncol 2016;27(3):e25.

11. Wright AA, Bohlke K, Armstrong DK, et al. Neoadjuvant chemotherapy for newly diagnosed, advanced ovarian cancer: society of gynecologic oncology and American society of clinical oncology clinical practice guideline. Journal of Clinical Oncology 2016;34(28):3460–73.

12. Vergote I, Coens C, Nankivell M, et al. Neoadjuvant chemotherapy versus debulking surgery in advanced tubo-ovarian cancers: pooled analysis of individual patient data from the EORTC 55971 and CHORUS trials. Lancet Oncol 2018;19(12):1680–7.

13. Xiong J, Zhang Z, Liu Y, Fan G, Wu K, Zhang W. Prevalence and outcomes of unilateral versus bilateral oophorectomy in women with ovarian cancer: A population-based study. Front Oncol 2022;12:866443.

14. Horowitz NS, Miller A, Rungruang B, et al. Does aggressive surgery improve outcomes? interaction between preoperative disease burden and complex surgery in patients with advanced-stage ovarian cancer: an analysis of GOG 182. Journal of Clinical Oncology 2015;33(8):937–43.

15. Chandra A, Pius C, Nabeel M, et al. Ovarian cancer: Current status and strategies for improving therapeutic outcomes. Cancer Med 2019;8(16):7018–31.

16. Perren TJ, Swart AM, Pfisterer J, et al. A Phase 3 Trial of bevacizumab in ovarian cancer. New England Journal of Medicine 2011;365(26):2484–96.

17. Falandry C, Rousseau F, Mouret-Reynier M-A, et al. Efficacy and safety of first-line single-agent carboplatin vs carboplatin plus paclitaxel for vulnerable older adult women with ovarian cancer.. JAMA Oncol 2021;7(6):853.

18. Chan JK, Brady MF, Penson RT, et al. Weekly vs. every-3-week paclitaxel and carboplatin for ovarian cancer. New England Journal of Medicine 2016;374(8):738–48.

19. Brahmer JR, Tykodi SS, Chow LQM, et al. Safety and activity of anti–PD-L1 antibody in patients with advanced cancer. New England Journal of Medicine 2012;366(26):2455–65.

20. Moore K, Colombo N, Scambia G, et al. Maintenance olaparib in patients with newly diagnosed advanced ovarian cancer. New England Journal of Medicine 2018;379(26):2495–505.

21. DiSilvestro P, Colombo N, Scambia G, et al. Efficacy of maintenance olaparib for patients with newly diagnosed advanced ovarian cancer with a BRCA mutation: subgroup analysis findings from the SOLO1 trial. Journal of Clinical Oncology 2020;38(30):3528–37.

22. Hall JM, Lee MK, Newman B, et al. Linkage of early-onset familial breast cancer to chromosome 17q21. Science (1979) 1990;250(4988):1684–9.

23. Jasiewicz A, Rudnicka H, Kluźniak W, et al. Frequency of BRCA1 and BRCA2 mutations in ovarian cancer patients in South-East Poland. Hered Cancer Clin Pract 2022;20(1):12.

24. Cham S, Landrum MB, Keating NL, Armstrong J, Wright AA. Use of germline *BRCA* testing in patients with ovarian cancer and commercial insurance. JAMA Netw Open 2022;5(1):e2142703.

25. Kwon Y, Rösner H, Zhao W, et al. DNA binding and RAD51 engagement by the BRCA2 C-terminus orchestrate DNA repair and replication fork preservation. Nat Commun 2023;14(1):432.

26. Tarsounas M, Sung P. The antitumorigenic roles of BRCA1–BARD1 in DNA repair and replication. Nat Rev Mol Cell Biol 2020;21(5):284–99.

27. Prakash R, Zhang Y, Feng W, Jasin M. Homologous recombination and human health: the roles of BRCA1, BRCA2, and associated proteins. Cold Spring Harb Perspect Biol 2015;7(4):a016600.

28. Roy R, Chun J, Powell SN. BRCA1 and BRCA2: different roles in a common pathway of genome protection. Nat Rev Cancer 2012;12(1):68–78.

29. Gorodetska I, Kozeretska I, Dubrovska A. BRCA genes: the role in genome stability, cancer stemness and therapy resistance. J Cancer 2019;10(9):2109–27.

30. Rebbeck TR, Mitra N, Wan F, et al. Association of type and location of BRCA1 and BRCA2 mutations with risk of breast and ovarian cancer. JAMA 2015;313(13):1347.

31. Clark SL, Rodriguez AM, Snyder RR, Hankins GDV, Boehning D. Structure-function of the tumor suppressor BRCA1. Comput Struct Biotechnol J 2012;1(1):e201204005.

32. Andreassen PR, Seo J, Wiek C, Hanenberg H. Understanding BRCA2 function as a Tumor suppressor based on domain-specific activities in DNA damage responses. Genes (Basel) 2021;12(7):1034.

33. Wen WX, Leong C-O. Association of BRCA1- and BRCA2-deficiency with mutation burden, expression of PD-L1/PD-1, immune infiltrates, and T cell-inflamed signature in breast cancer. PLoS One 2019;14(4):e0215381.

34. Oshi M, Gandhi S, Wu R, et al. Development of a novel BRCAness score that predicts response to PARP inhibitors. Biomark Res 2022;10(1):80.

35. Lord CJ, Ashworth A. BRCAness revisited. Nat Rev Cancer 2016;16(2):110–20.

36. Gowen LC, Johnson BL, Latour AM, Sulik KK, Koller BH. Brca1 deficiency results in early embryonic lethality characterized by neuroepithelial abnormalities. Nat Genet 1996;12(2):191–4.

37. Weghofer A, Tea M-K, Barad DH, et al. *BRCA1/2* mutations appear embryo-lethal unless rescued by low (CGG) FMR1 sub-genotypes: explanation for the "BRCA paradox"? PLoS One 2012;7(9):e44753.

38. Rodgers K, McVey M. Error-prone repair of DNA double-strand breaks. J Cell Physiol 2016;231(1):15–24.

39. Kim D-S, Challa S, Jones A, Kraus WL. PARPs and ADP-ribosylation in RNA biology: from RNA expression and processing to protein translation and proteostasis. Genes Dev 2020;34(5–6):302–20.

40. Kim MY, Zhang T, Kraus WL. Poly(ADP-ribosyl)ation by PARP-1: `PAR-laying' NAD $^{+}$ into a nuclear signal. Genes Dev 2005;19(17):1951–67.

41. Wei H, Yu X. Functions of PARylation in DNA damage repair pathways. Genomics Proteomics Bioinformatics 2016;14(3):131–9.

42. Loeffler PA, Cuneo MJ, Mueller GA, DeRose EF, Gabel SA, London RE. Structural studies of the PARP-1 BRCT domain. BMC Struct Biol 2011;11(1):37.

43. Katsyuba E, Mottis A, Zietak M, et al. De novo NAD+ synthesis enhances mitochondrial function and improves health. Nature 2018;563(7731):354–9.

44. Xie N, Zhang L, Gao W, et al. NAD+ metabolism: pathophysiologic mechanisms and therapeutic potential. Signal Transduct Target Ther 2020;5(1):227.

45. Tang Q, Çağlayan M. The scaffold protein XRCC1 stabilizes the formation of polβ/gap DNA and ligase IIIα/nick DNA complexes in base excision repair. Journal of Biological Chemistry 2021;297(3):101025.

46. Masson M, Niedergang C, Schreiber V, Muller S, Menissier-de Murcia J, de Murcia G. XRCC1 is specifically associated with poly(ADP-ribose) polymerase and negatively regulates its activity following DNA damage. Mol Cell Biol 1998;18(6):3563–71.

47. Purnell MR, Whish WJ. Novel inhibitors of poly(ADP-ribose) synthetase. Biochemical Journal 1980;185(3):775–7.

48. Murai J, Huang SN, Das BB, et al. Trapping of PARP1 and PARP2 by clinical PARP inhibitors. Cancer Res 2012;72(21):5588–99.

49. Creeden JF, Nanavaty NS, Einloth KR, et al. Homologous recombination proficiency in ovarian and breast cancer patients. BMC Cancer 2021;21(1):1154.

50. Kondrashova O, Topp M, Nesic K, et al. Methylation of all BRCA1 copies predicts response to the PARP inhibitor rucaparib in ovarian carcinoma. Nat Commun 2018;9(1):3970.

51. Li S, Topatana W, Juengpanich S, et al. Development of synthetic lethality in cancer: molecular and cellular classification. Signal Transduct Target Ther 2020;5(1):241.

52. Liu JF, Barry WT, Birrer M, et al. Combination cediranib and olaparib versus olaparib alone for women with recurrent platinum-sensitive ovarian cancer: a randomised phase 2 study. Lancet Oncol 2014;15(11):1207–14.

53. Kaufman B, Shapira-Frommer R, Schmutzler RK, et al. Olaparib monotherapy in patients with advanced cancer and a germline *BRCA1/2* mutation. Journal of Clinical Oncology 2015;33(3):244–50.

54. Tinker A V., Altman AD, Bernardini MQ, et al. A pan-Canadian consensus statement on first-line PARP inhibitor maintenance for advanced, high-grade serous and endometrioid tubal, ovarian, and primary peritoneal cancers. Current Oncology 2022;29(6):4354–69.

55. Rudolph J, Jung K, Luger K. Inhibitors of PARP: Number crunching and structure gazing. Proceedings of the National Academy of Sciences 2022; ;119(11):e2121979119.

56. Byers LA, Bentsion D, Gans S, et al. Veliparib in in combination with carboplatin and etoposide in patients with treatment-naïve extensive-stage small cell lung cancer: a phase 2 randomized study. Clinical Cancer Research 2021;27(14):3884–95.

57. Leal TA, Sharifi MN, Chan N, et al. A phase I study of talazoparib (BMN 673) combined with carboplatin and paclitaxel in patients with advanced solid tumors (NCI9782). Cancer Med 2022;11(21):3969–81.

58. Zhang H, Zhang Y. Olaparib and paclitaxel in combination with carboplatin in treatment of ovarian cancer: influence on disease control. Am J Transl Res 2022;14(1):468–75.

59. Gajan A, Sarma A, Kim S, Gurdziel K, Wu GS, Shekhar MP. Analysis of adaptive olaparib resistance effects on cisplatin sensitivity in triple negative breast cancer cells. Front Oncol 2021;11.

60. Gao J, Wang Z, Fu J, A. J, Ohno Y, Xu C. Combination treatment with cisplatin, paclitaxel and olaparib has synergistic and dose reduction potential in ovarian cancer cells. Exp Ther Med 2021;22(3):935.

61. Rose M, Burgess JT, O'Byrne K, Richard DJ, Bolderson E. PARP inhibitors: clinical relevance, mechanisms of action and tumor resistance. Front Cell Dev Biol 2020;8:564601.

62. Anderson NM, Simon MC. The tumor microenvironment. Current Biology 2020;30(16):R921–5.

63. Rodriguez GM, Galpin KJC, Cook DP, et al. The tumor immune profile of murine ovarian cancer models: an essential tool for ovarian cancer immunotherapy research. Cancer Research Communications 2022;2(6):417–33.

64. Rodriguez G, Galpin K, McCloskey C, Vanderhyden B. The tumor microenvironment of epithelial ovarian cancer and its influence on response to immunotherapy. Cancers (Basel) 2018;10(8):242.

65. Mabuchi S, Sasano T, Komura N. Targeting myeloid-derived suppressor cells in ovarian cancer. Cells 2021;10(2):329.

66. Sato S, Matsushita H, Shintani D, et al. Association between effector-type regulatory T cells and immune checkpoint expression on CD8+ T cells in malignant ascites from epithelial ovarian cancer. BMC Cancer 2022;22(1):437.

67. Hensler M, Kasikova L, Fiser K, et al. M2-like macrophages dictate clinically relevant immunosuppression in metastatic ovarian cancer. J Immunother Cancer 2020;8(2):e000979.

68. Kandalaft LE, Odunsi K, Coukos G. Immune Therapy Opportunities in Ovarian Cancer. American Society of Clinical Oncology Educational Book 2020;(40):e228–40.

69. Lieber S, Reinartz S, Raifer H, et al. Prognosis of ovarian cancer is associated with effector memory CD8 $^{+}$ T cell accumulation in ascites, CXCL9 levels and activation-triggered signal transduction in T cells. Oncoimmunology 2018;7(5):e1424672.

70. Nersesian S, Schwartz SL, Grantham SR, et al. NK cell infiltration is associated with improved overall survival in solid cancers: A systematic review and meta-analysis. Transl Oncol 2021;14(1):100930.

71. Macciò A, Gramignano G, Cherchi MC, Tanca L, Melis L, Madeddu C. Role of M1-polarized tumor-associated macrophages in the prognosis of advanced ovarian cancer patients. Sci Rep 2020;10(1):6096.

72. Jiang T, Shi T, Zhang H, et al. Tumor neoantigens: from basic research to clinical applications. J Hematol Oncol 2019;12(1):93.

73. Wu M, Huang Q, Xie Y, et al. Improvement of the anticancer efficacy of PD-1/PD-L1 blockade via combination therapy and PD-L1 regulation. J Hematol Oncol. 2022;15(1):24.

74. Paul S, Lal G. The molecular mechanism of natural killer cells function and its importance in cancer immunotherapy. Front Immunol 2017;8:1124.

75. Strome SE, Dong H, Tamura H, et al. B7-H1 blockade augments adoptive T-cell immunotherapy for squamous cell carcinoma. Cancer Res 2003;63(19):6501–5.

76. Oh DY, Fong L, Newell EW, et al. Toward a better understanding of T cells in cancer. Cancer Cell 2021;39(12):1549–52.

77. Dumitru A, Dobrica E-C, Croitoru A, Cretoiu SM, Gaspar BS. Focus on PD-1/PD-L1 as a Therapeutic Target in Ovarian Cancer. Int J Mol Sci 2022;23(20):12067.

78. Zhu J, Yan L, Wang Q. Efficacy of PD-1/PD-L1 inhibitors in ovarian cancer: a single-arm meta-analysis. J Ovarian Res 2021;14(1):112.

79. Kuchenbaecker KB, Hopper JL, Barnes DR, et al. Risks of breast, ovarian, and contralateral breast cancer for BRCA1 and BRCA2 mutation carriers. JAMA 2017;317(23):2402.

80. Bolton KL. Association Between BRCA1 and BRCA2 mutations and xurvival in women with invasive epithelial ovarian cancer. JAMA 2012;307(4):382.

81. Wen WX, Leong CO. Association of BRCA1- And BRCA2-deficiency with mutation burden, expression of PD-L1/ PD-1, immune infiltrates, and T cell-inflamed signature in breast cancer. PLoS One 2019;14(4): e0215381.

82. Sha D, Jin Z, Budczies J, Kluck K, Stenzinger A, Sinicrope FA. Tumor mutational burden as a predictive biomarker in solid tumors. Cancer Discov 2020;10(12):1808–25.

83. Wei Y, Ou T, Lu Y, et al. Classification of ovarian cancer associated with BRCA1 mutations, immune checkpoints, and tumor microenvironment based on immunogenomic profiling. PeerJ 2020;8:e10414.

84. Heijink AM, Talens F, Jae LT, et al. BRCA2 deficiency instigates cGAS-mediated inflammatory signaling and confers sensitivity to tumor necrosis factor-alpha-mediated cytotoxicity. Nat Commun 2019;10(1):100.

85. Abdolahi S, Ghazvinian Z, Muhammadnejad S, Saleh M, Asadzadeh Aghdaei H, Baghaei K. Patient-derived xenograft (PDX) models, applications and challenges in cancer research. J Transl Med 2022;20(1):206.

86. Roby KF, Taylor CC, Sweetwood JP, et al. Development of a syngeneic mouse model for events related to ovarian cancer. Carcinogenesis 2000;21(4):585–91.

87. McCloskey C, Rodriguez G, Galpin K, Vanderhyden B. Ovarian cancer immunotherapy: preclinical models and emerging therapeutics. Cancers (Basel) 2018;10(8):244.

88. Walton J, Blagih J, Ennis D, et al. CRISPR/Cas9-mediated Trp53 and Brca2 knockout to generate improved murine models of ovarian high-grade serous carcinoma. Cancer Res 2016;76(20):6118–29.

89. Walton JB, Farquharson M, Mason S, et al. CRISPR/Cas9-derived models of ovarian high grade serous carcinoma targeting Brca1, Pten and Nf1, and correlation with platinum sensitivity. Sci Rep 2017;7(1):16827.

90. Cook DP, Galpin KJC, Rodriguez GM, et al. Comparative analysis of syngeneic mouse models of high-grade serous ovarian cancer. bioRxiv [Internet] 2023;2023.03.09.531888. Available from: http://biorxiv.org/content/early/2023/03/10/2023.03.09.531888.1.abstract

91. Jiao S, Xia W, Yamaguchi H, et al. PARP inhibitor upregulates PD-L1 expression and enhances cancer-associated immunosuppression. Clinical Cancer Research 2017;23(14):3711–20.

92. Meng J, Peng J, Feng J, et al. Niraparib exhibits a synergistic anti-tumor effect with PD-L1 blockade by inducing an immune response in ovarian cancer. J Transl Med 2021;19(1):415.

93. Li CW, Lim SO, Xia W, et al. Glycosylation and stabilization of programmed death ligand-1 suppresses T-cell activity. Nat Commun 2016;7:12632.

94. Rampersad SN. Multiple applications of alamar blue as an indicator of metabolic function and cellular health in cell viability bioassays. Sensors (Switzerland) 2012;12(9):12347–60.

95. Fathalla MF. Incessant ovulation - a factor in ovarian neoplasia. The Lancet 1971;298(7716):163.

96. Kurman RJ, Shih I-M. Molecular pathogenesis and extraovarian origin of epithelial ovarian cancer—Shifting the paradigm. Hum Pathol 2011;42(7):918–31.

97. Cass I, Holschneider C, Datta N, Barbuto D, Walts AE, Karlan BY. BRCA-Mutation–Associated Fallopian Tube Carcinoma. Obstetrics & Gynecology 2005;106(6):1327–34.

98. Labidi-Galy SI, Rodrigues M, Sandoval JL, et al. Association of location of BRCA1 and BRCA2 mutations with benefit from olaparib and bevacizumab maintenance in high-grade ovarian cancer: phase III PAOLA-1/ENGOT-ov25 trial subgroup exploratory analysis. Annals of Oncology 2022;

99. Moore K, Colombo N, Scambia G, et al. Maintenance olaparib in patients with newly diagnosed advanced ovarian cancer. New England Journal of Medicine 2018;379(26):2495–505.

100. Pujade-Lauraine E, Ledermann JA, Selle F, et al. Olaparib tablets as maintenance therapy in patients with platinum-sensitive, relapsed ovarian cancer and a BRCA1/2 mutation (SOLO2/ENGOT-Ov21): a double-blind, randomised, placebo-controlled, phase 3 trial. Lancet Oncol 2017;18(9):1274–84.

101. Penn CA, Lester J, Bohrer K, et al. PD-1/PD-L1 expression in mutated ovarian cancers. Gynecol Oncol 2019;154:33.

102. Kornepati AVR, Boyd JT, Murray CE, et al. Tumor intrinsic PD-L1 promotes DNA repair in distinct cancers and suppresses PARP inhibitor-induced synthetic lethality. Cancer Res 2022;82(11):2156–70.

103. Dai Y, Sun C, Feng Y, Jia Q, Zhu B. Potent immunogenicity in BRCA1-mutated patients with high-grade serous ovarian carcinoma. J Cell Mol Med 2018;22(8):3979–86.

104. Pauken KE, Wherry EJ. Overcoming T cell exhaustion in infection and cancer. Trends Immunol 2015;36(4):265–76.

105. Schumann J, Stanko K, Schliesser U, Appelt C, Sawitzki B. Differences in CD44 Surface Expression Levels and Function Discriminates IL-17 and IFN-γ Producing Helper T Cells. PLoS One 2015;10(7):e0132479.

106. Kalia V, Sarkar S. Regulation of effector and memory CD8 T cell differentiation by IL-2 - a balancing act. Front Immunol 2018;9: 2987.

107. Lai Y-P, Lin C-C, Liao W-J, Tang C-Y, Chen S-C. CD4+ T cell-derived IL-2 signals during early priming advances primary CD8+ T cell sesponses. PLoS One 2009;4(11):e7766.

108. Toumi R, Yuzefpolskiy Y, Vegaraju A, et al. Autocrine and paracrine IL-2 signals collaborate to regulate distinct phases of CD8 T cell memory. Cell Rep 2022;39(2):110632.

109. Alam MS, Otsuka S, Wong N, et al. TNF plays a crucial role in inflammation by signaling via T cell TNFR2. Proceedings of the National Academy of Sciences 2021;118(50):e2109972118.

110. Mehta AK, Gracias DT, Croft M. TNF activity and T cells. Cytokine 2018;101:14–8.

111. Tay C, Kanellakis P, Hosseini H, et al. B Cell and CD4 T Cell Interactions Promote Development of Atherosclerosis. Front Immunol 2020;10:3046.

112. Xu H, Li X, Liu D, et al. Follicular T-helper cell recruitment governed by bystander B cells and ICOS-driven motility. Nature 2013;496(7446):523–7.

113. Garnelo M, Tan A, Her Z, et al. Interaction between tumour-infiltrating B cells and T cells controls the progression of hepatocellular carcinoma. Gut 2017;66(2):342–51.

114. Gilbert AE, Karagiannis P, Dodev T, et al. Monitoring the systemic human memory B cell compartment of melanoma patients for anti-tumor IgG antibodies. PLoS One 2011;6(4):e19330.

115. Floc'h A Le, Jalil A, Vergnon I, et al. αEβ7 integrin interaction with E-cadherin promotes antitumor CTL activity by triggering lytic granule polarization and exocytosis. Journal of Experimental Medicine 2007;204(3):559–70.

116. Jaime-Sanchez P, Uranga-Murillo I, Aguilo N, et al. Cell death induced by cytotoxic CD8 + T cells is immunogenic and primes caspase-3–dependent spread immunity against endogenous tumor antigens. J Immunother Cancer 2020;8(1):e000528.

117. Fu Q, Fu T-M, Cruz AC, et al. Structural basis and functional role of intramembrane trimerization of the Fas/CD95 death receptor. Mol Cell 2016;61(4):602–13.

118. Zhang L, Conejo-Garcia JR, Katsaros D, et al. Intratumoral T cells, recurrence, and survival in epithelial ovarian cancer. New England Journal of Medicine 2003;348(3):203–13.

119. Sato E, Olson SH, Ahn J, et al. Intraepithelial CD8 + tumor-infiltrating lymphocytes and a high CD8 + /regulatory T cell ratio are associated with favorable prognosis in ovarian cancer. Proceedings of the National Academy of Sciences 2005;102(51):18538–43.

120. Lieber S, Reinartz S, Raifer H, et al. Prognosis of ovarian cancer is associated with effector memory CD8 + T cell accumulation in ascites, CXCL9 levels and activation-triggered signal transduction in T cells. Oncoimmunology 2018;7(5):e1424672.

121. Preston CC, Maurer MJ, Oberg AL, et al. The Ratios of CD8+ T Cells to CD4+CD25+ FOXP3+ and FOXP3- T cells correlate with poor clinical outcome in human serous ovarian cancer. PLoS One 2013;8(11):e80063.

122. Waki K, Kawano K, Tsuda N, Komatsu N, Yamada A. CD4/CD8 ratio is a prognostic factor in IgG nonresponders among peptide vaccine-treated ovarian cancer patients. Cancer Sci 2020;111(4):1124–31.

123. Brodbeck T, Nehmann N, Bethge A, Wedemann G, Schumacher U. Perforin-dependent direct cytotoxicity in natural killer cells induces considerable knockdown of spontaneous lung metastases and computer modelling-proven tumor cell dormancy in a HT29 human colon cancer xenograft mouse model. Mol Cancer 2014;13(1):244.

124. Liu Y, Cheng Y, Xu Y, et al. Increased expression of programmed cell death protein 1 on NK cells inhibits NK-cell-mediated anti-tumor function and indicates poor prognosis in digestive cancers. Oncogene 2017;36(44):6143–53.

125. Benson DM, Bakan CE, Mishra A, et al. The PD-1/PD-L1 axis modulates the natural killer cell versus multiple myeloma effect: a therapeutic target for CT-011, a novel monoclonal anti–PD-1 antibody. Blood 2010;116(13):2286–94.

126. Movahedi K, Laoui D, Gysemans C, et al. Different tumor microenvironments contain functionally distinct subsets of macrophages derived from Ly6C(high) monocytes. Cancer Res 2010;70(14):5728–39.

127. Bruns H, Büttner M, Fabri M, et al. Vitamin D–dependent induction of cathelicidin in human macrophages results in cytotoxicity against high-grade B cell lymphoma. Sci Transl Med 2015;7(282):282ra47.

128. Pan Y, Yu Y, Wang X, Zhang T. Tumor-associated macrophages in tumor immunity. Front Immunol 2020;11:583084.

129. Dungan LS, McGuinness NC, Boon L, Lynch MA, Mills KHG. Innate IFN-γ promotes development of experimental autoimmune encephalomyelitis: A role for NK cells and M1 macrophages. Eur J Immunol 2014;44(10):2903–17.

130. Xaus J, Comalada M, Barrachina M, et al. The expression of MHC class II genes in macrophages is cell cycle dependent. The Journal of Immunology 2000;165(11):6364–71.

131. Iwanowycz S, Ngoi S, Li Y, et al. Type 2 dendritic cells mediate control of cytotoxic T cell resistant tumors. JCI Insight 2021;6(17): e145885.

132. Guilliams M, Dutertre C-A, Scott CL, et al. Unsupervised high-dimensional analysis aligns dendritic cells across tissues and species. Immunity 2016;45(3):669–84.

133. Chen R, Yang D, Shen L, Fang J, Khan R, Liu D. Overexpression of CD86 enhances the ability of THP-1 macrophages to defend against *Talaromyces marneffei*. Immun Inflamm Dis 2022;10(12): e740.

134. Yokosuka T, Takamatsu M, Kobayashi-Imanishi W, Hashimoto-Tane A, Azuma M, Saito T. Programmed cell death 1 forms negative costimulatory microclusters that directly inhibit T cell receptor signaling by recruiting phosphatase SHP2. Journal of Experimental Medicine 2012;209(6):1201–17.

135. Parry R V., Chemnitz JM, Frauwirth KA, et al. CTLA-4 and PD-1 receptors inhibit T-Cell activation by distinct mechanisms. Mol Cell Biol 2005;25(21):9543–53.

136. Herrero-Sánchez MC, Rodríguez-Serrano C, Almeida J, et al. Targeting of PI3K/AKT/mTOR pathway to inhibit T cell activation and prevent graft-versus-host disease development. J Hematol Oncol 2016;9(1):113.

137. Dong Y, Li X, Zhang L, et al. CD4+ T cell exhaustion revealed by high PD-1 and LAG-3 expression and the loss of helper T cell function in chronic hepatitis B. BMC Immunol 2019;20(1):27.

138. Ran G he, Lin Y qing, Tian L, et al. Natural killer cell homing and trafficking in tissues and tumors: from biology to application. Signal Transduct Target Ther 2022;7(1):205.

139. Nakajima Y, Chamoto K, Oura T, Honjo T. Critical role of the CD44 ^{low} CD62L ^{low} CD8 $^{+}$ T cell subset in restoring antitumor immunity in aged mice. Proceedings of the National Academy of Sciences 2021;118(23).

140. Narayanan S, Ahl PJ, Au Bijin V, et al. LAG3 is a Central Regulator of NK Cell Cytokine Production Corresponding bioRxiv [Internet] 2020.01.31.928200; Available from: https://www.biorxiv.org/content/10.1101/2020.01.31.928200v1.full

141. Thibult M-L, Mamessier E, Gertner-Dardenne J, et al. PD-1 is a novel regulator of human B-cell activation. Int Immunol 2013;25(2):129–37.

142. Li Q, Lao X, Pan Q, et al. Adoptive Transfer of tumor reactive B cells confers host T-cell immunity and tumor regression. Clinical Cancer Research 2011;17(15):4987–95.

143. Henriksen JR, Nederby L, Donskov F, et al. Prognostic significance of baseline T cells, B cells and neutrophil-lymphocyte ratio (NLR) in recurrent ovarian cancer treated with chemotherapy. J Ovarian Res 2020;13(1):59.

144. Huang R-Y, Francois A, McGray AR, Miliotto A, Odunsi K. Compensatory upregulation of PD-1, LAG-3, and CTLA-4 limits the efficacy of single-agent checkpoint blockade in metastatic ovarian cancer. Oncoimmunology 2017;6(1):e1249561.

145. Koyama S, Akbay EA, Li YY, et al. Adaptive resistance to therapeutic PD-1 blockade is associated with upregulation of alternative immune checkpoints. Nat Commun 2016;7(1):10501.

146. Miller BC, Sen DR, Al Abosy R, et al. Subsets of exhausted CD8+ T cells differentially mediate tumor control and respond to checkpoint blockade. Nat Immunol 2019;20(3):326–36.

147. Garcia-Diaz A, Shin DS, Moreno BH, et al. Interferon receptor signaling pathways regulating PD-L1 and PD-L2 expression. Cell Rep 2017;19(6):1189–201.

148. Gasteiger G, Hemmers S, Firth MA, et al. IL-2–dependent tuning of NK cell sensitivity for target cells is controlled by regulatory T cells. Journal of Experimental Medicine 2013;210(6):1167–78.

149. Rudnicka K, Matusiak A, Chmiela M. CD25 (IL-2R) expression correlates with the target cell induced cytotoxic activity and cytokine secretion in human natural killer cells. Acta Biochim Pol 2015;62(4):885–94.

150. Fehniger TA, Cai SF, Cao X, et al. Acquisition of murine NK cell cytotoxicity requires the translation of a pre-existing pool of granzyme B and perforin mRNAs. Immunity 2007;26(6):798–811.

151. McRitchie BR, Akkaya B. Exhaust the exhausters: Targeting regulatory T cells in the tumor microenvironment. Front Immunol 2022;13: 940052.

152. Long Y, Tao H, Karachi A, et al. Dysregulation of glutamate transport enhances Treg function that promotes VEGF blockade resistance in glioblastoma. Cancer Res 2020;80(3):499–509.

153. Ma J, Zheng B, Goswami S, et al. PD1Hi CD8+ T cells correlate with exhausted signature and poor clinical outcome in hepatocellular carcinoma. J Immunother Cancer 2019;7(1):331.

154. Quatrini L, Mariotti FR, Munari E, Tumino N, Vacca P, Moretta L. The immune checkpoint PD-1 in natural killer cells: expression, function and targeting in tumour immunotherapy. Cancers (Basel) 2020;12(11):3285.

155. Meng F, Li L, Lu F, et al. Overexpression of TIGIT in NK and T cells contributes to tumor immune escape in myelodysplastic syndromes. Front Oncol 2020;10:1595.

156. Zhang C, Wang H, Li J, et al. Involvement of TIGIT in natural killer cell exhaustion and immune escape in patients and mouse model with liver echinococcus multilocularis infection. Hepatology 2021;74(6):3376–93.

157. AstraZeneca, Roswell Park Cancer Institute. Olaparib, durvalumab, and tremelimumab in treating patients with recurrent or refractory ovarian, fallopian tube or primary peritoneal cancer with BRCA1 or BRCA2 mutation. Available from: https://clinicaltrials.gov/ct2/show/NCT02953457

158. Hodgins JJ, Abou-Hamad J, Hagerman A, et al. More than a ligand: PD-L1 promotes oncolytic virus infection via a metabolic shift that 2 inhibits the type I intderferon pathway. Corresponding bioRxiv [Internet] 2022.08.31.506095. Available from: https://www.biorxiv.org/content/10.1101/2022.08.31.506095v1

159. Bao T, Liu J, Leng J, Cai L. The cGAS–STING pathway: more than fighting against viruses and cancer. Cell Biosci. 2021;11(1):209.

160. Domizio J Di, Gulen MF, Saidoune F, et al. The cGAS–STING pathway drives type I IFN immunopathology in COVID-19. Nature 2022;603(7899):145–51.

161. Bunting K, Rao S, Hardy K, et al. Genome-Wide analysis of gene expression in T cells to identify targets of the NF-κB transcription factor c-Rel. The Journal of Immunology 2007;178(11):7097–109.

162. Wolfsberger J, Sakil HAM, Zhou L, et al. TAp73 represses NF-κB-mediated recruitment of tumor-associated macrophages in breast cancer. Proc Natl Acad Sci U S A. 2021;118(10):e2017089118.

163. Hua F, Tian Y. Original Article CCL4 promotes the cell proliferation, invasion and migration of endometrial carcinoma by targeting the VEGF-A signal pathway. Int J Clin Exp Pathol. 2017 Nov 1;10(11):11288-11299.

164. Sasaki S, Baba T, Nishimura T, et al. Essential roles of the interaction between cancer cell-derived chemokine, CCL4, and intra-bone CCR5-expressing fibroblasts in breast cancer bone metastasis. Cancer Lett 2016;378(1):23–32.

165. Lien M-Y, Tsai H-C, Chang A-C, et al. Chemokine CCL4 induces vascular endothelial growth factor C expression and lymphangiogenesis by miR-195-3p in oral squamous cell carcinoma. Front Immunol 2018;9:412.

166. Zhang L, Zhang M, Wang L, et al. Identification of CCL4 as an immune-related prognostic biomarker associated with tumor proliferation and the tumor microenvironment in clear cell renal cell carcinoma. Front Oncol 2021;11: 694664.

167. Kim M, Choi HY, Woo JW, Chung YR, Park SY. Role of CXCL10 in the progression of in situ to invasive carcinoma of the breast. Sci Rep 2021;11(1):18007.

168. Baj-Krzyworzeka M, Weglarczyk K, Szatanek R, Mytar B, Baran J, Siedlar M. The role of CD44H molecule in the interactions between human monocytes and pancreatic adenocarcinoma-derived microvesicles. Folia Histochem Cytobiol 2015;(1):28-34.

169. Rashighi M, Agarwal P, Richmond JM, et al. CXCL10 is critical for the progression and maintenance of depigmentation in a mouse model of vitiligo. Sci Transl Med 2014;6(223): 223ra23.

170. Yum S, Li M, Fang Y, Chen ZJ. TBK1 recruitment to STING activates both IRF3 and NF-κB that mediate immune defense against tumors and viral infections. Proceedings of the National Academy of Sciences 2021;118(14): e2100225118.

171. Schoonen PM, Kok YP, Wierenga E, et al. Premature mitotic entry induced by ATR inhibition potentiates olaparib inhibition-mediated genomic instability, inflammatory signaling, and cytotoxicity in BRCA2-deficient cancer cells. Mol Oncol 2019;13(11):2422–40.

172. Hatch EM, Fischer AH, Deerinck TJ, Hetzer MW. Catastrophic nuclear envelope collapse in cancer cell micronuclei. Cell 2013;154(1):47–60.

173. Schoonen PM, Talens F, Stok C, et al. Progression through mitosis promotes PARP inhibitor-induced cytotoxicity in homologous recombination-deficient cancer cells. Nat Com 2017;8(1):15981.

174. George J, Alsop K, Etemadmoghadam D, et al. Nonequivalent gene expression and copy number alterations in high-grade serous ovarian cancers with *BRCA1* and *BRCA2* mutations. Clinical Cancer Research 2013;19(13):3474–84.

175. Bruand M, Barras D, Mina M, et al. Cell-autonomous inflammation of BRCA1-deficient ovarian cancers drives both tumor-intrinsic immunoreactivity and immune resistance via STING. Cell Rep 2021;36(3):109412.

176. Kawai H, Li H, Chun P, Avraham S, Avraham HK. Direct interaction between BRCA1 and the estrogen receptor regulates vascular endothelial growth factor (VEGF) transcription and secretion in breast cancer cells. Oncogene 2002;21(50):7730–9.

177. Wang L, Di L-J. BRCA1 and estrogen/estrogen receptor in breast cancer: where they interact? Int J Biol Sci 2014;10(5):566–75.

178. Samstein RM, Krishna C, Ma X, et al. Mutations in BRCA1 and BRCA2 differentially affect the tumor microenvironment and response to checkpoint blockade immunotherapy. Nat Cancer 2020;1(12):1188–203.

179. Zampieri, LX, Sboarina, M, Cacace, et al. Olaparib Is a Mitochondrial Complex I Inhibitor That Kills Temozolomide-Resistant Human Glioblastoma Cells. Int J Mol Sci 2021;*22*(21), 11938.